Izuhara, Nagasaki, Japan

Αρ. 95 – ΟΚΤΩΒΡΙΟΣ 2016

ΕΛΛΗΝΙΚΗ
ΕΠΙΣΤΗΜΟΝΙΚΗ
ΕΤΑΙΡΕΙΑ
ΕΔΑΦΟΜΗΧΑΝΙΚΗΣ
& ΓΕΩΤΕΧΝΙΚΗΣ
ΜΗΧΑΝΙΚΗΣ

Τα Νέα της Ε Ε Ε Ε Γ Μ

95

Γροθιά στο στομάχι: Πόσα χάνει η Ελλάδα από το Brain Drain των νέων

Στοιχεία σοκ για το πραγματικό κόστος του Brain drain από την Ελλάδα φέρνει στο φως της δημοσιότητας η έρευνα του μη κερδοσκοπικού οργανισμού στήριξης της επιχειρηματικότητας, Endeavor Greece.

Στην επίμαχη έρευνα καταγράφεται η προστιθέμενη αξία και τα φορολογικά έσοδα που δημιουργούν στις χώρες υποδοχής οι Έλληνες που έφυγαν για το εξωτερικό κατά τη διάρκεια της κρίσης (2008-2016).

Σύμφωνα με στοιχεία από τις χώρες υποδοχής και εγχώριες έρευνες, η εκτιμώμενη φυγή ανθρώπινου κεφαλαίου από τον Ιανουάριο 2008 μέχρι σήμερα είναι μεταξύ 350.000 (εκτίμηση Endeavor) και 427.000 (εκτίμηση ΤτΕ).

Βάσει υπολογισμών την Endeavor, οι άνθρωποι αυτοί, κυρίως ανώτερης/ανώτατης εκπαίδευσης, συνεισφέρουν ετησίως €12,9 δισ. στο ΑΕΠ των χωρών υποδοχής (κυρίως Γερμανία και Αγγλία) και €9,1 δισ. σε φορολογικά έσοδα, εκ των οποίων €7,9 δισ. σε φόρους εισοδήματος και εισφορές και €1,2 δισ. σε ΦΠΑ. Αθροιστικά, από το 2008 μέχρι και σήμερα, οι Έλληνες του brain drain έχουν παραγάγει περισσότερα από €50 δισ. ΑΕΠ στις νέες «πατρίδες» τους.

Είναι ενδιαφέρον στοιχείο ότι το ποσό που έχει δαπανήσει το ελληνικό κράτος για την εκπαίδευση των ανθρώπων αυτών υπολογίζεται στα €8 δισ.

(συνέχεια στην σελίδα 3)

Π Ε Ρ Ι Ε Χ Ο Μ Ε Ν Α

(συνέχεια από την σελίδα 1)

Είναι εντυπωσιακό ότι σήμερα, μεταξύ όλων των εξαγόμενων «προϊόντων» της χώρας, το ανθρώπινο δυναμικό κατέχει την πρώτη θέση σε αξία με €12,9 δισ. Ακολουθούν τα προϊόντα πετρελαίου (€7,2 δισ.), τα προϊόντα αλουμινίου (€1,3 δισ.), τα φάρμακα (€0,7 δισ.), το ελαιόλαδο (€0,5 δισ.), τα ψάρια, οι ελιές, τα προϊόντα καπνού, τα πληροφοριακά συστήματα και τα τυροκομικά προϊόντα με €0,4 δισ., το βαμβάκι και τα ροδάκινα (€0,3 δισ.). Προφανώς, ενώ στις εξαγωγές προϊόντων, το παραγόμενο εισόδημα συγκεντρώνεται στην Ελλάδα, η δραστηριότητα των Ελλήνων του εξωτερικού ωφελεί κατά κύριο λόγο και βραχυ/μεσο-πρόθεσμα τις χώρες υποδοχής.

Είναι χαρακτηριστικό ότι περισσότεροι εργαζόμενοι (49%) παρά άνεργοι (43%) επιθυμούν να φύγουν από τη χώρα αναζητώντας καλύτερες ευκαιρίες εξέλιξης και ένα σταθερότερο περιβάλλον.

Η διαρροή ταλέντου αποτελεί σημαντικό πρόβλημα για τις εταιρείες στη χώρα με επιτυχημένη πορεία και προοπτική ανάπτυξης καθώς έχουν ανάγκη για καταρτισμένο προσωπικό αλλά αντιμετωπίζουν αυξανόμενη δυσκολία να κρατήσουν τα ταλέντα στην Ελλάδα ή να τους δώσουν κίνητρα για να επιστρέψουν.

Οι βασικοί λόγοι είναι κυρίως το υψηλό μη μισθολογικό κόστος που συμπιέζει περισσότερο τους ήδη χαμηλούς μισθούς, η απουσία προοπτικής επαγγελματικής εξέλιξης αλλά και η απουσία ευρύτερου αναπτυξιακού πλάνου, θετικού «αφηγήματος» και προοπτικής σε επίπεδο χώρας.

Μακροπρόθεσμα, το ανθρώπινο δυναμικό που φεύγει από τη χώρα μπορεί να φέρει πίσω τεχνογνωσία και καινοτόμες ιδέες και να βοηθήσει στην εξέλιξη της εγχώριας αγοράς.

Για να γίνει αυτό πρέπει να αναστραφούν οι αιτίες μετανάστευσής τους και να δοθεί η δυνατότητα να απορροφηθούν σε υγιείς εταιρείες με υψηλούς ρυθμούς ανάπτυξης ή να δημιουργήσουν δικές τους εταιρείες αξιοποιώντας την εμπειρία και τις γνώσεις που απέκτησαν διεθνώς.

http://www.tribune.gr/greece/news/article/267096/grothia-sto-stomachi-posa-chani-i-ellada-apo-to-brain-drain-ton-neon.html

ΣΕΒ: Δύο δισ. ευρώ το χρόνο χάνει το κράτος από τη μετανάστευση των ελλήνων

Η αποχώρησή τους από την εγχώρια αγορά εργασίας έχει οδηγήσει σε ετήσια απώλεια φόρων και εισφορών 2 δις ευρώ το έτος για το ελληνικό κράτος, ποσό που αντιστοιχεί στα 2/3 περίπου του ΕΝΦΙΑ που βεβαιώνεται ή στο 20% των εισφορών που εισπράττει το ΙΚΑ.

Όπως αναφέρεται στο εβδομαδιαίο δελτίο του ΣΕΒ για την ελληνική οικονομία, η Ελλάδα έχει το υψηλότερο ποσοστό εργαζομένων που έχουν υπερβάλλουσες δεξιότητες σε σχέση με αυτές που απαιτεί η εργασία τους (28% αντί 10% για τον μ.ο. του ΟΟΣΑ) ενώ το 41,4% (αντί 39,6% στον ΟΟΣΑ) εργάζεται σε άλλο αντικείμενο από αυτό που σπούδασε.

Την ίδια ώρα ωστόσο ένα ασυνήθιστα -σε σχέση με άλλες χώρες- μεγάλο μέρος του ενήλικου πληθυσμού στην Ελλάδα φαίνεται να στερείται σημαντικών δεξιοτήτων κατανόησης κειμένων (26,5%), μαθηματικών εννοιών, (28,5%) και πληροφορικής (47,9%). «Προβάλλει, συνεπώς, από αρκετές πλευρές η εικόνα μιας οικονομίας που δεν εκπαιδεύει τους εργαζόμενους στις δεξιότητες που απαιτεί η αγορά εργασίας: παρόλο που επενδύεται χρήμα και χρόνος, η εκπαίδευση αυτή δεν οδηγεί σε ιδιαίτερα αυξημένες δεξιότητες. Μια τέτοια αγορά εργασίας που αξιολογεί τυπικά προσόντα και όχι τις πραγματικές ικανότητες, είναι συμβατή με μια οικονομία που φαίνεται να αδυνατεί να μεταφράσει την εκπαίδευση σε αυξημένη παραγωγικότητα, ατομικά και συλλογικά», αναφέρει ο ΣΕΒ.

«Το ελληνικό εκπαιδευτικό σύστημα εξακολουθεί να προσφέρει, και η αγορά εργασίας να ανταμείβει, τυπικά, και όχι ουσιαστικά, προσόντα», προσθέτει, συνδέοντας το θέμα με το τρίτο κύμα μετανάστευσης από την Ελλάδα, εργαζομένων συνήθως υψηλής εξειδίκευσης και αυξημένων δεξιοτήτων.

Υπενθυμίζεται ότι πρόσφατη μελέτη της Τράπεζας της Ελλάδος καταγράφει ότι λόγω της κρίσης έχουν μεταναστεύσει 427.000 έλληνες που είναι άτομα υψηλής εξειδίκευσης, σε αντίθεση με τα δύο προηγούμενα κύματα μετανάστευσης της περιόδου 1903-17 και 1960.

Πηγή: ΣΕΒ: Δύο δισ. ευρώ το χρόνο χάνει το κράτος από τη μετανάστευση των ελλήνων | iefimerida.grhttp://www.iefimerida.gr/news/278155/sev-dyo-dis-eyro-hrono-hanei-kratos-apo-ti-metanasteysi-ton-ellinon#ixzz4FJqQFXnj

Ορέστης Παπαγεωργίου (1924 ÷ 2016)

Ο Ορέστης Παπαγεωργίου γεννήθηκε το 1924 στη Ναύπακτο. Φοίτησε στη Σχολή Πολιτικών Μηχανικών του ΕΜΠ κατά το διάστημα 1942 – 1947 και 1949 – 1950, οπότε απέκτησε το Δίπλωμα Πολιτικού Μηχανικού και την Άδεια Ασκήσεως Επαγγέλματος. Μετά την αποφοίτησή του εργάστηκε κατά το χρονικό διάστημα 1951 – 1957 στην εταιρεία Tippetts – Abbett – McCarthy – Stratton Σύμβουλοι Μηχανικοί και κατά το χρονικό διάστημα 1959 – 1962 στο U.S. Corps of Engineers, ως Προϊστάμενος Τμήματος στα Έργα Μεσογείου του Εργαστηρίου του, συμμετέχοντας σε μελέτες υδροηλεκτρικών και υδραυλικών έργων, γεφυρών και αεροδρομίων στην Ελλάδα, στην Τουρκία, στη Μέση Ανατολή και στην Αφρική. Ακολούθησαν διετείς μεταπτυχιακές σπουδές (1962 – 1964) σε Γεωτεχνική Μηχανική, Τεχνική Γεωλογία, Σεισμολογία και Υδραυλικά Έργα στο Imperial College of Science, Technology and Medicine, στο Λονδίνο.

Κατά την επιστροφή του στην Ελλάδα, εργάστηκε για σύντομο χρονικό διάστημα στο Γραφείο Δοξιάδη και στη συνέχεια (1965 – 1990) στη ΔΕΗ (Διεύθυνση Μελετών Παραγωγής, Μεταφοράς – Διεύθυνση Μελετών – Κατασκευών Υδροηλεκτρικών Έργων, Διεύθυνση Ανάπτυξης Υδροηλεκτρικών Έργων, συμμετοχή στη μελέτη και στη σύνταξη προδιαγραφών σε όλα τα μεγάλα Υδροηλεκτρικά Έργα της Ελλάδας με κορωνίδα το φράγμα και ΥΗΕ Θησαυρού Νέστου, σε επιτροπές φιλικού διακανονισμού και σε διαιτητικά δικαστήρια). Μετά την αφυπηρέτησή του το 1990 και μέχρι το 2010 απασχολήθηκε στον ιδιωτικό τομέα ως Σύμβουλος σε πλήθος από Υδροηλεκτρικά και Υδραυλικά έργα ανά την Ελλάδα.

Υπήρξε ιδρυτικό μέλος της Ελληνικής Επιστημονικής Εταιρίας Εδαφομηχανικής και Θεμελιώσεων το 1966, της ενώ το 1965 συμμετέχει, μέσω της ΔΕΗ, στην ίδρυση της Ελληνικής Επιτροπής Μεγάλων Φραγμάτων, σύμφωνα με τα πρότυπα των αντίστοιχων διεθνών επιτροπών. Υπήρξε επίσης ενεργό μέλος της Ελληνικής Επιτροπής Τεχνικής Γεωλογίας. Η εξωστρέφεια για αυτόν ήταν σημαντική και αυτήν υπηρέτησε και ως επί χρόνια Γενικός Γραμματέας της Ελληνικής Επιτροπής Μεγάλων Φραγμάτων, την οποία εκπροσώπησε με δικά του έξοδα σε εννέα διεθνή συνέδρια. Συνέγραψε άνω των είκοσι πέντε (25) άρθρων σε εθνικά και διεθνή συνέδρια Γεωτεχνικής Μηχανικής και Μηχανικής Φραγμάτων. Για την προσφορά του στην ανάπτυξη ανανεώσιμων πηγών ενέργειας στη χώρα μας τον τίμησε η Ελληνική Επιτροπή Μεγάλων Φραγμάτων το 2008.

Απεβίωσε στις 2 Οκτωβρίου 2016 πλήρης ημερών.

Αχιλλέας Παπαδημητρίου - Έλενα Παπαγεωργίου

ΑΡΘΡΑ

Παρουσίαση άρθρων, στην συγγραφή των οποίων μετείχαν Έλληνες, στο XVI European Conference on Soil Mechanics and Geotechnical Engineering, Edinburgh, 13-17 September 2015 (κατ' αλφαβητική σειρά, στα ελληνικά, του ονόματος του πρώτου συγγραφέα).

Simplified estimation of elastic response spectra for liquefied ground

Estimation simplifiée des spectres de réponse élastique pour sol liquéfié

Y.Z. Tsiapas, G.D. Bouckovalas and Y.K. Chaloulos

ABSTRACT A simplified methodology is proposed for the estimation of elastic response spectra under liquefiable ground conditions. In brief, the response spectrum is defined through linear interpolation between the corresponding spectra in absence of liquefaction and after complete liquefaction, obtained by equivalent linear (frequency domain) site response analyses. The interpolation is controlled by the factor of safety against liquefaction. In this way, the proposed methodology takes indirectly into account the time lag until the onset of liquefaction, a parameter of cornerstone importance for the evaluation of the overall ground response.

1 INTRODUCTION

The seismic response of liquefied ground can be numerically simulated using advanced constitutive models implemented into available non-linear (Finite Difference or Finite Element) numerical algorithms. However, due to the objective complexity of such analyses, simplified methodologies have been also proposed in the literature, based on simpler computational means (e.g. SHAKE-type equivalent linear analyses). A common assumption of these methodologies is that liquefaction occurs at the onset of the seismic excitation so that the analyses can be performed with the mechanical properties of the liquefied ground. Nevertheless, this assumption is valid only for intense seismic excitations and small factors of safety against liquefaction. As a result, these methodologies may prove significantly unconservative, as the important effect of the pre-liquefaction segment of the seismic excitation is overlooked.

To remedy this shortcoming, a new analytical methodology has been developed, which allows a simplified prediction of the elastic response spectra of liquefied ground while taking consistently into account the pre- as well as the post-liquefaction segments of the seismic excitation. For this purpose, it is assumed that the response spectra for non-liquefied and for totally liquefied ground constitute upper and lower bounds to the actual spectrum. The proposed methodology is calibrated against both the seismic motion recordings from 3 liquefaction case histories, and the results of parametric, fully coupled, nonlinear, numerical analyses. The simulation of the liquefiable sand response is achieved using the critical state plasticity constitutive model NTUA-SAND (Andrianopoulos et al. 2010), which has been extensively verified against laboratory tests and implemented in the finite difference code FLAC as a User Defined Model.

2 LITERATURE REVIEW

2.1 Effect of liquefaction on the seismic design parameters

The majority of the examined cases show deamplification of the peak ground acceleration (PGA) at the ground surface. However, there is also evidence for the opposite, in cases when liquefaction occurred after the strong motion part of the seismic excitation (e.g. the liquefaction case study in Wildlife Liquefaction Array, WLA, under Superstition Hills earthquake) or in the presence of relatively thin (e.g. approximately 3m thick) liquefiable soil layers (e.g. Dashti et al. 2010). The relative density of the liquefiable soil seems to be related to the PGA (e.g. Dashti et al. 2010, Taiebat et al. 2010), for one at least reason: the resistance to liquefaction increases with relative density and consequently the onset of liquefaction may occur after the strong motion part of the seismic excitation, leading thus to amplification of the PGA. Liquefaction effects on spectral accelerations are different for small and for large structural periods, T_{str}. In the low period range, the effect is similar to the above mentioned one for PGA. For the high period range (approximately for T_{str} > 0.8–1.0 sec), liquefaction of the subsoil generally leads to amplification of spectral accelerations (e.g. Youd & Carter 2005, Dashti et al. 2010, Kramer et al. 2011).

2.2 Simplified methodologies for the estimation of seismic design parameters in liquefiable sites

The literature survey did not reveal any widely accepted and adequately documented methodologies for the definition of design spectra for liquefied soils. The few available methods are grossly approximate, while they are not generally consistent with the conclusions of paragraph 2.1. For instance, Miwa & Ikeda (2006) propose to use equivalent linear analyses for the prediction of the seismic motion on the surface of the liquefied ground, using constant values of elastic shear modulus for the liquefied soil layers. The key parameter for this kind of analyses is the shear wave velocity of the liquefied ground, $V_{S,liq}$. Its values were estimated by inverse analyses of actual recordings in liquefied sites and were consequently related with the factor of safety against liquefaction, FS_L, and the initial shear wave velocity without liquefaction, V_S (Table 1). It must be noted that Miwa & Ikeda (2006) do not provide any details for the hysteretic damping ratio, ξ_{liq}, of the liquefied soil that should be used in their analyses. To fill this gap, one may recall previous findings of Pease & O'Rourke (1997) suggesting that the hysteretic damping ratio of liquefied sands, obtained from reverse analysis of relevant seismic recordings, is ξ_{liq} = 20 – 30%.

Table 1. Proposed $V_{S,liq}/V_S$ ratios by Miwa & Ikeda (2006).

FS_L	0.3 - 0.6	0.6 - 0.9	0.9 - 1.0
$V_{s,liq}/V_s$	0.10 - 0.14	0.12 - 0.16	0.14 - 0.19

Based on the conclusions of paragraph 2.1, it is realized that the methodology of Miwa & Ikeda is reliable only in the case of extensive liquefaction (e.g. FS_L < 0.40), when the liquefaction onset occurs early during shaking, i.e. well before the peak of the seismic excitation. In the opposite case, this approach may prove significantly non-conservative, since it totally ignores the possible amplification of the seismic excitation segment preceding the onset of liquefaction. This effect is taken indirectly into account by Kramer et al. (2011), who proposed numerically established spectral acceleration correction curves (ratio of liquefied over non-liquefied site response) in terms of FS_L. Nevertheless, the Authors accept that application of their correction curves in practice is premature due to the large scatter of the associated numerical predictions.

3 OUTLINE OF THE PROPOSED METHODOLOGY

3.1 Basic principles

The basic assumption of the proposed methodology is that the response spectrum of the liquefied ground, Sa_{REAL}, can be estimated through linear interpolation between the response spectra for "non-liquefied", Sa_{NL}, and for totally "liquefied" ground, Sa_L, which are obtained from equivalent linear analyses. Note that Sa_{NL} and Sa_L can be computed with conventional analysis methods, combined with the logic of Miwa & Ikeda (2006) in the later case. In particular, the elastic shear modulus, G_{max}, is reduced to a prescribed constant value ($G_{liq} = \rho V_{S,liq}^2$), whereas the hysteretic damping ratio is related to cyclic shear strain amplitude γ, using the common empirical ξ-γ curves for sands. For the linear interpolation between the aforementioned response spectra, the interpolation factor, α, is defined as a function of structural period, T:

$$\alpha(T) = \frac{Sa_{NL}(T) - Sa_{REAL}(T)}{Sa_{NL}(T) - Sa_{L}(T)} \quad (1)$$

In absence of liquefaction ($FS_L > 1$), it is evident that the recorded response spectrum, is equal to the spectrum for the "non-liquefied" ground, and hence α = 0. On the other hand, when the factor of safety is close to zero, the ground liquefies immediately and the real spectrum becomes equal to the "liquefied" one, so that α = 1. As a result, the values of the interpolation factor are restricted to the range: α = 0 – 1.

3.2 Inverse analyses for the calculation of the interpolation factor α

The calibration of the interpolation factor was based on: (a) three (3) liquefaction case histories, in sites with acceleration recordings both at the soil surface and at the base of the liquefied layer, and (b) the results of parametric, fully coupled, nonlinear, numerical analyses. The examined case histories come from the "Wildlife Liquefaction Array" (WLA) in U.S.A. and the "Port Island" array in Japan. The first site consists of 4.5m liquefiable silty sand (2.5–7.0m depth), with two accelerometers installed at the soil surface and at 7.5m depth. The respective soil profile, along with the variation of the average tip resistance from 5 CPT tests with depth, is presented in Figure 1a. Two strong motion recordings were obtained in WLA: Elmore Ranch earthquake (1987) of MW = 6.2 magnitude, which did not cause liquefaction (FSL ≈ 1.50) and Superstition Hills earthquake (1987) of MW = 6.6 magnitude, which led to liquefaction (FSL ≈ 0.80). The Port Island site, consists of loose sand and gravel, which liquefied between 3–16m depth during Kobe earthquake (1995) of MW = 6.9, as FSL ≈ 0.4. Acceleration time-histories have been recorded at the ground surface, at 16m depth, as well as at greater depths. The respective soil profile with SPT results is presented in Figure 1b.

The numerical analyses simulate the seismic response of an actual soil profile (Figure 1c), located within the riverbed of Strymonas river in Northern Greece, consisting of a 23m thick liquefiable silty sand layer. The seismic response of this site has been simulated with the finite difference code FLAC and the in-built Critical State soil plasticity model NTUA–Sand (Andrianopoulos et al. 2010). To capture the liquefaction resistance of the in-situ soils, NTUA-Sand was properly calibrated against the associated factors of safety against liquefaction, FSL, computed from the reported SPT results according to the Youd et al. (2001) empirical method. The numerical model consists of a single element column with element dimensions 1m x 0.50m (width x height). Tied–node conditions were considered at the side boundaries, which impose the same vertical and horizontal displacements to grid points of the same elevation.

To examine the effect of shaking magnitude, two different seismic excitation scenarios were considered:

- Scenario A, for 1000yrs return period, MW = 7 and PGA = 0.32g at the outcropping bedrock.

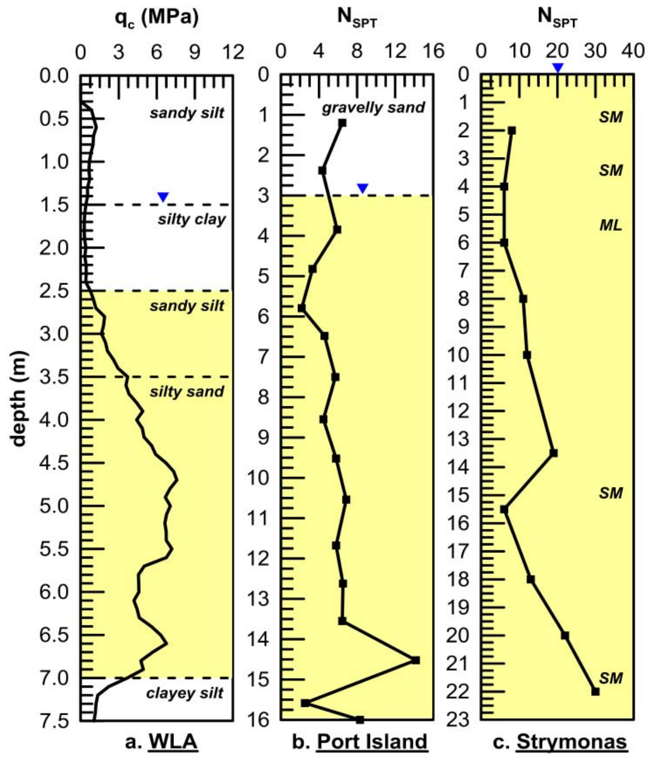

Figure 1. Soil profile and CPT/SPT results for (a) WLA site, (b) Port Island site, and (c) the numerical simulations (at Strymonas river).

- Scenario B, for 225yrs return period, MW = 6.7 and PGA = 0.22g at the outcropping bedrock.

For each scenario, a suite of seven earthquake motions, recorded on bedrock outcrop and having the target magnitude, is selected and properly scaled so that the average response spectrum is in good agreement with the design spectra of Eurocode 8 for soil type B (Figure 2). These seismic motions, along with the respective FSL values, as estimated from SPT results (Youd et al. 2001), are summarized in Table 2.

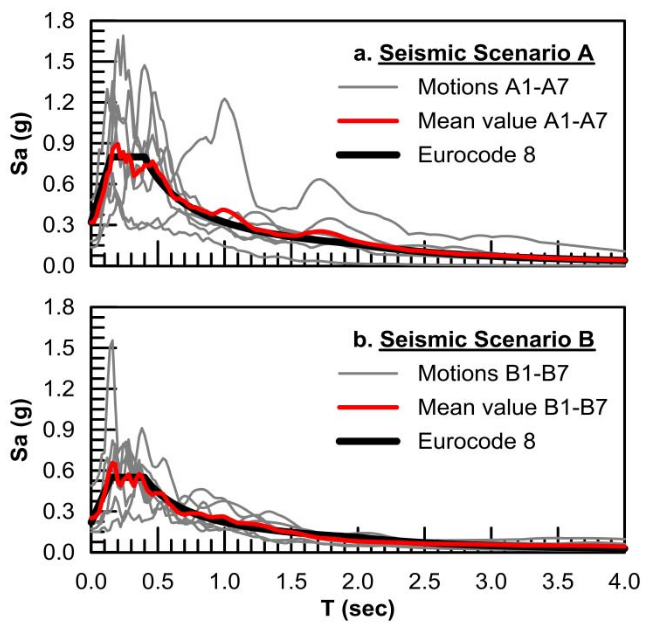

Figure 2. Comparison of the average elastic response spectra at bedrock outcrop for the seismic scenarios A and B with the respective design spectra of EC8.

Table 2. Summary of earthquake motions and average FSL for the numerical simulations.

Motion #	Seismic Scenario A			Seismic Scenario A		
	Seismic Motion	PGA (g)	FS_L	Seismic Motion	PGA (g)	FS_L
1	*ITALY-BAG*	0.180	1.03	*NEWZEAL*	0.280	0.78
2	*ITALY-VLT*	0.136	1.36	*NORTHR-BLD*	0.251	0.80
3	*KOBE-AMA*	0.394	0.47	*NORTHR-CEN*	0.589	0.41
4	*KOBE-KAK*	0.330	0.56	*NORTHR-FLE*	0.172	1.17
5	*KOBE-TDO*	0.383	0.49	*SFERN-L*	0.150	1.38
6	*LOMAP-AND*	0.320	0.58	*SFERN-PEL*	0.211	0.99
7	*LOMAP-GIL*	0.484	0.38	*SPITAK*	0.207	0.91

Inverse calculation of interpolation factors α, was based on equivalent linear analyses of each soil profile in Figure 1, separately for "non-liquefied" and for "liquefied" ground conditions. For the examined case histories, the respective recording at the base of the liquefied layer (Figure 3) was applied, whereas the 14 seismic motions of Figure 2 were used for the numerical simulations.

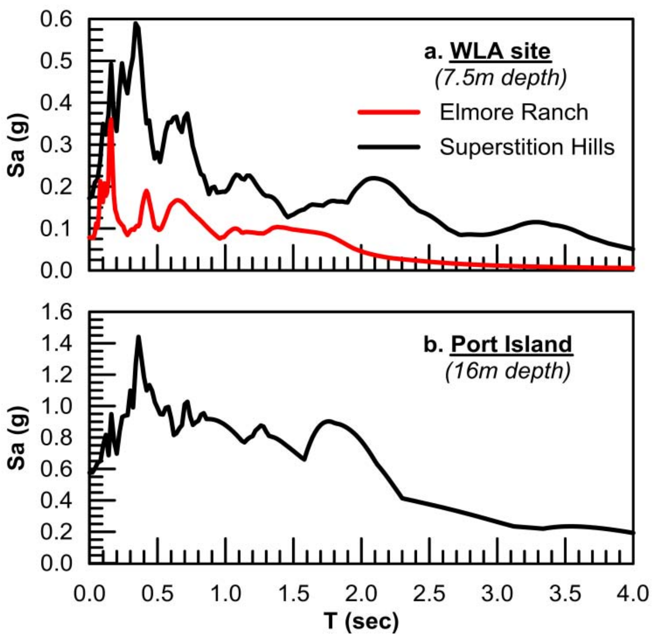

Figure 3. Response spectra at the base of the liquefied layer at (a) WLA (Elmore Ranch and Superstition Hills earthquakes) and (b) Port Island (Kobe earthquake).

A parametric investigation was conducted in order to define the value of the $V_{S,liq}/V_S$ ratio which provides best fit in the analyses of "liquefied" ground. In each case, the $V_{S,liq}/V_S$ ratio for which the corresponding response spectrum for "liquefied" ground matches with the real one in long periods ($T > 0.8$–1.0sec) is selected for the next steps of the statistical processing. Typical results for the variation of coefficient α with period are presented in Figure 4 for two numerical simulations.

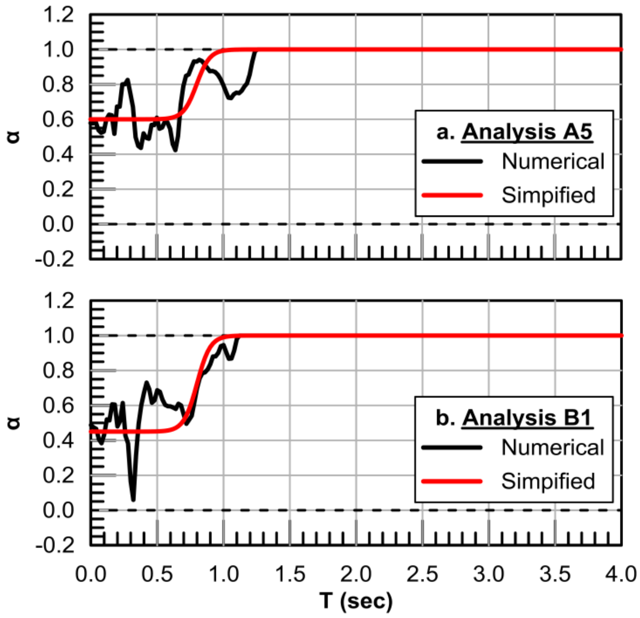

Figure 4. Actual and fitting curves of the coefficient "α".

4 CALIBRATION AND EVALUATION OF THE PROPOSED METHODOLOGY

4.1 Calibration of the interpolation factors

There are two (2) key parameters that need to be determined, in order to apply the proposed methodology in practice: the $V_{S,liq}/V_S$ ratio and the variation of coefficient "α" with period. Starting with the $V_{S,liq}/V_S$ ratio, the values obtained from the inverse analyses are plotted against FS_L in Figure 5a, in comparison with the range proposed by Miwa & Ikeda (2006) for $FS_L \leq 1$ (Table 1). The observed agreement is fairly good and suggest that the same chart, properly extended for $FS_L > 1.0$, may be used for the a-priori selection of $V_{S,liq}/V_S$ ratio.

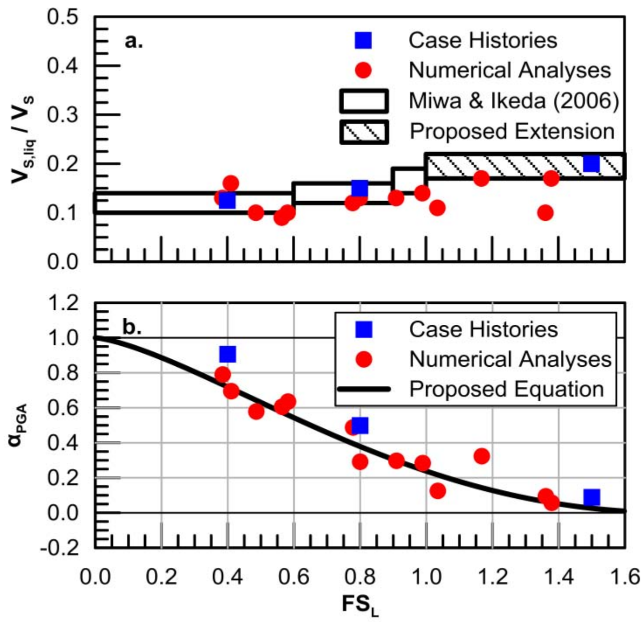

Figure 5. Empirical charts for the computation of $V_{S,liq}/V_S$ and α_{PGA} in terms of FS_L.

In addition, it is observed that the values of coefficient α for peak ground acceleration (α_{PGA}) are uniquely related to FS_L (Figure 5b) and can be expressed analytically as follows:

$$\alpha_{PGA} = \frac{1}{2}\left\{1+\cos\left[\frac{\pi}{2}\left(\frac{FS_L}{0.65}\right)^{0.70}\right]\right\} \quad (2)$$

Finally, the shape of the statistically estimated curves for the variation of coefficient α with the period T of Figure 4 is fitted with the following approximate relation which predicts a step-like increase from $\alpha = \alpha_{PGA}$ for T < 0.8sec to α = 1 for T > 1sec:

$$\alpha(T) = \left(\frac{1+\alpha_{PGA}}{2}\right) + \left(\frac{1-\alpha_{PGA}}{2}\right)\tanh\left[10(T-0.8)\right] \quad (3)$$

4.2 valuation of the analytical predictions

To evaluate the accuracy of the proposed methodology, the predicted response spectra, Sa_{PRED}, are compared in Figure 6 with the recorded response spectra at WLA and Port Island liquefaction sites and the numerically simulated ones for seismic scenarios A5 and B1 in Table 1. In all cases, the comparison between the predictions with the proposed methodology and the target response spectra is consistently good, over the entire range of period T. To further appreciate the capabilities of the proposed methodology, predictions using the approach of Miwa & Ikeda (2006) are also plotted in Figure 6. Observe that this early approach provides reliable predictions only in the high period range, and significantly underestimates spectral accelerations in the period range of common structures (T = 0.30–0.60sec). Exception is the case of Port Island liquefaction site, where liquefaction occurs at the initial stages of shaking ($FS_L \approx 0.40$), and consequently the Miwa & Ikeda (2006) approach provides a reasonable fit of the recorded seismic response.

5 CONCLUDING REMARKS

A new method has been established to predict the elastic response spectrum of liquefiable sites using simple analysis methods, developed and widely applied for non liquefiable soils (e.g. the equivalent linear analysis method). The novel assumption of the proposed methodology is that the liquefied ground response is significantly affected by the preliquefaction segment of the seismic excitation, and, consequently, it may even exhibit amplification of the seismic motion parameters at the low period range, of common structures. This effect is indirectly incorporated via the introduction of the factor of safety against liquefaction FS_L as the basic parameter for the interpolation between the response spectra for the two limiting conditions: the immediate liquefaction (FS_L<0.30) and the total absence of it (FS_L> 1.0).

Until now, the new methodology has been calibrated against the few available case histories and a limited number of parametric numerical simulations for an actual soil profile. Work is currently in progress in order to gain insight to the possible effect on the interpolation factor α(T) of additional problem parameters, such as the thickness of the liquefied layer and the frequency content of the seismic excitation.

ACKNOWLEDGEMENT

This research has been co-financed by the European Union (European Social Fund – ESF) and Greek national funds through the Operational Program "Education and Lifelong Learning" of the National Strategic Reference Framework (NSRF)-Research Funding Program: THALES. Investing in knowledge society through the European Social Fund.

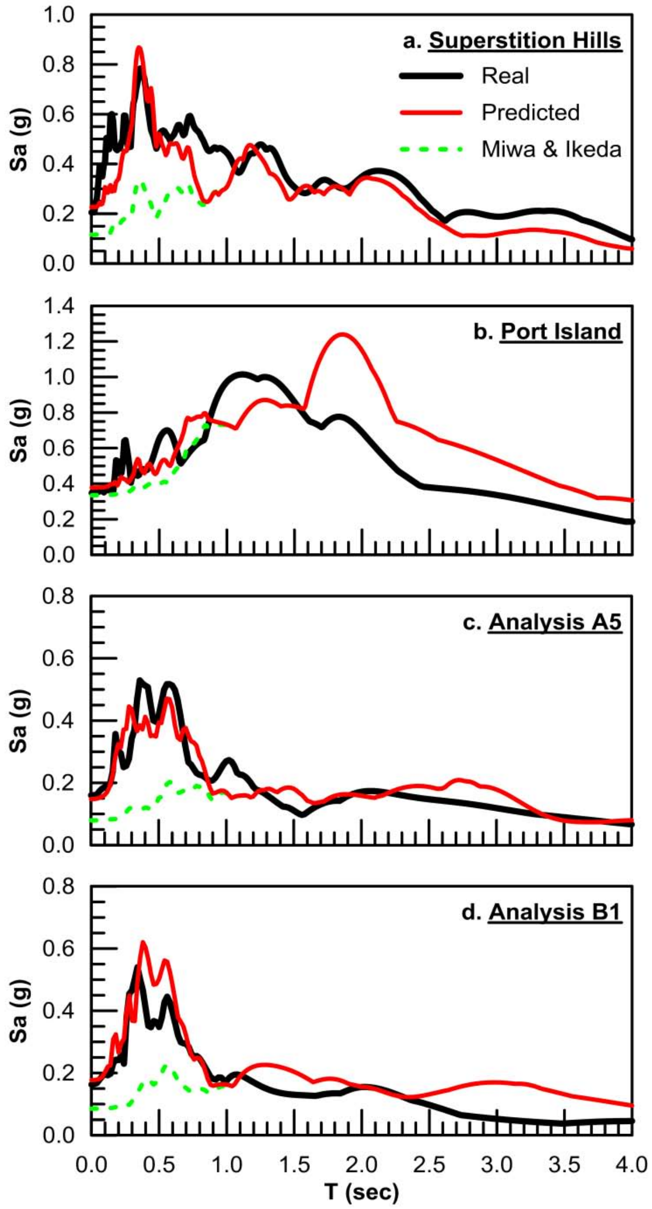

Figure 6. Evaluation of the proposed methodology for (a) WLA during Superstition Hills earthquake, (b) Port Island, (c) analysis A5 and (d) analysis B1.

REFERENCES

Andrianopoulos, K. I., Papadimitriou, A. G., and Bouckovalas, G. D. (2010). "Bounding surface plasticity model for the seismic liquefaction analysis of geostructures." *Soil Dynamics and Earthquake Engineering*, 30(10), pp. 895–911.

Dashti, S., Bray, J. D., Pestana, J. M., Riemer, M., and Wilson, D. (2010). "Mechanisms of Seismically Induced Settlement of Buildings with Shallow Foundations on Liquefiable Soil." *Journal of Geotechnical and Geoenvironmental Engineering*, ASCE, 136(1), 151–164.

Kramer, S. L., Hartvigsen, A. J., Sideras, S. S., and Ozener, P. T. (2011). "Site response modeling in liquefiable soil deposits." *4th IASPEI / IAEE International Symposium: Effects of Surface Geology on Strong Ground Motion*.

Miwa, S., and Ikeda, T. (2006). "Shear modulus and strain of liquefied ground and their application to evaluation of the response of foundation structures." *Structural Engineering/Earthquake Engineering*, 23(1), 167s–179s.

Pease, J. W., and O'Rourke, T. D. (1997). "Seismic response of liquefaction sites." *Journal of Geotechnical Engineering*, 123(1), 37–45.

Schnabel, P. B., Lysmer, J., and Seed, H. B. (1972). "SHAKE: A computer program for earthquake response analysis of horizontally layered sites." *SHAKE: A Computer Program for Earthquake Response Analysis of Horizontally Layered Sites*.

Taiebat, M., Jeremić, B., Dafalias, Y. F., Kaynia, A. M., and Cheng, Z. (2010). "Propagation of seismic waves through liquefied soils." *Soil Dynamics and Earthquake Engineering*, 30(4),.

Youd, T., Idriss, I., Andrus, R., Arango, I., Castro, G., Christian, J., Dobry, R., Finn, W., Harder, L., Hynes, M., Ishihara, K., Koester, J., Liao, S., Marcuson, W., Martin, G., Mitchell, J., Moriwaki, Y., Power, M., Robertson, P., Seed, R., and Stokoe, K. (2001). "Liquefaction Resistance of Soils: Summary Report from the 1996 NCEER and 1998 NCEER/NSF Workshops on Evaluation of Liquefaction Resistance of Soils." *Journal of Geotechnical and Geoenvironmental Engineering*, American Society of Civil Engineers, 127(10), 817–833.

Youd, T. L., and Carter, B. L. (2005). "Influence of Soil Softening and Liquefaction on Spectral Acceleration." *Journal of Geotechnical and Geoenvironmental Engineering*, 131(7), 811–825.

On the seismic response of shallow rectangular tunnels in soft soils

Etude expérimentale et numérique du comportement sismique des tunnels rectangulaires en terrain meubles

G. Tsinidis, K. Pitilakis, G. Madabhushi and C. Heron

ABSTRACT A series of dynamic centrifuge tests was performed on a rectangular tunnel model embedded in dry sand at the centrifuge facility of the University of Cambridge. An extensive instrumentation array was implemented to monitor the soil-tunnel response, which comprised of miniature accelerometers, pressure cells and position sensors in addition to strain gauges that recorded the strains within the tunnel lining. In the second phase of this research program representative test cases were numerically investigated by means of full dynamic analysis of the coupled soil-tunnel system using ABAQUS. The paper discusses several crucial aspects of the seismic response, as revealed by comparisons between the numerical and the experimental data, namely the lining dynamic internal forces, the magnitude and distribution of the dynamic earth pressures and shear stresses which develop around the rectangular tunnel and the effect of burial depth on the response characteristics. The interpretation of both the experimental and numerical data reveals, among others: (i) a rocking response of the model tunnel in combination with the racking mode and (ii) residual earth pressures on the side-walls and residual internal forces, after shaking, which are amplified by the tunnel's flexibility.

1 INTRODUCTION

Although recent earthquake events have demonstrated that underground structures in soft soils may undergo extensive deformations or even collapse, their seismic response has received considerably less attention compared to aboveground structures. The seismic response of underground structures is quite distinct from that of above ground structures as the kinematic loading introduced by the surrounding soil is prevalent, while the inertia loads are often of secondary importance. Generally, the knowledge shortfall is more evident for rectangular embedded structures (e.g. cut and cover tunnels), where the soil-structure interaction effects are expected to be more pronounced. In addition, design specifications in modern seismic codes are based primarily on simplified methods, which may lead to substantially different seismic design loads and internal lining stresses (Pitilakis & Tsinidis 2014).

Given the need for further research, a series of dynamic centrifuge tests was performed on flexible aluminum square tunnel models embedded in dry sand models pluviated to differing relative densities. Representative tests were numerically modeled by means of full dynamic analysis of the coupled soil-tunnel system. The paper presents a series of comparisons between the numerical predictions and the experimental results. Throughout this paper, crucial response characteristics are discussed.

2 DYNAMIC CENTRIFUGE TESTING

The centrifuge tests were performed at the "Turner beam centrifuge" of the University of Cambridge, under a centrifugal acceleration of 50 g (scale factor N = 50). The models were constructed within an equivalent shear beam (ESB) container, while a specially designed Stored Angular Momentum actuator was used to apply the earthquake input motions at the model base. The actuator is capable of applying sinusoidal or sine-sweep inputs (Madabhushi et al. 1998).

Soil deposits were made of dry Hostun HN31 sand reconstituted at two different relative densities of 50 % and 90 %.

Table 1. Sand mechanical properties

Parameter	Values
ρ_s (g/cm^3)	2.65
e_{max} / e_{min}	1.01 / 0.555
d_{10} / d_{50} / d_{60} (mm)	0.209 / 0.335 / 0.365
φ_{crit} (°)	33

A 100 × 100 × 210 (mm) square model tunnel was manufactured by an extruded section of 6063A aluminum alloy having a thickness of 2 mm (Figure 1). This selection, with such a reduced lining thickness was chosen so as to study the effects of tunnel flexibility at an extreme end of possible real structure flexibilities. To study the effect of the soil-tunnel interface friction Hostun sand was stuck to the external face of the tunnel-model, creating a rough surface for the final test (Test 2).

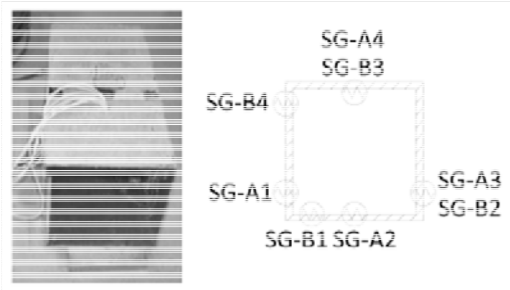

Figure 1. Model tunnel; strain gauges: SG-Ai: axial force strain gauges, SG-Bi: bending moment strain gauges.

Table 2. Model tunnel mechanical properties

Parameter	Values
Unit weight, γ (kN/m^3)	2.70
Young's Modulus, E (GPa)	69.5
Poisson ratio, ν	0.33
Tensile strength, f_{bk} (MPa)	33

Figure 2 presents a typical model layout and the instrumentation scheme, while Table 3 tabulates the sequence and characteristics of the input motions during each test.

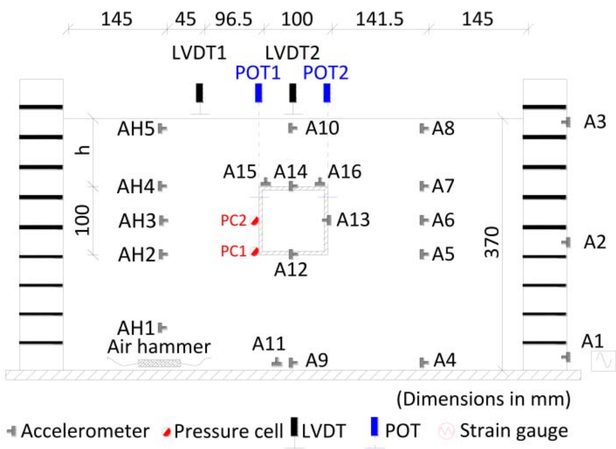

Figure 2. Typical model layout; h = 60 mm for Test 1; h = 100 mm for Test 2.

Table 3. Input motions (bracketed values in prototype scale)

Test ID	D_r (%)	EQ ID	Frequency (Hz)	Amplitude (g)	Nominal Duration (s)
Test 1	51	EQ1	60 (1.2)	10.5 (0.21)	0.4 (20)
		EQ2	60 (1.2)	12.9 (0.26)	0.4 (20)
		EQ3	60 (1.2)	15.7 (0.31)	0.4 (20)
		EQ4	60 (1.2)	18.3 (0.37)	0.4 (20)
Test 2	89	EQ1	30 (0.6)	1.0 (0.02)	0.4 (20)
		EQ2	45 (0.9)	4.0 (0.08)	0.4 (20)
		EQ3	50 (1)	6.5 (0.13)	0.4 (20)
		EQ4	50 (1)	12.0 (0.24)	0.4 (20)
		EQ5*	60 (1.2)	12.0 (0.24)	3.0 (150)
		EQ6**	50 (1)	5.8 (0.116)	0.4 (20)
		EQ7**	50 (1)	6.0 (0.12)	0.6 (30)
		EQ8**	50 (1)	11.0 (0.22)	0.5 (25

* Sine sweep / ** Fired during a second flight

A dense monitoring array was implemented to record the soil-tunnel system response, comprising of miniature accelerometers (As), linear variable differential transformers (LVDTs), position sensors (POTs) and miniature total earth pressure cells (PCs) (Figure 2). Resistance strain gauges were also used to measure the tunnel lining axial and bending moment strains at several locations (Figure 1). Unfortunately, the strain gauges did not record during the first test (Test 1) due to a wiring problem, while they worked properly during the second test (Test 2). To estimate the soil shear wave velocity gradient, air hammer tests were performed prior shaking.

In each test, the centrifuge was spun up in steps until 50 g and then the earthquakes were fired in a row, leaving some time between them to acquire the data. The data was recorded at a sampling frequency of 4 Hz during the centrifuge swing up and at 4 kHz during shaking. More details about the experimental program may be found in Tsinidis et al. (2014).

3 NUMERICAL ANALYSIS

The tests were simulated by means of full dynamic time history analyses, using the finite element code ABAQUS (ABAQUS 2012). The analyses were performed in prototype scale under plane strain conditions. Figure 3 presents a typical numerical model layout.

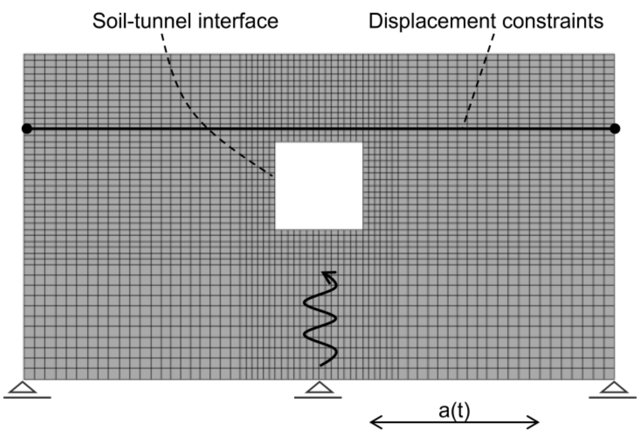

Figure 3. Numerical model in ABAQUS.

The soil was adequately meshed with quadratic plane strain elements, while the tunnel was modelled with beam elements. The base boundary of the model was simulated as rigid bedrock, while for the vertical boundaries kinematic tie constrains were introduced, simulating in that simplified way the ESB container.

For the soil-tunnel interface, a finite sliding hard contact algorithm was implemented (ABAQUS 2012). The interface friction effect was investigated applying different Coulomb friction coefficients μ, namely μ = 0 for the full slip and 0.4 and 0.8 for nonslip conditions. In a final analysis, the soil and the tunnel were fully bonded assuming no slip conditions and precluding separation.

The lining behaviour was simulated using an elastic-perfectly plastic material model, with yield strength equal to 220 MPa.

The dynamic sand response was modeled in two ways. For a first series of analyses a visco-elastic model was implemented using the equivalent linear approximation. In a second stage, the analyses were performed with a non-associated elasto-plastic Mohr-Coulomb model in order to account for the soil permanent deformations. Sand stiffness and damping were properly tuned, in order to reproduce the recorded inertial response of the soil (e.g. horizontal acceleration amplification and time histories at free field). In particular, 1D soil response analyses were performed assuming a small strain shear modulus according to Hardin and Drenvich (1972) and using different sets of G-γ-D curves for cohesionless soils. Computed acceleration was compared to the recorded data. This procedure revealed that a reduced distribution according to Hardin and Drenvich (1972) was adequately describing the sand shear modulus:

$$G = a \times 100 \frac{(3-e)^2}{1+e} (\sigma')^{0.5} \tag{1}$$

where: e is the void ratio, σ' is the mean effective stress (in MPa), G is the degraded shear modulus (in MPa) and a is the reduction value for each shake, ranging between 0.3-0.4 for the different cases studied. Viscous damping (15 %) was employed in the frequency depended Rayleigh type. For the elastoplastic analyses additional energy dissipation was introduced by the hysteretic soil response (e.g. near the tunnel). Regarding the soil strength parameters, the friction angle φ was assumed equal to 33° (critical angle for the specific sand fraction), while the dilatancy angle ψ was assumed equal to 3° for all the examined cases. To avoid numerical problems a small amount of cohesion was introduced in the model (c = 1 kPa).

Seismic input motion was introduced at the base of the numerical model in terms of acceleration time histories referring to the motion recorded at the reference accelerometer (A1). All the records were properly processed (filtering, baseline correction) before being used in the numerical analysis. Analyses were performed in two steps; first the gravity loads were introduced, while in a second step the earthquake motions were applied in a row replicating each test flight.

4 RESULTS

This section summarizes representative comparison examples between the experimental results and the numerical predictions. The results are generally shown at model scale, if not differently stated.

4.1 Horizontal acceleration

Figure 4 presents representative comparisons between the recorded and computed horizontal acceleration amplification along accelerometers vertical arrays. Both visco-elastic and elasto-plastic analyses revealed similar responses and amplification. The numerical predictions are generally in good agreement with the records for the horizontal acceleration. The differences, generally minor, are mainly attributed to the differences between the assumed soil mechanical properties (stiffness and damping) and their actual values during the test. The larger deviation of the acceleration amplitude at the tunnel roof slab in the presented example is attributed to an erroneous record at this location.

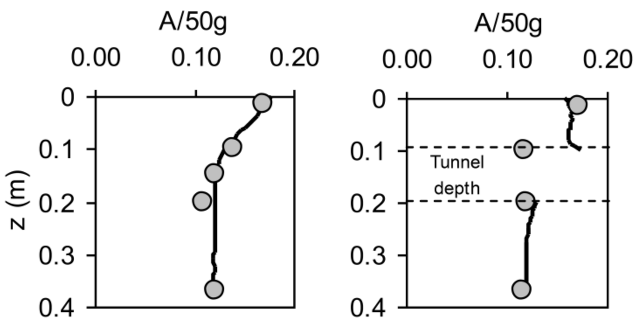

Figure 4. Horizontal acceleration amplification along the free field (left) and the tunnel (right) accelerometer vertical arrays; solid lines: numerical results (elasto-plastic analysis), circles: experimental data, EQ6-Test 2.

4.2 Tunnel deformed shapes

Figure 5 presents representative time-windows of the recorded vertical acceleration at the sides of the tunnels roof slabs. Time histories for the deeper tunnel (Test 2) are out of phase indicating a rocking mode of vibration for the tunnel in addition to the racking distortion. Numerical results reveal a similar tendency. This observation is less evident for the shallower tunnel (Test 1); however this rocking response still exists. Figure 6 presents typical tunnel deformed shapes during shaking, indicating this complex racking-rocking response. Due to the high flexibility of the tunnel, inward deformations are also observed for the slabs and the walls.

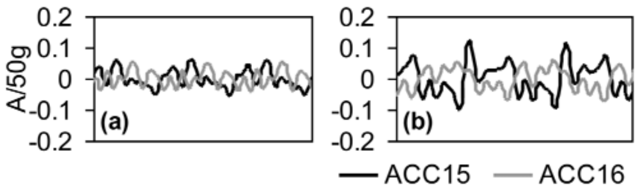

Figure 5. Time windows of the recorded vertical acceleration at the sides of the tunnels roof slabs; (a) EQ2-Test 1, (b) EQ4 -Test 2.

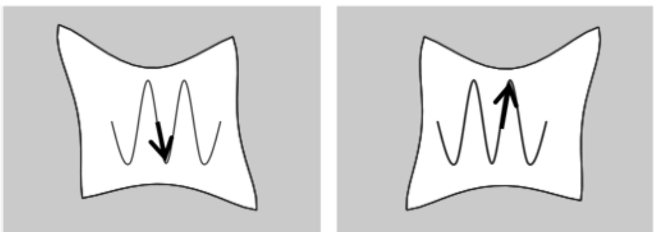

Figure 6. Tunnel deformed shapes for time steps of maximum racking distortion; EQ2-Test 1, no slip conditions (deformations scale × 60).

4.3 Dynamic earth pressures

Recorded dynamic earth pressures generally increased with increasing burial depth and increasing soil relative density (Test 2), both in terms of dynamic increments and residual values after shaking.

Figure 7 presents typical comparisons between the computed and the recorded dynamic earth pressures time histories at the left side-wall. Numerical results refer to elasto-plastic analysis assuming no-slip conditions. Residual values were reported after shaking, as a result of the soil yielding and densification around the tunnel. This post-earthquake residual response that can not be reproduced by the viscoelastic analyses is amplified with the flexibility of the tunnel. In addition, dynamic pressure increments were found to be larger near the stiff corners of the tunnel. For the deeper tunnel case (Test 2) numerical results for no-slip conditions were closer to the experimental records. For the shallow tunnel (Test 1) full slip conditions were found to describe better the recorded response. It is noteworthy that for Test 2 sand was stack on the external face of the tunnel leading to a rough interface.

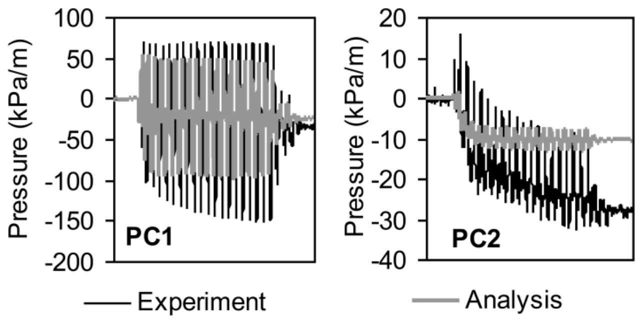

Figure 7. Dynamic earth pressure time histories on the left side wall; EQ8-Test 2, no slip conditions.

Figure 8 presents typical dynamic earth pressure distributions around the tunnel perimeter, as affected by the soil-tunnel interface characteristics. The results refer to the time step of the tunnel maximum racking distortion. Soil yielding around the tunnel results in stress redistributions leading to a different response between elasto-plastic and visco-elastic analyses.

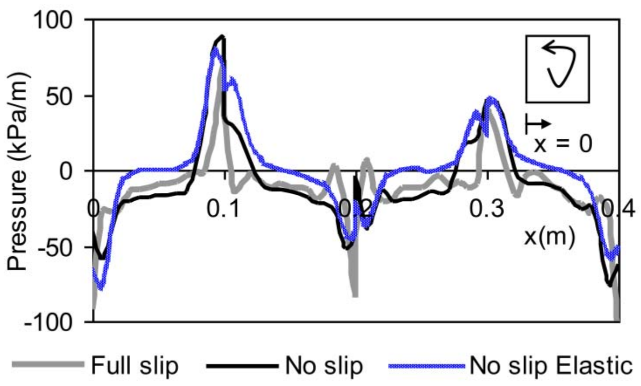

Figure 8. Dynamic earth pressure distributions around the tunnel for the time step of maximum racking distortion determined from numerical analysis; EQ8-Test 2.

4.4 Soil dynamic shear stresses

Figure 9 presents dynamic shear stress distributions computed for the time step of maximum racking distortion. Similar to the earth pressures, soil yielding affects the shear stress distribution around the tunnel. Generally, shear stresses tend to increase near the tunnel corners due to the higher earth pressures (confining pressures for the tunnel) at these locations. As expected, interface friction affects significantly the soil shear stresses distributions and magnitudes.

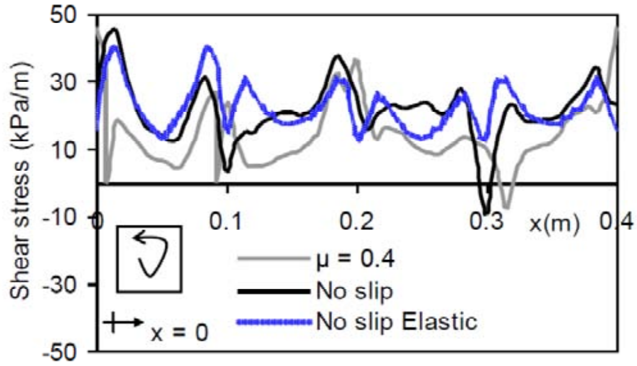

Figure 9. Soil dynamic shear stress distributions around the tunnel for the time step of maximum racking distortion determined from numerical analysis; EQ8-Test 2.

4.5 Lining dynamic bending moment

A representative comparison between recorded and computed dynamic bending moment time histories is presented in Figure 10. Generally, the numerical results are in good agreement with experimental data. Both the experimental data and the numerical predictions indicate a post-earthquake residual response, similar to that of the earth pressures. This residual response is highly affected by the tunnel's flexibility and as expected it is affecting the bending moment distributions around the tunnel (Figure 11).

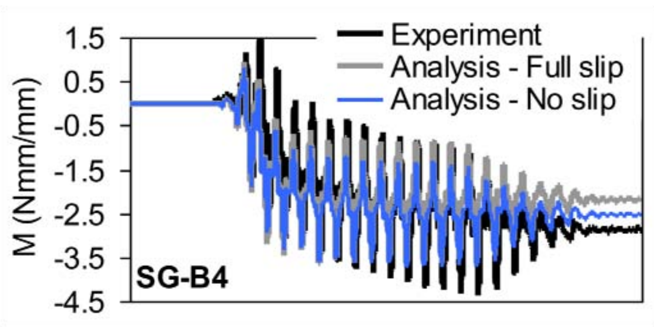

Figure 10. Dynamic bending moment at SG-B4; EQ3-Test 2.

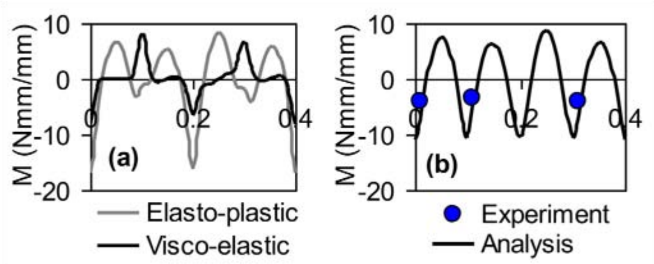

Figure 11. Dynamic bending moment distributions; (a) at the time of maximum racking distortion, (b) residual values after shaking, EQ4-Test 2.

Similar observations are made for the shallow tunnel (Test 1), with the residuals being close to those computed for the deeper tunnel.

4.6 Lining dynamic axial forces

Residual values were also recorded for the lining dynamic axial forces and were generally larger along the slabs. The effect of the mobilized friction (along the interface) on the lining axial forces is very important (Figure 12).

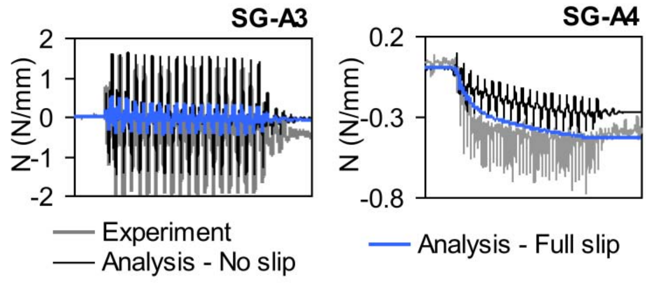

Figure 12. Dynamic axial forces time histories; EQ8-Test 2.

Similar to what was observed for the dynamic earth pressures recorded axial forces for the deeper tunnel are in better agreement with the numerical predictions assuming no-slip conditions. This can be attributed to the inward deformations of the model tunnel that are amplified by the tunnel's high flexibility. The surrounding sand is actually squeezing the tunnel leading to a more rigid soil-tunnel interface (no separation-no slip conditions). This effect is less evident for the shallower tunnel in the looser sand deposit.

It is noteworthy that both visco-elastic and elastoplastic analyses reproduce the recorded bending moment and axial force dynamic increments quite well (Figure 13). These increments are generally amplified near the tunnel corners.

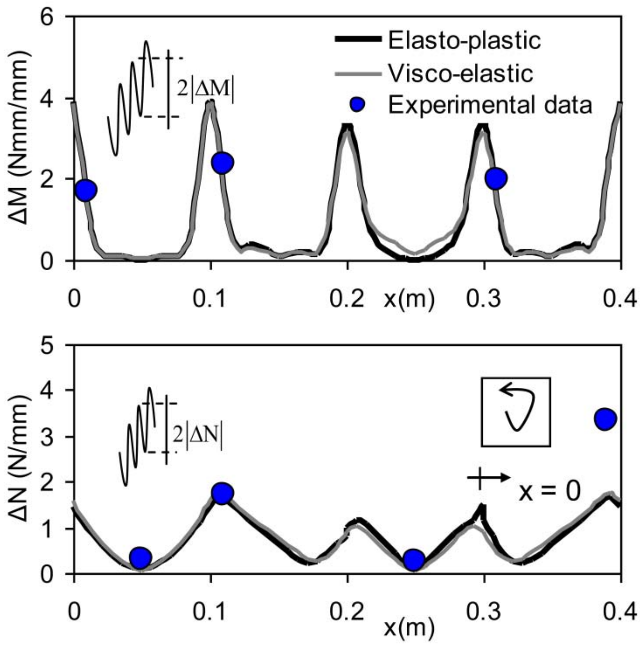

Figure 13. Dynamic bending moment increment (ΔM) along the perimeter of the tunnel for EQ4-Test 2; Dynamic axial force increment (ΔN) along the perimeter of the tunnel for EQ6-Test 2.

5 CONCLUSIONS

Summarizing, both the numerical and the experimental results revealed a rocking mode of vibration for the tunnel in addition to the racking distortion and the inward deformations of the slabs and the walls. Post-earthquake residual values were reported for both the dynamic earth pressures and the lining internal forces, mainly due to soil yielding and densification around the tunnel. These response characteristics were amplified with the tunnel's flexibility.

ACKNOWLEDGEMENT

The research leading to these experimental results has received funding from the European Community's Seventh Framework Programme [FP7/2007–2013] for access to the

Turner Beam Centrifuge, Cambridge, UK, under grant agreement no 227887 [SERIES, www.series.upatras.gr/TUNNELSEIS].

REFERENCES

ABAQUS. 2012. *Analysis user's manual-version 6.10*, Dassault Systemes, SIMULIA Inc, USA.

Hardin, B.O. & Drnevich, V.P. 1972. Shear modulus and damping in soils: design equations and curves. *Journal of Soil Mechanics and Foundations*, **98**, 667–692.

Madabhushi, S.P.G., Schofield A.N. & Lesley S. 1998. A new stored angular momentum (SAM) based earthquake actuator. *Proceedings of the international conference Centrifuge '98,* Balkema, Rotterdam, 111–116, 1998.

Pitilakis, K. & Tsinidis, G. 2014. Performance and Seismic Design of Underground Structures. *Earthquake Geotechnical Engineering Design.* Geotechnical Geological and Earthquake Engineering **28**, 279–340, Springer International Publishing, Switzerland.

Tsinidis, G., Heron, C., Pitilakis, K. & Madabhushi G. 2014. Physical modeling for the evaluation of the seismic behavior of square tunnels. *Seismic evaluation and rehabilitation of structures.* Geotechnical Geological and Earthquake Engineering **26**, 389–406, Springer International Publishing, Switzerland.

Dynamic compaction of collapsible soils – case study from a motorway project in Romania

Compactage Dynamique des Sols Pliants – Cas Réel d'après un Projet d'Autoroute en Roumanie

G. Tsitsas, V. Dimitriadi, D. Zekkos, M. Dumitru, R. Ciortan and S. Manea

ABSTRACT Dynamic compaction is a widely used ground improvement method applicable to a variety of soils including collapsible loess. The paper presents site characterization and ground improvement performance results obtained from a 22 kilometer motorway project in Constanta, Romania. High energy dynamic compaction was utilized to treat 240.000 square meters of ground to depths ranging from 6 to 8 meters in order to reduce settlements and mitigate collapse potential. The field results are compared to the results of a finite difference numerical model, developed to simulate the dynamic compaction.

1 INTRODUCTION

Dynamic compaction (DC) is one of the most widely used ground improvement technologies to densify soils in-situ and improve their properties in depth. The technique is particularly effective for moist or saturated cohesionless soils that are largely free draining as well as finer soils above the water table. This paper presents the case history of the densification of loess deposits in southeastern Romania for the construction of a major motorway. Dynamic compaction was used to improve the bearing capacity of the soil below embankments, reduce differential settlements to 25 mm every 100 m, and reduce the possibility of soil collapse. The densification scheme and site characterization results before and after improvement are presented and compared to the results of a finite difference numerical model.

2 PROJECT DESCRIPTION

The motorway project involved the design and construction of 22 km of highway including 26 bridges and 5 interchanges as well as 11-m high embankments between Ovidiu and Agigea (Fig. 1).

Soil profile consists of loess deposits to a depth of 12 m with the top 6 m considered prone to collapse. Below these deposits is a red clay with limestone concretions and thickness of 16 to 18 m which tops degraded limestone. Groundwater level was measured below 12 m.

Figure 1. Location of the site

2.1 Characterization of collapsible loess soils

Geotechnical investigation included SPT, CPT and laboratory tests to characterize the subsurface conditions. The loess deposits in the top 12 m consist of alternating layers of clayey silt, clay and silty clay. Collapsible loess deposits are known for porosity greater than 40%, low Plasticity Index and unit weight, irreversible changes of their internal structure upon contact with water calculated by the additional settlement index (i_{m300}). This index is determined in the laboratory by double odometer tests. Loess is classified as collapsible when i_{m300} exceeds 2%.

Figure 2 illustrates the soil profile at a project location. The average dry density ρ_d, at the top 10 m, is equal to 1.57 to 1.69 g/cm^3, natural moisture content is about 20%, and the void ratio is approximately 0.61. Fines significantly exceed 50% and two Atterberg test results indicate a Liquid Limit (LL) of 37 and Plasticity Index (PI) of 24.

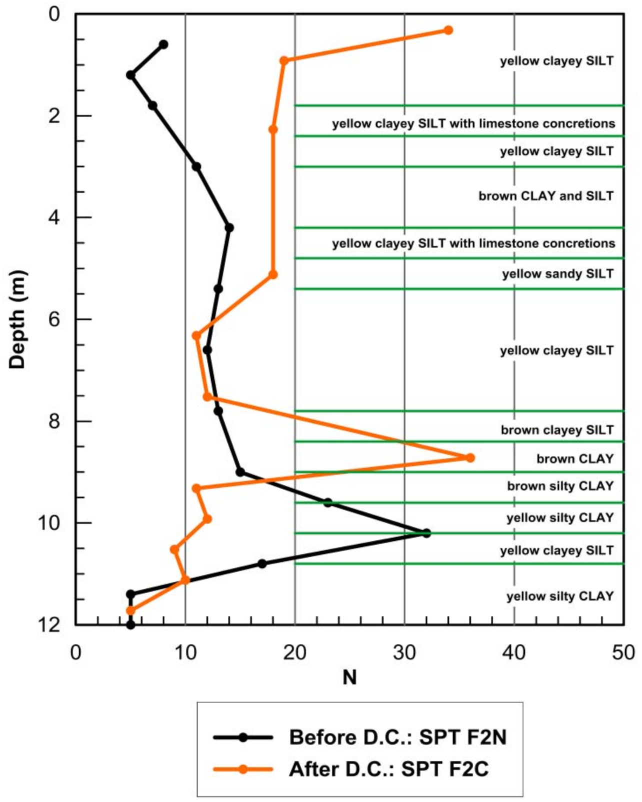

Figure 2. SPT profile in the study area before and after Dynamic compaction at km 11+750 to km 12+260.

CPT tests were conducted in 15 locations prior to as well as after ground improvement took place. The mean (μ) and variance (μ±σ) in cone penetration tip resistance with depth, before (CPT 1-15) and after dynamic compaction (CPT 1A – 15A) are summarized in Figure 3. Mean CPT tip resistance values, were used in deriving the soil properties for the baseline and parametric numerical analyses. Of interest is also the coefficient of variation (C.o.V.), defined as the ratio of standard deviation (σ) to mean and is shown in Figure 4. The C.o.V. values indicate fairly uniform site conditions, with an increase in variability at a depth of approximately 8 m and deeper. The CPT data were used to estimate constrained modulus M and, for an assumed Poisson's ratio of 0.25, to calculate Young's modulus E, Bulk modulus B and Shear modulus G. Shear strength parameters were also derived on the basis of the CPT, SPT, and laboratory shear data. Average soil properties are summarized in Table 1.

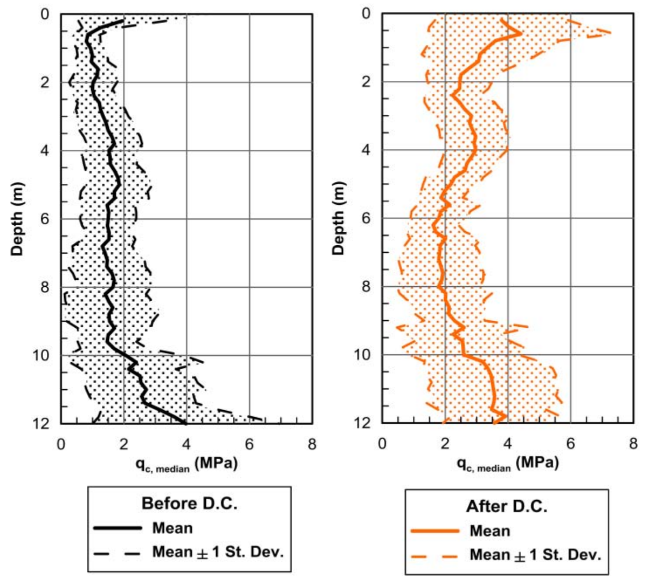

Figure 3. Mean CPT values with depth before and after Dynamic compaction.

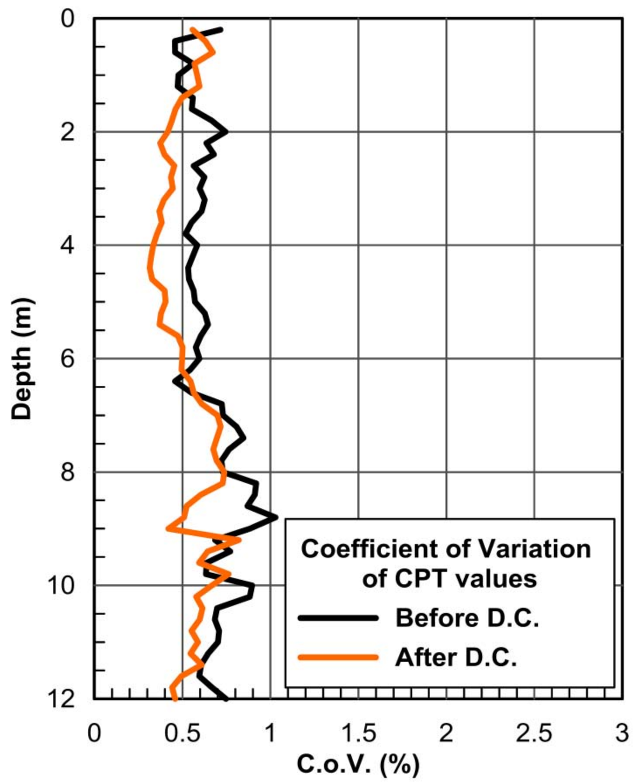

Figure 4. Coefficient of variation (C.o.V.) of tip resistance before and after soil improvement.

Table 1. Stiffness properties as estimated before and after Dynamic compaction.

	Before D.C.	After D.C.
E (kPa)	7,000	11,000
B (kPa)	4,700	7,365
G (kPa)	2,800	4,420
φ (deg)	17	30
c (kPa)	15	15
ψ (deg)	0	0

2.2 Implementation of Dynamic Compaction

Three-phase dynamic compaction was carried out using an 18 metric tons steel pounder with a surface area of 3.8 m2. The compaction grid varied throughout the site from 6×6 m to 7×7 m, based on results obtained from pilot tests. Phase I consisted of a high energy input based on a densification grid, followed by Phase II in intermediate points. Phase III was the "ironing" phase that involved lower energy input and aimed at densifying the shallower, disturbed, soil layers.

The number of drops, reported in Table 2, was determined based on pilot dynamic compaction tests paired with in situ and laboratory measurements executed prior to the final design of the improvement scheme. During the pilot tests, the optimum number of drops was selected, based on the observed ground response that involved heave and/or settlement measurements and the assessed depth of improvement.

Energy input (pounder mass, drop height and number of drops) for each Phase is shown in Table 2. Applied energy during the ironing phase was calculated using a grid spacing equal to the area of the pounder. Energy input is expressed in terms of Applied Energy, given by the following expression:

$$Applied\_Energy = \frac{WHN(P)}{grid\_spacing} \tag{1}$$

where W = mass of pounder (metric tons or Mg), H = drop height (m), N = number of drops, (P) = number of passes, grid spacing (in m^2).

Table 2. Pounder mass, drop height, and number of drops.

	M metric tons	H m	# of drops	AE ton.m/m²
Phase I	18	23	12/14	101.4/118.3
Phase II	18	23	12/14	101.4/118.3
Phase III (ironing)	18/14	20/14.5	2/4	189.5/169.2

2.3 Assessment of Dynamic Compaction

The impact of densification was assessed on the basis of the evolution of crater depths during DC, as well as pre- and post-improvement CPT, SPT and laboratory results. As shown in Figure 5, the evolution of crater depth varied, but overall reached 2.0 to 2.7 m. SPT and CPT results prior to and after improvement are shown in Figures 2 and 3 respectively. On the basis of the SPT and CPT results, the depth of improvement is 6 to 8 m. For the pounder mass and drop height used in the project, the empirical site coefficient *n* is 0.3 to 0.4, which is consistent with other dynamic compaction projects in fine silty soils (Lukas, 1995).

3 NUMERICAL MODELING

Dynamic compaction was numerically simulated with a 2-D axi-symmetric model using the Finite Difference Code FLAC (Itasca, 2005). The modeling space is illustrated in Figure 6. In the vicinity of the pounder, 0.1×0.1 m zones are defined. Zone size is increased with depth and horizontal distance from the pounder up to 0.2×0.2 m at the edges of the configuration.

In the stage of geostatic stress generation, horizontal displacements were constrained along the lateral boundaries, and both vertical and horizontal movement was restrained along the bottom boundaries. During dynamic loading, vertical boundaries were allowed to move freely along the vertical direction under the application of the loading sequence.

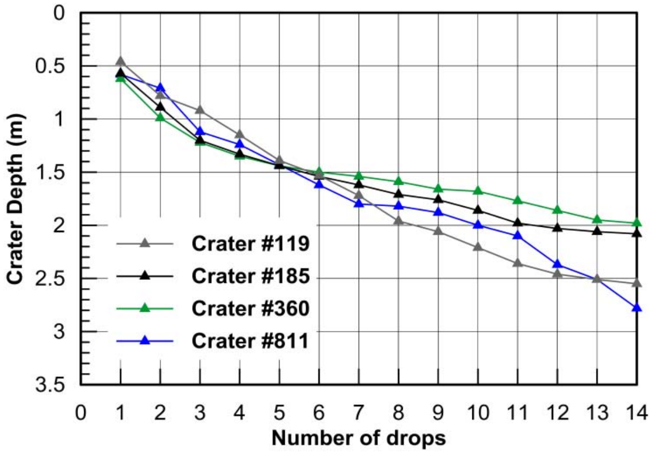

Figure 5. Evolution of pounder penetration with number of drops.

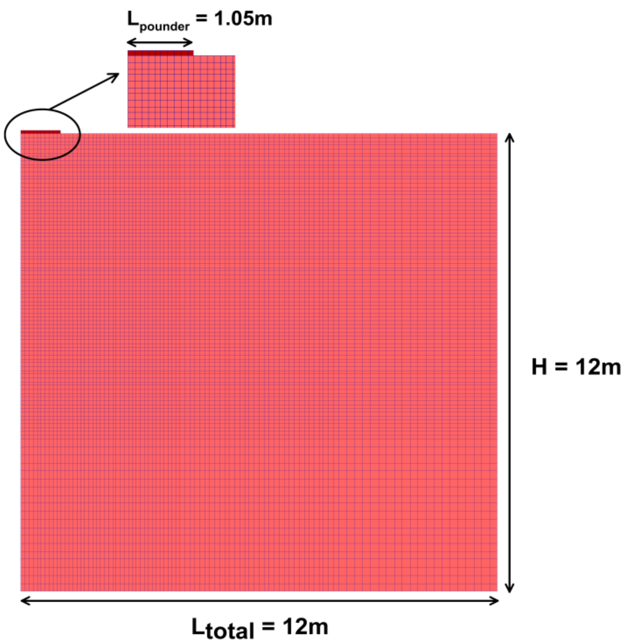

Figure 6. Mesh discretization with the pounder simulated as a rigid steel body.

The pounder was simulated as an elastic rigid body on the top of the grid, (Figure 6), with a width equal to 1.05 m, upon which a velocity (loading) time history was applied. The pounder was assigned properties of steel (mass density ρ=7.85Mg/m^3, Es=200,000kPa, v=0.2).

The loading sequence was simulated with a series of triangular pulses of period T with a maximum impact velocity imposed upon the rigid pounder. Recurrent pulses were separated by intervals of zero loading. Maximum impact velocity was initially computed based on the free fall equation. Parametric analyses were conducted for a combination of velocity amplitudes and periods of triangular loading. The baseline analyses were performed for 20 tamper drops of period T = 0.1 sec, separated by a break time of 1 sec, and an amplitude of 2.12 m/sec, as shown in Figure 7.

Soil response was simulated using a Mohr – Coulomb elasto-plastic constitutive model. For this constitutive model the following parameters are required: (i) bulk modulus (kPa), (ii) shear modulus (kPa), (iii) friction angle (deg), (iv) cohesion (kPa) and (v) dilatancy angle, also summarized in Table 1. Dilatancy angle was considered zero throughout the numerical simulation. The soil properties before dynamic compaction were used in the analyses. Based on the site characterization results, it was considered reasonable to use uniform properties throughout the soil profile (total thickness of 12 m). Local, nonviscous damping of 5% was assumed for the baseline case. Parametric analyses were also conducted to evaluate the sensitivity of the results to the assumed damping value, which was found to be significant.

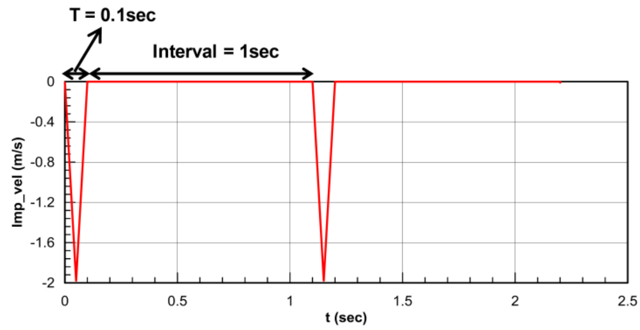

Figure 7. Applied loading sequence.

4 COMPARISONS

4.1 Evolution of ground settlements with number of drops

As shown in Figure 8, the permanent displacement time history is generally similar in magnitude to the measured crater depth time history of crater #360 located in the vicinity of the SPT test location (F2N location in Figure 2). The most significant difference is in the shape of the relationship. The settlement time history from the model is linear, as opposed to the hyperbolic relationship observed in the field data. This difference is due to the manner by which the loading input is simulated, the high energy input and the lack of soil property updating during densification. The crater depth (or settlement) at around 20 drops is, however, similar.

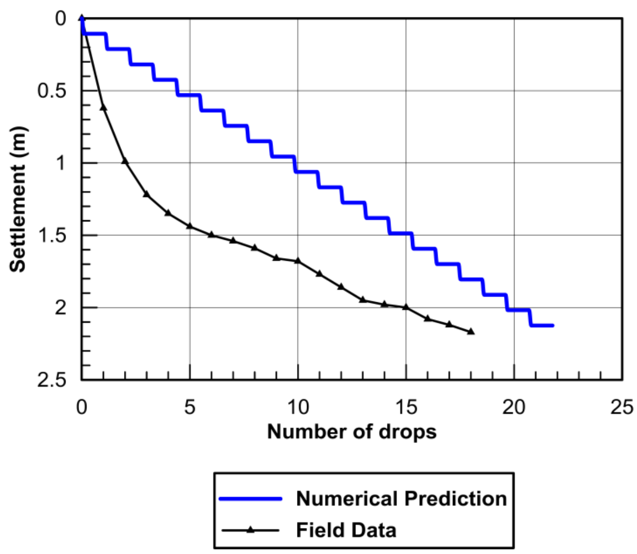

Figure 8. Evolution of ground settlements with number of drops.

4.2 Evolution of shear and volumetric strains with number of drops

The evolution of shear and volumetric strains with increasing number of drops is qualitatively similar to the expected strain contours during dynamic compaction. A strain bulb is observed that extends primarily with depth, but also laterally.

Shear strain evolution illustrated in Figure 9, indicates the occurrence of excessive shearing in the vicinity of the impact zone. Note that shear strain contours are shown up to a maximum shear strain of 10%. Numerically calculated strains that exceed 10% are shown as white-out areas. Shear strains (1% or higher) appear to be extending up to a depth of about 5 m and laterally reaching up to 3 m.

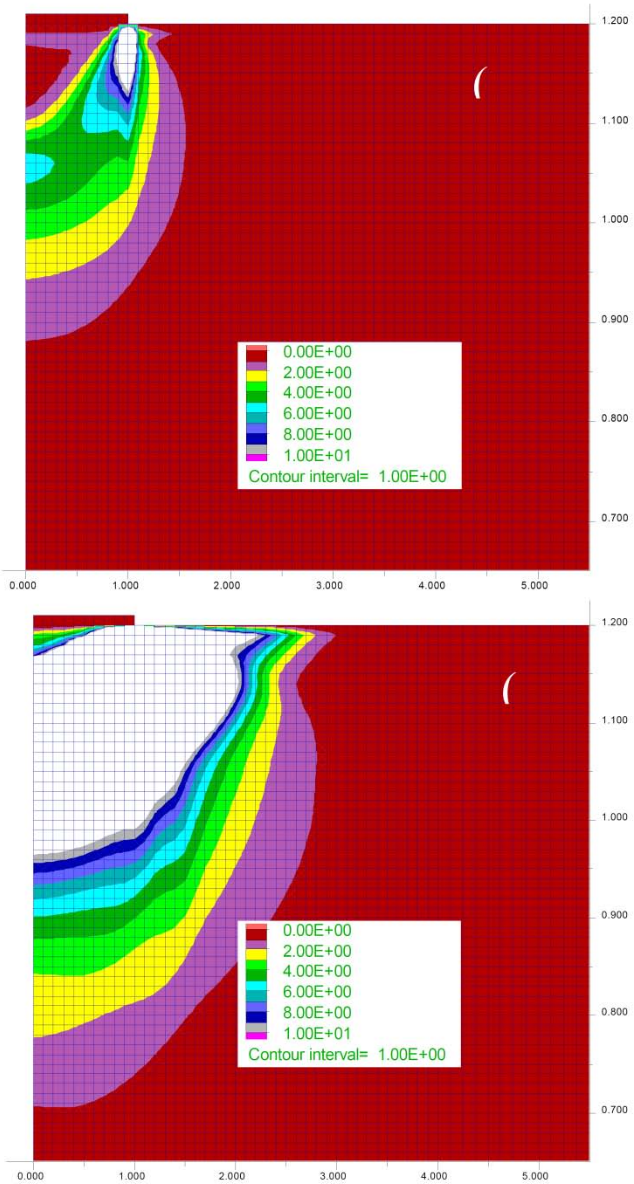

Figure 9. Evolution of shear strain contours (%) around the pounder after (a) 1st drop, and (b) 10th drop.

Similar results are observed in terms of the volumetric strain contours, presented in Figure 10. Compressive strains are observed in the soil below the tamper, whereas, heave (i.e., negative volumetric strains) is developing at the edge of the tamper already from the first drop. The area with significant compressive strains has a width that is almost twice the radius of the tamper, that is approximately 2 m, and depth in the order of 4 m.

Depth of improvement is practically defined as the depth at which no change in penetration resistance (and by extension, no change in the state of soil) is observed prior to and after DC. In the numerical analyses, the depth of improvement is evaluated based on the shearing and volumetric strain distribution, given that a change in strain within a soil should result in a change in soil properties. In this study, a volumetric or shear strain threshold of 1% was used as the criterion to define the depth of improvement. The depth of improvement, in that case, varies from 4-6 m, which is comparable to the 7 m that would be predicted for fine soils, and the 6 to 8 m measured at the site.

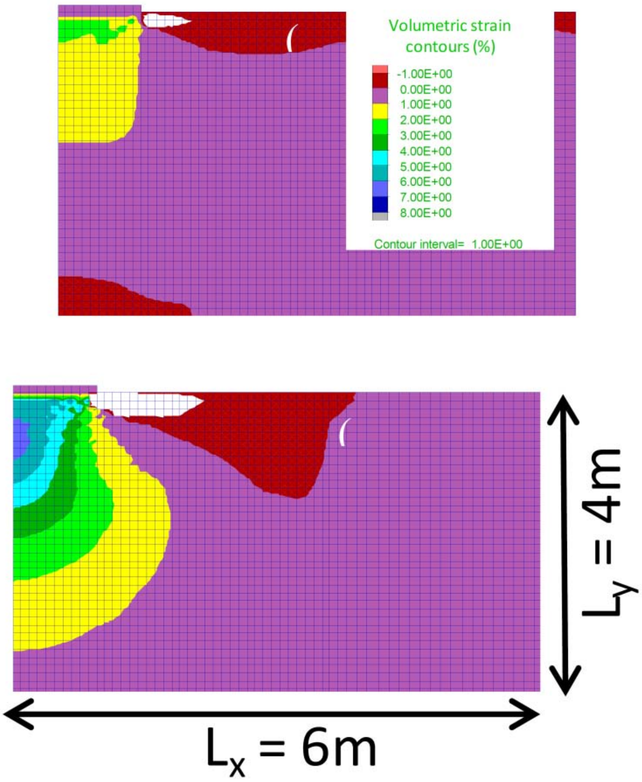

Figure 10. Evolution of volumetric strain contours around the pounder after (a) 1st drop, and (b) 10th drop.

Additional parametric analyses were conducted to evaluate the sensitivity of the results to the assumed material properties. It was found that a reduction in soil stiffness increases the volumetric strains, whereas a higher friction angle results in a larger volumetric strain bulb. In both cases, shear strains extend deeper, indicating higher "depths of improvement." Although, the properties of the soil model are not updated with increasing densification, the parametric analyses with increased shear strength indicate that the "depth of improvement" may reach approximately 6.5 m.

The reasons for the smaller depth of improvement predicted by the model are most likely associated with the definition used to assess the numerical results as well as model limitations that include: (a) modeling of the impact of the tamper on the ground with a velocity pulse with certain amplitude and frequency characteristics; (b) simplifications and limitations of the constitutive elastoplastic Mohr-Coulomb model, e.g., the use of a constant modulus in the elastic region, and the absence of material property updating during densification.

5 CONCLUSIONS

A dynamic compaction project executed for the construction of a motorway in southeastern Romania to reduce the collapsible characteristics of loess deposits is presented. The results of the ground improvement program are compared to a numerical model that was employed for simulation using the available site characterization data. The simplified model was able, in a qualitative sense, to predict the impact of the energy (velocity) input on the loess deposits. The shape of the volumetric and shear strain contours is generally reasonable. The model indicates significant changes in the soil (in terms of volume and shear) below the tamper for a prescribed energy input. The results of the analyses were sensitive to the values of the model input parameters; hence, particular attention is required in their selection. Overall, for the definition of “depth of improvement” used in this study, the simulations indicated that it was about 4 to 6 m for the baseline case, which is comparable to a depth of improvement of 7 m using the dynamic compaction equation and the 6 to 8 m measured in the field.

ACKNOWLEDGEMENT

We would like to express our appreciation to Mr. Jose Martinez Salazar, representative of JV FCC/ASTALDI for his support during the course of this project.

REFERENCES

Itasca. 2005. FLAC: Fast Lagrangian Analysis of Continua, Online Manual.

Manea, S, Ciortan, R, Tsitsas, G, Dumitru, M. 2012. “Verification of improvement for collapsible soils treated with High Energy Dynamic Compaction”. Proceedings of the 12th National Conference in Geotechnical and Foundation engineering in Iasi, Romania

Lukas, R. 1995. Geotechnical Engineering Circular 1: Dynamic Compaction, FHWA report No SA-95-037.

Analyzing the reliability of predictive models for earthquake-induced displacements of slopes

Analyse de la fiabilité des modèles de prédiction des déplacements sismiques des pentes

S.D. Fotopoulou and K.D. Pitilakis

ABSTRACT The aim of the paper is twofold: first, to evaluate earthquake-induced slope displacements using numerical dynamic analysis considering different real acceleration time histories as input motion and varying the resistance and the compliance of the sliding mass; then, to assess the reliability of the numerical approach by comparing the numerically calculated seismically induced slope displacements with predictions using available Newmark-type empirical models. In general the Newmark-type empirical models predict comparable displacements, at least in the order of magnitude, with the numerical analysis. The final goal of this systemic analysis is to pave the road to a more reliable analytical model to predict co-seismic slope displacements, taking into account the most influencing parameters of the problem and treating better the uncertainties involved.

1 INTRODUCTION

It has been shown that the magnitude of seismically induced slope displacements presents good correlations with observations of seismic performance of slopes (e.g., Jibson et al. 2000), and thus it is considered a crucial parameter in seismic design and hazard assessment. Typically, two different approaches of increased complexity are proposed to assess permanent ground displacements in case of seismically triggered slides: Newmark-type displacement methods and advanced stress- strain dynamic methods. Newmark-type methods are based on the sliding block assumption first proposed by Newmark (1965) providing an index of the dynamic slope performance. Advanced stress-deformation analyses based on continuum mechanics or discontinuum formulations are more computationally expensive and may be cost-ineffective for conventional design purposes. However, they are becoming attractive for complex critical projects providing approximate solutions to problems which otherwise cannot be solved by simplified methods e.g. the complex geometry including topographic and basin effects, material anisotropy and non-linear behavior under seismic loading, in situ stresses, pore water pressure built-up, progressive failure of slopes due to strain localization.

The aim of this study is two-fold: (a) to assess earthquake induced slope displacements using numerical dynamic analysis by performing a comprehensive parametric study for different slope geometries, soil properties and input motions and (b) to compare the numerical results in terms of co-seismic permanent slope displacements with available and widely used empirical displacement based models.

2 NUMERICAL PARAMETRIC ANALYSIS

Two dimensional (2D) fully non-linear numerical analyses are performed for idealized step-like slope configurations applying the finite difference code FLAC2D (Itasca, 2011) considering different real acceleration time histories as input motion and varying the resistance and the compliance of the sliding mass (characterized by the yield coefficient, k_y, and the fundamental period of the sliding mass, T_s, respectively). In particular, 12 typical slope soil models are analyzed with varying geometrical characteristics, material properties of the surface layer as well as strength and stiffness of the potential sliding surface. Figure 1 describes the layout of the problem under study whereas Table 1 summarizes the analyzed models.

The discretization allows for a maximum frequency of at least 10Hz to propagate through the grid without distortion. A finer discretization is adopted in the slope area, whereas towards the lateral boundaries of the model the mesh is coarser. Free field absorbing boundaries are applied along the lateral boundaries whereas quiet boundaries are applied along the bottom of the dynamic model to minimize the effect of trapped energy and artificially reflected waves. The soil materials are modeled using an elastoplastic constitutive model with the Mohr-Coulomb failure criterion (shear yield) with tension cutoff (tension yield function), assuming a non-associated flow rule for shear failure and an associated rule for tension failure.

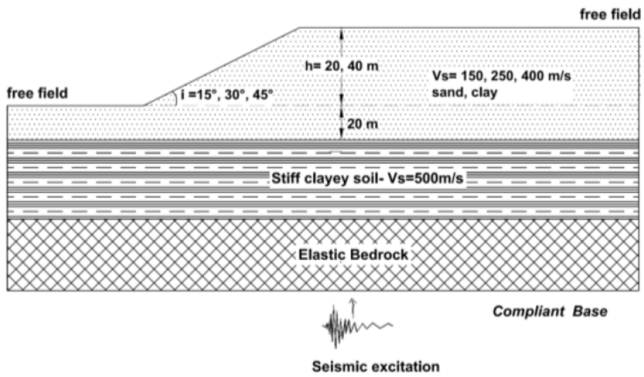

Figure 1. Layout of the problem under study.

Table 1. Analyzed models

k_y	h (m)	i (°)	Soil properties (surface layer)	T_s (s)	Model
0.05	40	45	Vs=400m/s, c=5KPa, φ=44°	0.050	m5
	40	45	Vs=400m/s, c=50KPa, φ=25°	0.300	m6
0.1	20	45	Vs=400m/s, c=5KPa, φ=44°	0.040	m3
	20	45	Vs=400m/s, c=30KPa, φ=25°	0.100	m4
0.15	20	30	Vs=250m/s, c=0.5KPa, φ=37°	0.032	m1
	20	30	Vs=250m/s, c=15KPa, φ=25°	0.130	m2
	40	30	Vs=400m/s, c=30KPa, φ=25°	0.150	m11
0.2	20	15	Vs=150m/s, c=15KPa, φ=18°	0.373	m12
	40	15	Vs=150m/s, c=30KPa, φ=18°	0.690	m7
0.25	40	15	Vs=150m/s, c=0.5KPa, φ=27°	0.130	m8
0.3	40	30	Vs=400m/s, c=5KPa, φ=44°	0.040	m9
	20	15	Vs=250m/s, c=15KPa, φ=24°	0.224	m10

A small amount of mass and stiffness - proportional Rayleigh damping (3% for the soil materials and 0.5% for the elastic bedrock) is also assigned to account for the energy dissipation during the elastic part of the cyclic response. Generic soil properties are considered based on the available literature and engineering judgment. These are selected to vary for the surface layer (see Table 1) while they are kept constant for the intermediate clayed layer (V_s=500m/s, c=50KPa, φ=27°) and the elastic bedrock (V_s=850m/s).

The initial fundamental period of the sliding mass (T_s) is estimated using the simplified expression: $T_s = 4H/V_s$, where H is the depth and Vs is the shear wave velocity of the potential sliding mass. The depth of the sliding surface as well as the horizontal yield coefficient, k_y, are evaluated by means of pseudostatic slope stability analyses utilizing the Bishop's simplified method for the critical sliding surface. It's worth noticing that a fixed value of k_y is calculated assuming that no significant strength loss is anticipated in the slope soil material (e.g. no liquefaction or strain softening).

The dynamic input motion consists of SV waves vertically propagating from the base. The seismic input applied along the base of the dynamic model consists of a set of 40 real acceleration time histories recorded on rock outcrop or very stiff soil (soil classes A and B according to EC8) and derived from the SHARE database (Seismic Hazard Harmonization in

Europe, www.share-eu.org). The input accelerograms represent motions from moment magnitudes, Mw, varying from 5 to 7.62 recorded at epicentral distances, R, between 3.4 to 71.4 km with shear wave velocity at the first 30m, $V_{s,30}$, between 602 to 2016 m/s. The input peak ground acceleration (PGA) values range from 0.065g to 0.91g, the peak ground velocity (PGV) values range from 3.1cm/s to 78.5cm/s and the mean period T_m ranges from 0.16s to 1.14s. To obtain the appropriate input motion at the base of the FLAC2D model, the selected time histories are first subjected to baseline correction and filtering (f_1=0.25Hz, f_2=10 Hz) to assure accurate representation of wave transmission through the model. Moreover, due to the compliant base used in the model, the appropriate input excitation corresponds to the upward propagating wave train that is taken as one-half the target outcrop motion.

Prior to the dynamic simulations, a static analysis is carried out to establish the initial effective stress field throughout the model. It is noticed that only the cases that result to nonzero displacement (≥0.001m) due to seismic loading are addressed. Thus, the number of dynamic analyses performed for each model depends on the considered k_y value in relation to the PGA values of the selected input motions. For instance, 40 dynamic analyses were carried out for model m6 (k_y=0.05, see Table 1) while only 13 analyses were possible for model m10 (k_y=0.3, see Table 1).

3 COMPARISON OF THE NUMERICAL APPROACH WITH EMPIRICAL METHODS

The dynamic analysis results are extracted in terms of permanent horizontal displacements within the sliding mass for the idealized step-like slopes, characterized by different flexibility and resistance of the potential sliding surface. Figure 2 presents the distribution of the computed numerical horizontal displacements that vary from very small values (smaller than 0.01m) to large ones (>1m). In total, 285 nonzero permanent horizontal displacements are calculated for all considered analysis cases.

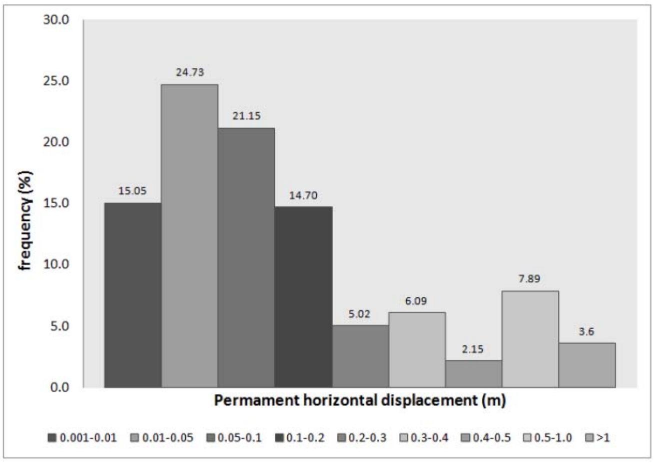

Figure 2. Histogram of the computed numerical horizontal displacements (for all models, N=285)

These displacements are then compared with the slope displacement (D) predicted with four empirical models commonly used in earthquake engineering practice, namely the conventional analytical Newmark rigid block model (Newmark 1965), Jibson (2007) rigid block model, Rathje and Antonakos (2011) decoupled sliding block model and Bray and Travasarou (2007) coupled stick-slip sliding block model.

The Newmark conventional analytical rigid block method is used to predict average slope displacements obtained by integrating twice with respect to time the parts of an earthquake acceleration-time history that exceed the critical or yield acceleration, a_c ($k_y \cdot g$) (i.e. threshold acceleration required to overcome shear soil resistance and initiate sliding). The second approach is a simplified rigid block model proposed by Jibson (2007), which predicts slope displacement as a function as Arias intensity (I_a) and critical acceleration ratio (a_c/PGA). This method was selected considering that Arias intensity was found to be the most efficient intensity measure for stiff, weak slopes (Travasarou 2003). The third method is a two parameter vector (PGA, PGV) model proposed by Rathje and Antonakos (2011). This model is often recommended for use in practice due to its ability to significantly reduce the variability in the displacement prediction (Saygili and Rathje 2008). For flexible sliding, k_{max} (e.g. peak value of the average acceleration time history within the sliding mass) is used in lieu of PGA and $k\text{–}vel_{max}$ (e.g. peak value of the k-vel time history provided by numerical integration of the k-time history) is used to replace PGV. The last one is the Bray and Travasarou (2007) model. In this model cumulative displacements are calculated using the nonlinear fully coupled stick-slip deformable sliding block model proposed by Rathje and Bray (2000) to capture the dynamic response of the sliding mass. They use a single intensity parameter to characterize the equivalent seismic loading on the sliding mass, i.e. the ground motion's spectral acceleration Sa at a degraded period equal to $1.5T_s$, which was found to be the optimal one in terms of efficiency and sufficiency (Bray 2007).

It is noted that Newmark method is an analytical rigid block approach whereas Jibson (2007), Rathje and Antonakos (2011) and Bray and Travasarou (2007) models are essentially regression models of the analytical form of the rigid-block, decoupled and coupled methods respectively. As such, Newmark analytical method uses the entire time history to characterize the seismic loading as opposed to the simplified methods of Jibson (2007), Bray and Travasarou (2007) and Rathje and Antonakos (2011) that use one (I_a, S_a(1.5 T_s)) and two (PGA, PGV) intensity parameters respectively. In this way, uncertainties (and potential biases) associated to the selection of the ground motion intensity parameters are limited in the Newmark conventional analytical approach. The herein models yield mean (Jibson 2007) or median (Rathje and Antonakos 2011, Bray and Travasarou 2007) values of seismic slope displacement when the standard deviation is ignored. These median or mean displacement values are used in this study for the comparison with the herein calculated numerical displacements. This comparison aspires not only to enhance the reliability of the numerical analysis results but also to assess the relative accuracy of the different displacement based approaches with respect to the present a priori more advanced numerical approach. It is noted that Newmark-type methods capture the part of seismically induced displacement attributed to the deviatoric induced deformation while the corresponding part attributed to the volumetric compression is not account for. This displacement due to deviatoric deformation is largely horizontal (Bray and Travasarou 2007) justifying the use of the horizontal (instead of the vector) numerical displacement for the comparison.

To derive the appropriate inputs for the Newmark-type methods that include the effect of soil conditions, and to allow a direct comparison with the numerical results, we computed the acceleration time histories and the corresponding intensity parameters at the depth of the sliding surface through a one-dimensional (1D) non-linear site response analysis using FLAC 2D considering the same soil properties as in the 2D dynamic analysis (Figure 3). In particular, as for 2D analysis, 12 1D soil models are constructed that are then subjected to the same recorded earthquake motions described previously. It is noticed that the 1D soil profile is located at the section that approximately corresponds to the maximum slide mass thickness H of the potential sliding surface (Section A in Figure 3). The maximum slide mass thickness H (or otherwise the maximum depth of the sliding surface), which is calculated by means of pseudostatic slope stability analysis for the critical sliding surface, varies between 2 and 26 m for the different analyzed slope cases.

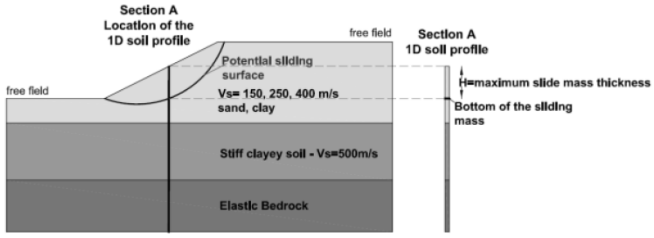

Figure 3. Schematic view of the model used to perform the 1D dynamic analyses.

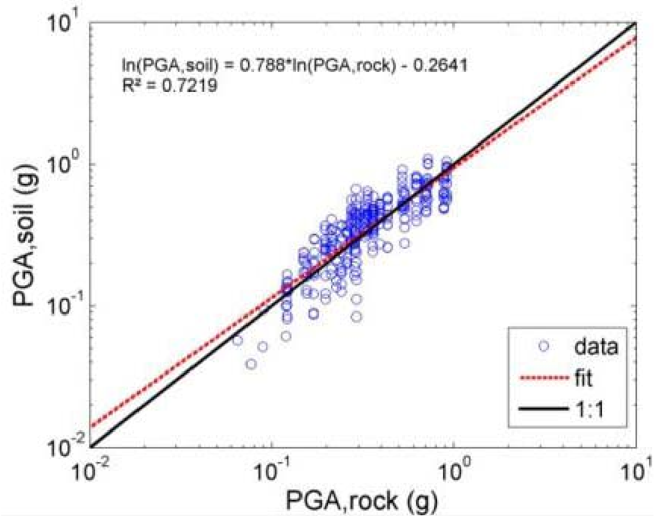

Figure 4. Variation of PGA of the input accelerograms with the corresponding calculated PGA at the depth of the sliding surface

Figure 4 presents representative correlations between the PGA of the input motions at the rock basement and the corresponding PGA at the depth of the sliding surface calculated via 1D dynamic analysis. A considerable variability with respect to the considered site conditions (soil or rock) is shown. A linear regression fit of the logarithms of the PGA,rock – PGA,soil which minimizes the regression also be derived for the other IMs. Such log-linear relationships could be used in practice to calculate the required IMs for soil conditions (e.g. at the bottom of the potential sliding mass) given the corresponding IMs at the rock outcrop. The latter parameters are normally more easily obtained from a seismic hazard analysis.

Figure 5 shows a direct comparison between analytical Newmark's, Jibson (2007) Bray and Travasarou (2007) and Rathje and Antonakos (2011) displacements with the horizontal displacements calculated from the 2D dynamic numerical analyses. It is observed that numerical displacements generally are not inconsistent with the predicted Newmark-type displacements enhancing the reliability and robustness of the dynamic analysis results. However, a relatively large dispersion in the displacement estimation is shown. This dispersion is also displayed in Figure 6, which presents the cumulative distribution of the *difference* (Difference (m) = $D_{numerical}$-$D_{empirical}$) (Figure 6, top) and the *relative difference*

$$(\text{Relative difference }(\%) = \frac{D_{numerical} - D_{empirical}}{D_{numerical}} \cdot 100\%)$$

(Figure 6, bottom) respectively between the numerical and empirical slope displacements for each of the empirical sliding block model. It is noted that for positive values of the

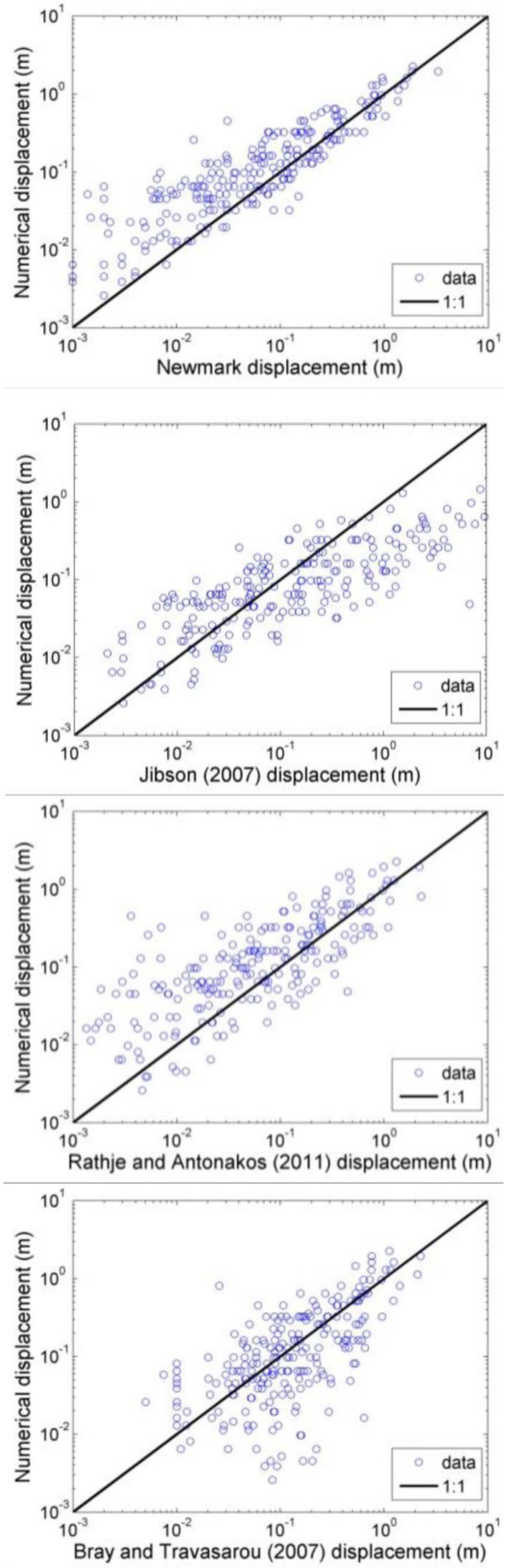

Figure 5. Numerically versus empirically calculated displacements

difference and *relative difference* the empirical methods underpredict the displacements derived from the numerical analysis and vice versa.

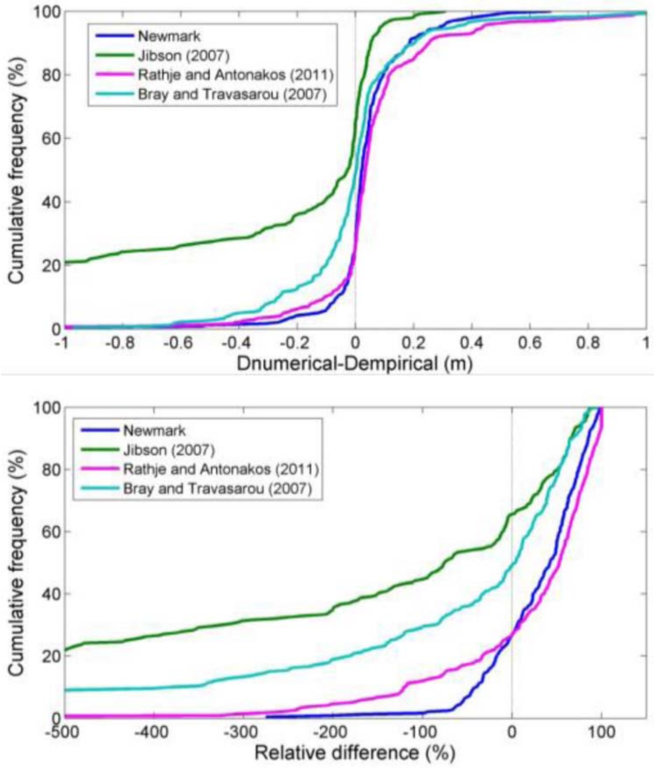

Figure 6. Cumulative distribution of the *difference* (top) and the *Relative difference* (%) (bottom) between numerical and empirical slope displacements for each of the empirical sliding block model.

By examining the cumulative distribution functions we see that Newmark analytical rigid block model and Rathje and Antonakos (2011) decoupled model generally tend to predict smaller displacements compared to the numerically derived ones. In particular, positive values of the *difference* and *relative difference* in the displacement prediction are presented for cumulative frequencies from around 20÷30% to 100%. On the other hand, Bray and Travasarou (2007) coupled model may either overpredict or underpredict the numerical displacements yielding positive values of the *difference* and *relative difference* in the displacement prediction for cumulative frequencies from around 49% to 100%.

This is in line with the inherent coupled stick-slip assumption adopted in the method that offers a conceptual improvement over the rigid block and decoupled approaches for modeling the physical mechanism of earthquake-induced slope displacement.

Finally, Jibson (2007) simplified rigid block model tends to predict larger displacements compared the numerically calculated ones dominated by negative predictions of the *difference* and *relative difference* for cumulative frequencies up to 65%. The latter model is also associated with a very large dispersion in the median displacement estimation with respect to the numerical analysis compared to the former ones. This dispersion is obvious in both the cumulative distribution of the *difference* and *relative difference* diagrams resulting to *differences* and *relative differences* greater than -500% for cumulative frequencies up to - 1m and 20% respectively. This observation is in accordance with the findings of previous researchers (e.g. Saygili and Rathje 2008) confirming the author's recommendation regarding the avoidance of using his regression equations for site-specific applications where accurate estimates of displacement are required for design purposes.

4 CONCLUSIONS

Within the framework of this study, earthquake induced slope displacements were calculated using an advanced numerical parametric analysis considering different slope geometries, material properties and input motions. The computed numerical displacements were compared with some of the most widely used empirical Newmark-type displacement procedures, namely the conventional analytical Newmark rigid block model (Newmark 1965), Jibson (2007) rigid block model, Rathje and Antonakos (2011) decoupled sliding block model and Bray and Travasarou (2007) coupled stick-slip sliding block model. Relatively good correlations were observed enhancing the reliability of the numerical analysis results. However, a large dispersion in the displacement estimation is shown. Generally, it is seen that the simplified empirical models displayed greater variability with respect to the numerical analysis compared to the analytical Newmark method. The results highlight the need for the development of a more reliable analytical model to predict co-seismic slope displacements, taking into account the most influencing parameters of the problem and treating more rigorously the uncertainties involved.

REFERENCES

Bray, J.D. & Travasarou, T. 2007. Simplified procedure for estimating earthquake-induced deviatoric slope displacements*, Journal of Geotechnical and Geoenvironmental Engineering ASCE* **133**(4), 381-392.

Bray, J.D. 2007. *Simplified seismic slope displacement procedures. Earthquake Geotechnical Engineering*. K. D. Pitilakis, Editor, 2007 Springer.

Itasca Consulting Group 2011. *Inc. FLAC (Fast Lagrangian Analysis of Continua), ver. 7.0*. Itasca Consulting Group, Inc., Minneapolis.

Jibson, R.W. 2007. Regression models for estimating co seismic landslide displacement, *Engineering Geology* **91**, 209–218.

Jibson, R.W. Harp, E.L. & Michael, J.A. 2000. A method for producing digital probabilistic seismic landslide hazard maps, *Engineering Geology* **58**, 271–289.

Newmark, N.M. 1965. Effects of earthquakes on dams and embankments, *Geotechnique* **15** (2), 139–159.

Rathje, E.M. & Antonakos, G. 2011. A unified model for predicting earthquake-induced sliding displacements of rigid and flexible slopes, *Engineering Geology* **122**(1-2), 51-60.

Rathje, E.M. & Bray, J.D. 2000. Nonlinear coupled seismic sliding analysis of earth structures, *Journal of Geotechnical and Geoenvironmental Engineering ASCE* **126**(11), 1002–1014.

Saygili, G. & Rathje, E.M. 2008. Empirical Predictive Models for Earthquake-Induced Sliding Displacements of Slopes, *Journal of Geotechnical and Geoenvironmental Engineering* **134**(6),790-803.

Travasarou, T. 2003. Optimal ground motion intensity measures for probabilistic assessment of seismic slope displacements. Ph.D. Dissertation, U.C. Berkeley.

Pile response to lateral spreads: analysis of ultimate soil pressures

Réponse d'un pieu à l'écoulement lateral: Analyse des pressions de sol ultimes

Y.K. Chaloulos, G.D. Bouckovalas and D.K. Karamitros

ABSTRACT Recent experimental results suggest that available methods for the design of piles under liquefaction-induced lateral spreading may underestimate soil pressures and lead to un-conservative solutions. Due to this evidence, the kinematic interaction between single piles and liquefied ground has been thoroughly examined by means of 3-D numerical analyses and new empirical relations are established which take into account the dilative soil response at the upper part of the pile and the associated increase of pile reaction. Example application of the new relations shows that the aforementioned effect becomes important for liquefiable soils with relatively low permeability (e.g. fine, silty sands).

1 INTRODUCTION

Pile damage due to soil liquefaction and lateral spreading first drew the attention of the Geotechnical Community in the 1964 Niigata earthquake. Currently, pile design against such phenomena is performed with the "Beam on Nonlinear Winkler Foundation" method, alternatively known as the p-y method. Namely, the pile is simulated with beam elements, while soil-pile interaction is modeled through horizontal Winkler springs which follow a certain force displacement law (p-y curve). Under these conditions, lateral ground displacements are imposed at the fixed end of the springs.

It is realized that the accuracy of the simulation mainly depends on the nonlinear force-displacement relationship adopted for the Winkler springs. Thus, it is no surprise that a large number of studies, mostly experimental, have been dedicated to the investigation of the parameters that affect the shape of p-y curves, as well as to the development of empirical correlations for their evaluation. The majority of the existing correlations are based on relations for non liquefied soil [e.g. (API 2002)], while the effects of liquefaction are incorporated either through appropriate reduction factors [e.g. Brandenberg et al. (2005)] or through empirical correlations for the residual strength of the liquefied soil [e.g. Cubrinovski and Ishihara (2007)]. In either case, the pursued reduction is solely related to the relative density (Dr) of the sand.

Nevertheless, there are recent experimental data [e.g. Tokimatsu and Suzuki (2009)] which imply the effect of additional parameters, such as the properties of the pile itself (bending stiffness, installation method, head constraints), as well as, the insitu drainage conditions. Along the same line, González et al. (2009) provide experimental evidence for the potential development of negative excess pore pressures near the head of the pile, caused due to shear-induced dilation of the liquefied soil during its flow around the pile.

In view of the above, the problem of pile response into laterally spreading ground was revisited by means of 3-D numerical analyses, and a new set of empirical relations was proposed to evaluate appropriate p-y curves form pile design. The main assumptions and findings of this study are summarized herein, while a more detailed presentation is given by Chaloulos et al. (2013) and Chaloulos et al. (2014).

2 NUMERICAL METHODOLOGY

The 3-D mesh built to simulate the problem is shown in **Figure 1**: a single pile, rigidly fixed at the tip, is installed in a uniform, fully saturated and slightly inclined layer of Nevada sand. Both drilled (reference case) and driven piles are considered, while the head of the pile is either free (reference case), rigidly fixed or with restricted rotation. In total 26 parametric analyses were performed for the following pile, soil and excitation characteristics: diameter D=0.4-1.0m, bending stiffness EI=1.3e5 - 9.75e6 kNm2, relative density Dr=25-70%, soil permeability $k=1.8x10^{-5}$ - $1.8x10^{-3}$ m/s and harmonic excitation period T=0.20-0.50sec.

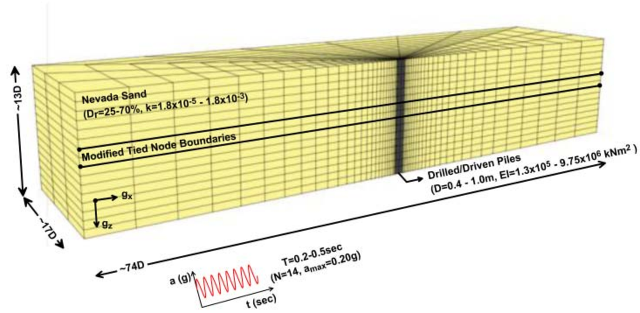

Figure 1. 3D mesh and parameters considered in the parametric investigation.

Note that, when one of the problem parameters is varied, all other are kept equal to their reference values i.e. D_r=50%, k=6.1x10-5m/s, D=0.60m, EI=1.3e6 kNm^2 and T=0.30s. In addition, it is clarified that the analyses investigating diameter effects were performed by uniformly scaling all mesh dimensions **shown in Figure 1.**

The basic aspects of the numerical simulation are the following:

(a) All analyses are performed with the finite difference code FLAC3D v4.0. A major advantage of this code is that it allows coupling between effective stress analyses and pore fluid flow, as well as the use of user-defined advanced constitutive models through a special C++ plug-in option.

(b) In this context, sand response under dynamic loading and liquefaction was simulated via NTUA Sand constitutive model (Andrianopoulos et al. 2010; Papadimitriou and Bouckovalas 2002), Karamitros (2010). NTUA Sand incorporates the critical state theory of soil mechanics and is calibrated against monotonic and cyclic tests performed on specimens of Nevada Sand.

(c) Contact (slip and separation) elements are used to simulate the pile-soil interface. The use of interface elements is essential to accurately capture the relative soil-pile movement which largely controls the aforementioned development of negative excess pore pressures near the pile head.

(d) Soil inclination is modeled by introducing in the mesh a horizontal component of the gravity vector, while the lateral constraints of the saturated infinite slope are simulated through a new type of boundary conditions. The new concept is based on the well-known tied-nodes method properly modified to account for the fact that the water table remains horizontal, thus yielding a hydrostatic pore pressure surplus at the downslope free-field boundary.

(e) The response of driven piles was simulated by incorporating Vesic's (1972) analytical solution for the calculation of stresses around cylindrical cavities. The analytical methodology was calibrated against axisymmetric plane strain numerical tests simulating the expansion of pie slices of Nevada Sand, and subsequently implemented in the analysis through a special subroutine.

The overall performance of the numerical methodology was verified against the centrifuge test results of Gonzalez et al. (2009), as shown in the comparisons of Figure 2 and Figure 3.

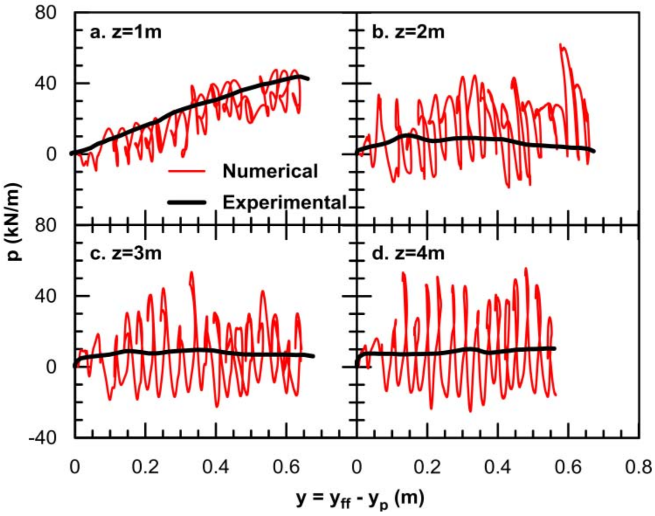

Figure 2. Experimental and numerical p-y predictions.

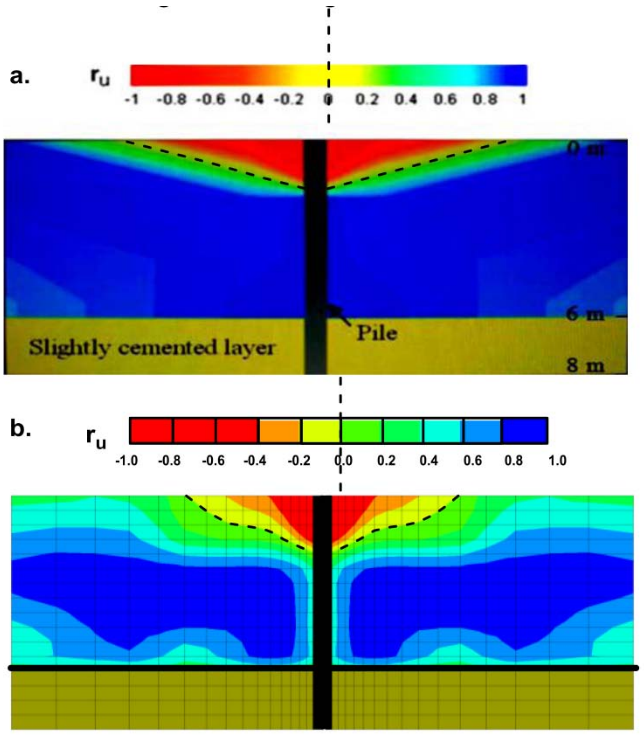

Figure 3. Excess pore pressure ratio contours at the end of shaking: (a) experimental recordings, (b) numerical predictions.

3 IMPROVED P-Y CURVES FOR LATERALLY SPREADING GROUND

3.1 Nonlinear shape of p-y curves

Typical p-y curves obtained from the baseline analysis are shown in Figure 4 for two different depths along the length of the pile (red line). It can be observed that despite the fact that soil response during each loading cycle exhibits hardening, the average (end of cycle) response through the entire excitation reveals softening.

Hence, taking also into account previous studies for non-liquefied sands (e.g. Det Norske Veritas 1980; Georgiadis et al. 1992), as well as laterally spreading soils (e.g. Brandenberg et al., 2007; Cubrinovski and Ishihara, 2007; Tokimatsu and Suzuki 2009), the following hyperbolic function was introduced to analytically describe the average p-y curves (black line in Figure 4):

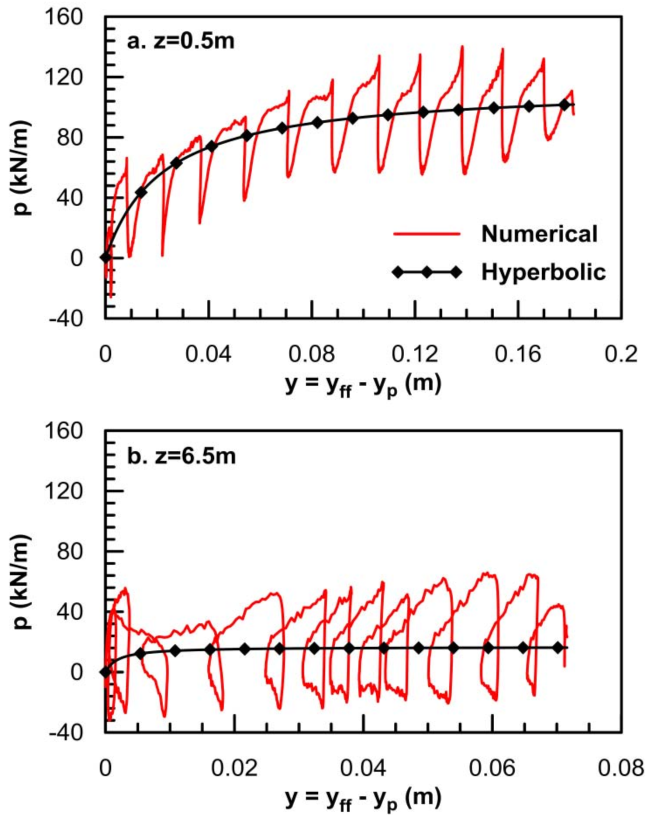

Figure 4. Adjustment of a hyperbolic curve on the numerically obtained p-y curve for the estimation of ultimate soil pressure.

$$p = \frac{y_{rel}}{\dfrac{1}{k_{ini,liq}\, z} + \dfrac{y_{rel}}{p_{ult,liq}}} \qquad (1)$$

where p (kN/m) is the soil pressure, y_{rel} (m) is the relative pile-soil displacement, $k_{ini,liq}$ (kN/m^3) is the initial subgrade modulus coefficient and $p_{ult,liq}$ (kN/m) is the ultimate soil pressure.

3.2 Initial subgrade modulus coefficient, k_{ini}

Best-fit values for $k_{ini,liq}$ and $p_{ult,liq}$ were subsequently obtained for the whole set of 26 analyses and 8 depths along the pile, through a trial-and-error procedure. Interpretation of the results revealed that the most consistent average fit of the numerical p-y curve is obtained assuming that $k_{ini,liq}$ is approximately equal to one-half of the corresponding value for the nonliquefied case ($k_{ini,firm}$), i.e.:

$$k_{ini,liq} = ½\, k_{ini,firm} \qquad (2)$$

Note that $k_{ini,liq}$ does not represent the elastic (small strain) stiffness of the soil, but a secant stiffness at very small (in the order of some millimeters) pile-soil displacements. This rather simplifying assumption is adopted herein taking into account that $p_{ult,liq}$, which is the focus of the present study, is reached early during shaking, so that the initial stiffness of the p-y curve becomes of secondary importance. Along the same direction, Dobry et al. (2003) recommend the apply directly $p_{ult,liq}$ on the pile rather than performing a complete p-y analysis in order to assess the response of the pile.

3.3 Ultimate soil pressures, $p_{ult,liq}$

Interpretation of the numerical results with regard to the ultimate soil pressures, $p_{ult,liq}$, revealed that they are uniquely related to the excess pore pressure ratio of the soil close to the pile ($r_{u,pile}$). For relatively low permeability soils, the latter can obtain large negative values close to the ground surface, as a result of soil dilation induced by the large pile-soil relative displacements, whereas it approaches unity (liquefaction) for middle and large depths, where the relative displacements are small. Graphically, this variation is demonstrated in Figure 5 where the normalized ultimate pressures $p_{ult,liq}/(\sigma'_{vo} D)$ are correlated with $1\text{-}r_{u,pile}$.

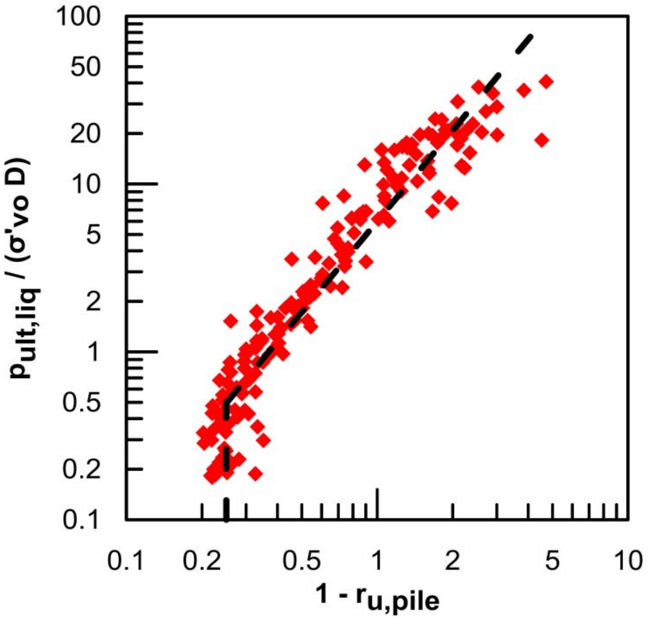

Figure 5. Relation between $p_{ult,liq}/(\sigma'_{vo} D)$ and $1\text{-}r_{u,pile}$

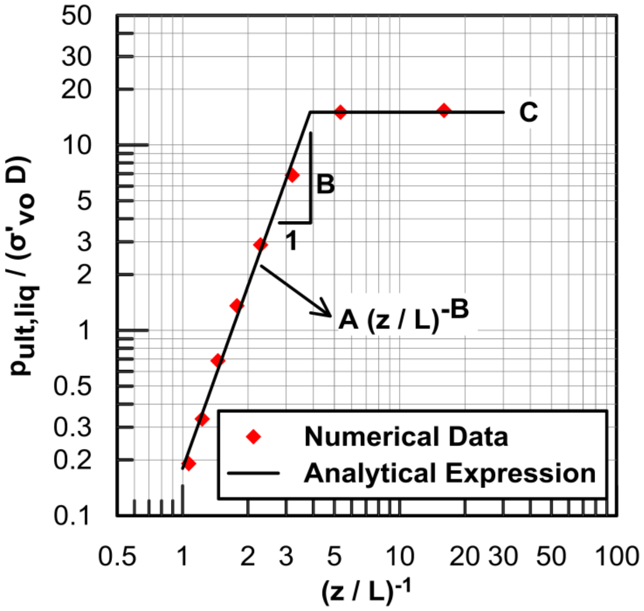

Figure 6. Relation between $p_{ult,liq}/(\sigma'_{vo} D)$ and (z/L) for the whole set of analyses.

Towards the development of a simple empirical relation, Figure 6 correlates the values of $p_{ult,liq}/(\sigma'_{vo} D)$ with the length ratio z/L, obtained from the baseline analysis. Mathematically their relation can be described as follows:

$$\frac{p_{ult,liq}}{\sigma'_{vo} D} = A\left(\frac{z}{L}\right)^{-B} \leq C \qquad (3)$$

The coefficients A, B and C above depend on the soil, pile and excitation characteristics and can be evaluated as follows, based on the results of the parametric analyses:

$$A = 0.045 \, . \, D_r(\%)^{0.9} \, . \, T^{1.55} \, . \, (k.10^4)^{0.06} \qquad (4)$$

$$B = 1.35 \exp[-0.023 \, D_r] \, . \, T^{-0.95} \, . \, (k.10^4)^{-0.11} . \exp[1.3D] \qquad (5)$$

$$C = 0.063 \exp[-0.025 \, D_r].[(k.T)/D]^{-0.6} \, .\min[(EI.10^{-5})^{0.3}, 8.6.(EI.10^{-5})^{-0.45}] \qquad (6)$$

In physical terms, coefficient A reflects soil resistance at large depths, where the excess pore pressure ratio is close to unity, thus its value is related to the mechanisms that govern the residual strength of the liquefied soil. On the other hand coefficient C represents soil resistance near the ground surface, i.e. in areas with pronounced dilation and large soil pressures. Finally, note that the effect of pile head constraint and installation method was minor on the overall response and was not incorporated in the relationships.

The accuracy of the proposed relationships is evaluated in Figure 6a, where analytical predictions are one-to-one compared with the numerical results, and in Figure 7b which shows the relative error. In both figures different symbols are used for the upper part (where $r_{u,pile}$<0.0), for the middle part (where $r_{u,pile}$=0.0-0.5) and for the lower part of the pile (where $r_{u,pile}$>0.5). The agreement is fairly consistent with less than 50% relative error for 95% of the data.

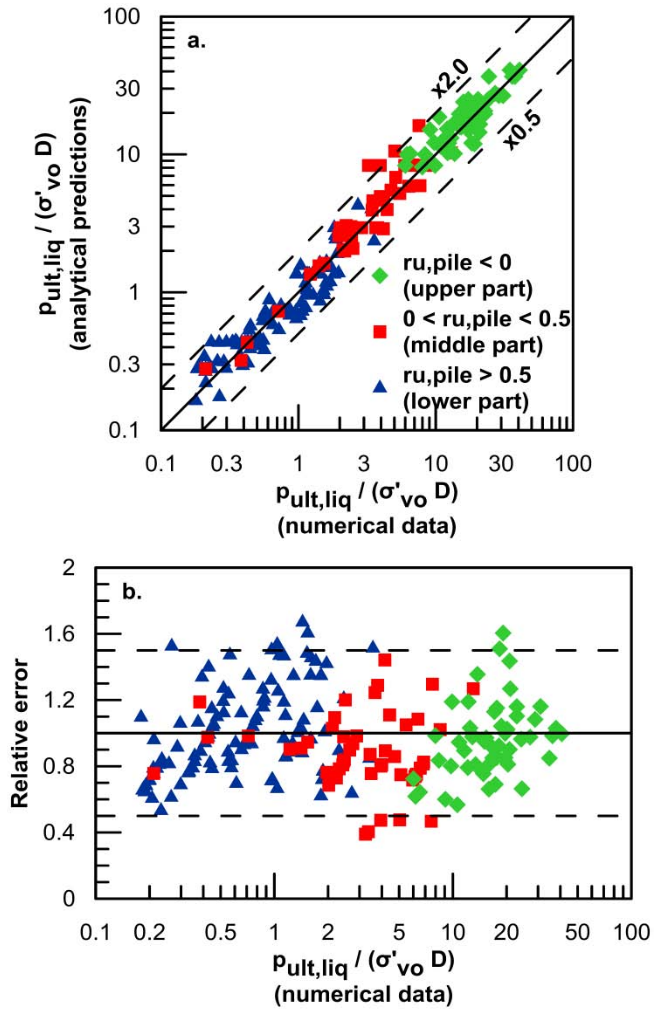

Figure 7. Evaluation of analytical relationships: (a) one-to-one comparison; (b) relative error.

4 CONCLUDING REMARKS

The major contribution of the proposed relationships is that they can capture the dilative response of the soil at the upper part of the pile and the subsequent increase in soil pressures. To appreciate the practical significance of this finding, the proposed relations are compared with the widely used methodologies of Brandenberg et al. (2007), Cubrinovski and Ishihara (2004, 2007) and Tokimatsu and Suzuki (2009). Note that the latter were developed based on data from centrifuge or shaking table tests, and do not make explicit reference to dilation phenomena.

The comparison is shown in Figure 8a, in terms of predicted ultimate soil pressures for a typical concrete pile with length L=8m, diameter D=0.60m and bending stiffness EI=190000kNm^2 installed in a uniform sand layer with relative density Dr=50%. The friction angle and the buoyant weight of the sand were taken equal to φ=33° and γ'=9.81kN/m^3 respectively, while the empirical relationships were applied for excitation period T=0.30sec.

The equivalent SPT blow count was estimated as $(N^1)_{60\text{-}cs}$ ≈ 11 (Tokimatsu and Seed 1987). The predictions by Brandenberg et al. are shown as a range for values of the reduction multiplier m_p=0.05 and 0.165, while the assumed reduction factor for Tokimatsu και Suzuki was β≈0.10 (for z<10m).

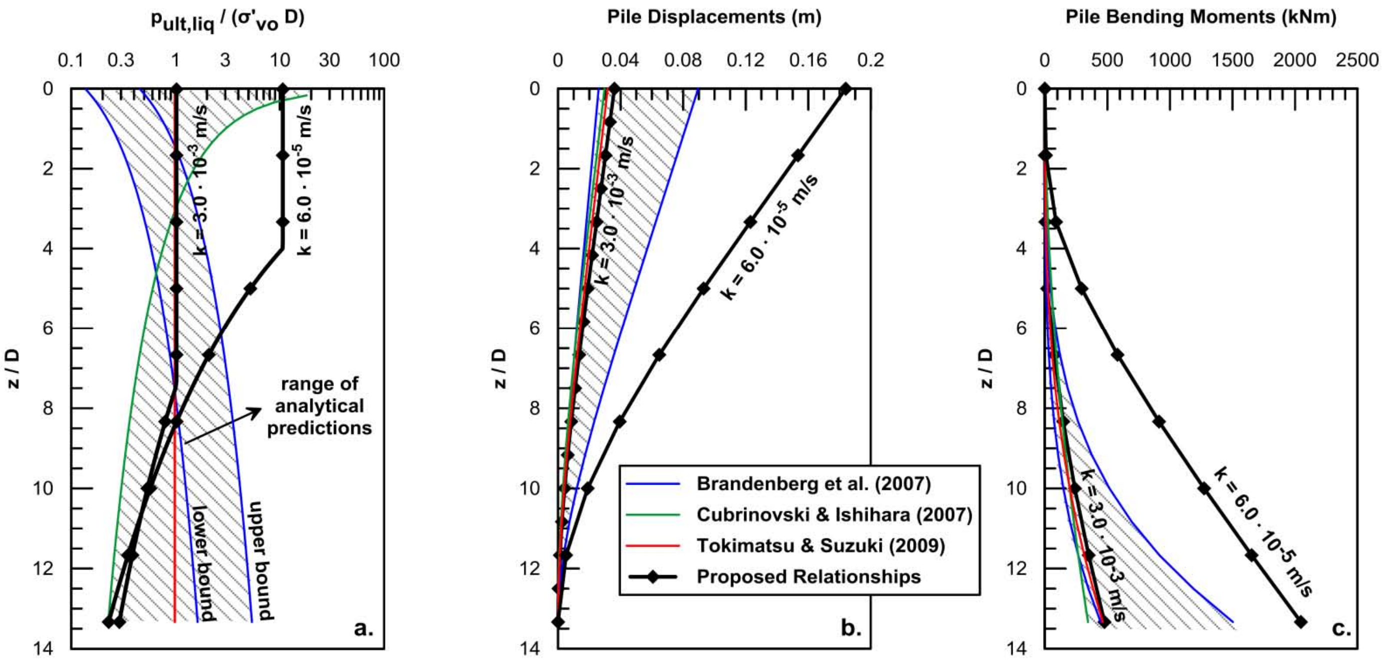

Figure 8. Effect of permeability and dilation on (a) ultimate soil pressures; (b) pile displacements; and (c) pile bending moments.

In order to investigate potential dilation effects, predictions with the proposed methodology are shown for two soil permeability coefficients: k=3.05 x 10-3 m/s, e.g. representative for sand-gravel mixtures, and k=6.1 x 10-5 m/s, e.g. representative for silty sands. Given that existing methodologies do not account for permeability effects, their predictions independent of k. The comparison reveals the following:

(a) The proposed and the existing relationships are in good agreement for cases where no significant dilation is expected, i.e. at large depths and large permeability coefficients.

(b) On the contrary, when significant dilation occurs, i.e. at small depths and low permeability coefficients, the existing methodologies significantly underestimate soil pressures.

The previous observations are further verified in Figure 8b and 8c which compare pile displacements and bending moments respectively. Namely, observe that pile head displacements and maximum bending moments for the low permeability case are increased by approximately 5-6 and 4 times relative to the predictions for high permeability, as well as the predictions with existing methods.

REFERENCES

Andrianopoulos, K. I., Papadimitriou, A. G., and Bouckovalas, G. D. (2010). "Explicit integration of bounding surface model for the analysis of earthquake soil liquefaction." Int. Journal for Numerical and Analytical Methods in Geomechanics, 34(15)

API. (2002). "Recommended Practice for Planning, Design, and Constructing Fixed Offshore Platforms, API RP 2A-WSD." American Petroleum Institute, Washington, D.C.

Brandenberg, S. J., Boulanger, R. W., Kutter, B. L., and Chang, D. (2005). "Behavior of pile foundations in laterally spreading ground during centrifuge tests." J. of Geotech. Geoenviron. Eng., 131(11)

Brandenberg, S. J., Boulanger, R. W., Kutter, B. L., and Chang, D. (2007). "Static pushover analyses of pile groups in liquefied and laterally spreading ground in centrifuge tests." J. of Geotech. Geoenviron. Eng., 133(9)

Chaloulos, Y. K., Bouckovalas, G. D., Karamitros, D. K. (2013). "Pile response in submerged lateral spreads: Common pitfalls of numerical and physical modeling techniques." Soil Dynamics and Earthquake Engineering, 55, 275–287.

Chaloulos, Y. K., Bouckovalas, G. D., Karamitros, D. K. (2014). "Analysis of Liquefaction Effects on Ultimate Pile Reaction to Lateral Spreading." J. of Geotech. Geoenviron. Eng., 140(3)

Cubrinovski, M., and Ishihara, K. (2007). "Simplified Analysis of Piles Subjected to Lateral Spreading: Parameters and Uncertainties." 4th International Conference on Earthquake Geotechnical Engineering, K. Pittilakis, ed., Thessaloniki, Greece.

Det Norske Veritas. (1980). Rules for the design, construction and inspection of offshore structures.

Dobry, R., Abdoun, T., O'Rourke, T. D., and Goh, S. H. (2003). "Single piles in lateral spreads: Field bending moment evaluation." Journal of Geotechnical and Geoenvironmental Engineering, 129(10), pp. 879–889.

Georgiadis, M., Anagnostopoulos, C., and Saflekou, S. (1992). "Centrifugal testing of laterally loaded piles in sand." Canadian Geotechnical Journal, NRC Research Press, 29(2), pp. 208–216.

González, L., Abdoun, T., and Dobry, R. (2009). "Effect of soil permeability on centrifuge modeling of pile response to lateral spreading." Journal of Geotechnical and Geoenvironmental Engineering, 135(1), pp. 62–73.

Papadimitriou, A. G., and Bouckovalas, G. D. (2002). "Plasticity model for sand under small and large cyclic strains: A multiaxial formulation." Soil Dynamics and Earthquake Engineering, 22(3)

Tokimatsu, K., and Seed, H. B. (1987). "Evaluation of Settlement in Sands due to Earthquake Shaking." Journal of geotechnical engineering, 113(8), pp. 861–878.

Tokimatsu, K., and Suzuki, H. (2009). "Seismic soil-pile-structure interaction based on large shaking table tests." Performance-Based Design in Earthquake Geotechnical Engineering, T. Kokusho, Y. Tsukamoto, and M. Yoshimine, eds., Taylor & Francis.

Vesic, A. S. (1972). "Expansion of cavities in infinite soil mass." ASCE J Soil Mech Found Div, 98(SM3), pp. 265–290.

Avoiding Whales in Anaerobic Digesters

Ian D. Peggs, P.E.

In 2014, shortly after being placed in service, one of two geomembrane-lined and covered anaerobic digesters generated extensive whales—"bubbles" in the lining system. Attempts to remove the apparent gas from under the cover were made unsuccessfully until it was realized that the cover was being uplifted by gas under the liner. Within two or three days, there were whales several meters high in the cover.

The liner had leaked, microbiological action in the leaked water had continued, biogas was generated under the liner, but the gas venting grid strips had been filled with water, and the biogas could not be vented. The whales formed instead.

ANAEROBIC DIGESTERS AND WASTEWATER

Many waste water treatment plants (WWTP) are adding anaerobic digesters to the process stream for the generation and collection of biogas for power generation. They are quite common in the food and meat processing industries. These lagoons and basins have a bottom geomembrane liner and a floating cover or a ballasted low-dome cover. Biogas is collected in a piping system inside the periphery of the system at the crests of the slopes/walls. Many of these lagoons have experienced whales as biogas develops and collects under the bottom geomembrane.

In the case noted here, two reactors were built side by side, one after the other. They were simple 150 x 100 m rectangular ponds with 3H:1V side slopes. They were lined with a single 1.5 mm thick high-density polyethylene (HDPE) geomembrane on a nonwoven geotextile cushion. They had ballasted low-dome covers. Filling commenced in June. By September, a whale was spotted.

Despite efforts to remove the gas build up, roughly 30% of the surface area wound up covered with whales. At this point the pond was taken out of service. The second reactor showed no signs of whales.

The affected liner was removed for dewatering, desludging, and degreasing. Pipe penetrations and other risk points were carefully examined in the search for how and why the bubbles had formed.

DESIGN AND INSTALLATION ISSUES

Several of the pipe penetrations in the slope liner—including sludge withdrawal pipes—needed to be placed along the floor. A strap over the pipe was welded to a patch and the patch welded to the liner to hold the pipe in place. Straps were placed about every 3 m. The pipe penetrations through the liner were located approximately half way up the slopes. The design of the pipe boot seal at the open end of the pipe was unusual.

The two steel straps will not form a seal without gaskets and it is difficult to imagine the straps exerting sufficient compression by the geomembrane on the gasket midway between them to effect a seal, especially when the straps are not tightened and provide leakage pathways.

When the boot is slipped over the pipe it should be a close fit to avoid wrinkles under the clamps. The inner strap will be attached first. Then the flexible gasket will have to be pushed between pipe and boot in such a way that it does not bend/kink and so that cut ends overlap evenly or butt tightly together or that a good scarf joint is made. This will probably be impossible. Then the outer strap has to be added in such a way that the geomembrane between the straps exerts sufficient uniform bridging compression on the gasket to make a seal. This is also probably impossible to do. The liner installer recognized this problem and tried to remedy it by cutting holes between the straps and injecting a caulk in the void space between geomembrane and pipe between the two straps.

When the seal was disassembled and sectioned, it was evident that the caulk was not uniformly distributed, that bonding to the PVC pipe was better than to the HDPE, and that leakage had occurred as shown by the dirt on the caulk/HDPE interface. Very little will bond with HDPE.

There were two more undesirable features of the pipe boots. Excessive wrinkling of the boot occurred along the pipe, and a neat fold/pleating effect of the excess skirt material was observed above the pipe. Since HDPE geomembranes are susceptible to stress cracking, project specifications usually require that the geomembrane be in intimate contact with the subgrade in order that it acts solely as a barrier and not as a load-bearing member of the lining system. Therefore, wrinkles and folds are most undesirable.



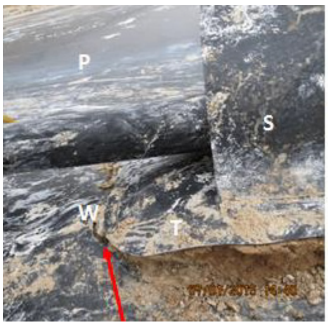

With this installation, several of the pipe boots had torn along the weld between the upper and lower parts of the boot under the pipe.

There were also tears in the liner at the corners of a patch to which a pipe strap was welded. Certainly the pipe needs to be restrained to prevent it moving and damaging the liner, but to do that by attaching it to the liner seems counterproductive. At the very least, the patch should have been welded to the liner around its full periphery, not just at the corners where the liner has been highly stressed.

There were two short cracks/tears along the edge of a patch extrusion weld at the toe of slope which when removed revealed a geocomposite vent strip to be full of sludge. The vent strips were unable to transmit gas.

The net result of the liner inspections was that there were many holes in the geomembrane liner through which water was leaking into the subgrade. The geocomposite vent strips became clogged with sludge and full of water, so they would not vent the biogas that continued to be generated under the liners. Whales formed.

Even though the geocomposite drain/vent strips were sloped towards a central drain, the system was again clogged which prevented venting of the gas. However, the second reactor appeared to be working satisfactorily which may reflect a lower more manageable leakage rate. However, there is no guarantee that the second liner will not suffer whaling.

SOME SOLUTIONS

As seen in this case and with a number of other anaerobic digesters, a grid pattern of geocomposite strips might not be effective in venting biogas from the leak detection system. Of course, it helps if the geomembrane can be installed such that it does not leak in the first place. Extrusion welds should not overheat the liner causing it to be locally oxidized and to be deformed with many stress concentrating notch geometries. All grinding marks/gouges should be covered by weld extrudate, and there should be no more than two welds in any one location.

This is a matter of using an experienced design engineer, an experienced liner installer, and a knowledgeable CQA firm. And the final phase of CQA should be to perform a geoelectric integrity survey on the liner to assure a minimum number of holes and cracks that might leak.

In anaerobic digesters, leaks often occur at pipe penetrations. As such, every effort should be made to avoid penetrations. If they cannot be avoided, they should be supported by concrete thrust blocks or something equivalent. There must be a means of removing leaked water very quickly and an effective venting system to remove any biogas generated under the liner.

**

Ian D. Peggs is principal of I-CORP INTERNATIONAL, www.geosynthetic.com. A full version of this article was published in the GeoAmericas 2016 Proceedings. GeoAmericas was held in April 2016 in Miami. The conference was hosted by the International Geosynthetics Society North American Chapter. Learn more about the event and acquire a copy of the three-volume digital proceedings at www.geoamericas2016.org.

(October 20, 2016, http://www.geosynthetica.net/designing-anaerobic-digesters-whales)

Natural Sheet Piling

A natural phenomenon from the dawn of time could well be the ultimate substitute for standard sheet piling. A seal is created within a few hours. This is the story of bog iron.

by Janneke Ijmker
Image Janderzel

When iron-rich groundwater comes into contact with oxygen, dams and nuggets with a rusty brown colour form in the ground: bog iron. In prehistoric times, our ancestors made grateful use of it to produce cast iron. By today's standards, the metal isn't pure enough but researchers Wim de Lange, Jos Vink, Rob Zwaan and Marco de Kleine have thought of a modern application for bog iron. Not by mining it but precisely by using a smart method to inject it into the ground.

Iron injection

Bog iron is - at least in theory - an ideal way of making underground sheet piling. There is no digging and the approach is environmentally friendly and invisible. 'The iron-rich liquid goes to where you want the sheet and it only goes to work once it's there,' says project manager Wim de Lange. In that sense, it resembles the existing injection technology with sodium silicate or water glass. Unfortunately, that technique produces highly alkaline results and it isn't environmentally friendly. 'It's like injecting ammonia into the soil,' says Jos Vink, the team's chemical expert. So bog iron is preferable: it is something that is already present in the ground. But how do you make it, and how do you get it into the right place in the right form?

Search

There is actually only one drawback to the idea: it really is difficult to adjust the interaction between the rate of the chemical reactions, spreading the injection fluid and blocking off the soil. And that process can also be affected by local conditions, as was seen during every step of the search that began in the Deltares chemical laboratory, Utrecht Castel, where Jos Vink and his colleagues looked at a range of mixtures to see how they blocked off the soil and tested them at the centimetre scale. A mixture was then tested in a glass container measuring 2 m^3 to see how it worked in real soil. 'You see the bog iron forming as you watch,' says researcher Rob Zwaan in his laboratory. 'It's a beautiful process.

Once this step was completed, the next challenge was: how can you spread the mixture evenly across a large surface area? Wim de Lange: 'We insert a large number of lances - they're like big syringes - into the soil. We induce groundwater flows between two rows of lances and the groundwater can only move in one direction between the lances. Then we inject the iron-rich water. In the future, we will be using several rows of lances that will move along canals or roads like a roller with the aim of installing a large sheet of bog iron beneath the surface.'

Rolling in the deep

Then it was time to prove that the idea actually worked on a large scale. The team of researchers tested the 'roller' in a trial with three tons of injection material in a 2.5-metre-deep, 40-square-metre container in the laboratory in Delft. The engineering firm Hektec designed a special plant for making the mixtures and injecting the right amounts into the ground. There was also an opportunity to conduct tests in natural conditions when a pond had to be enlarged in the Veluwe area of the Netherlands. The researchers wanted to show that you can do this by extending the impermeable layer below the pond using bog iron.

Those experiments identified a new challenge: you can't, of course, see anything below the ground. Marco de Kleine and his team therefore designed a monitoring system to watch the injection of bog iron. 'We can now pinpoint the location and the spread of the new bog iron. So we know immediately whether the job has been done right.'

Application

The team is now waiting to put the idea into practice. There are numerous possibilities. Flows of groundwater into construction pits can be reduced. Bog iron can also be used to deepen canals and roads. Injecting bog iron is more environmentally friendly than sodium silicate and water glass and it may, depending on the situation, be significantly cheaper than traditional sheet piling. Wim de Lange gives an example: 'Let's say a canal has to be made wider and deeper to accommodate larger and taller ships. If you don't want to replace all the bridges, you have to lower the water level. But then the groundwater level will be lower on either side of the canal. Homes and nature areas alongside may subside or dry up and that is certainly not a good idea. We think bog iron could be a great option here.'

More information:

wim.delange@deltares.nl

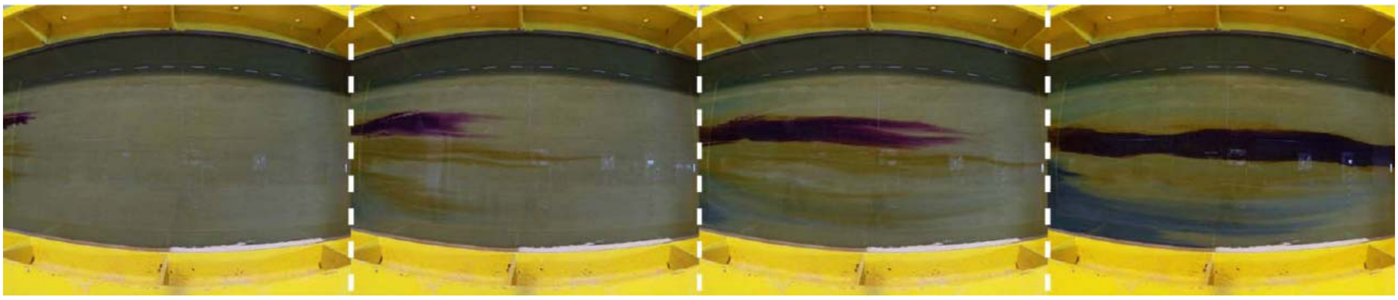

The development of bog iron in the test set-up.

ΝΕΑ ΑΠΟ ΕΛΛΗΝΙΚΕΣ ΚΑΙ ΔΙΕΘΝΕΙΣ ΓΕΩΤΕΧΝΙΚΕΣ ΕΝΩΣΕΙΣ

International Society for Soil Mechanics and Geotechnical Engineering

Prediction event ISSMGE TC212 B.E.S.T.

Hello all,

I believe you will be interested in taking a look at the Pile Prediction event that I am in the process of organizing in connection with the forthcoming 3rd CFPB in Santa Cruz, Bolivia,(www.cfpbbolivia.com) scheduled for April 27 - 29. The event comprises a series of static loading pile tests at the ISSMGE TC212 B.E.S.T. site. I have described the details of the site, tests, and prediction submission in the attached document. I hope that you will be interested in submitting a prediction and, also, that you will give me a hand with spreading the news by disseminating the invitation amongst those on your own contact list. (Some of the addresses I direct this message to may also be included on such lists. I apologize if you are bothered by receiving more than one copy of the message).

Four single piles of the same embedment length, 9.5 m, are included in the prediction event. The piles differ in width and type: a 620-mm bored pile, a 450-mm CFA-pile, a 450-mm FDP pile, and a 220-mm FDP pile. The latter has a an Expander Base (EBI) at the pile toe that is inflated to 300-mm diameter after the pile is constructed. The soil profile consists of a silty compact sand and has been explored using conventional boreholes (SPT) with lab tests, CPTU-soundings, Pressuremeter test, and Dilatometer tests. People who register intent to submit predictions on the pile-head load-movement curves and capacity for each test will receive a Prediction Package that will contain all necessary soil and pile information.

A loading test will also be carried out on a pile group consisting of thirteen 220-mm diameter FDP piles at 3 diameter c/c joined with a rigid pile cap. The prediction participants are asked to predict the response of the center pile and a corner pile.

The prediction effort is a part of a large field study involving soil in-situ exploration tests, head-down and bidirectional pile tests, and dynamic pile tests to demonstrate the state-of-the art and practice of analysis of the response and design of single piles and pile groups with regard to settlement and load distribution.

I will send the prediction package that includes site and soil information and submission template to all who register intent to submit a prediction at:

{https://secure.webforum.com/form/cfpbolivia/form.asp?sid=709626496},

Best regards,

Bengt

Bengt H. Fellenius, Dr.Tech., P.Eng.
2475 Rothesay Avenue
Sidney, BC, Canada
V8L 2B9
e-address: Bengt@Fellenius.net
Web site: www.Fellenius.net

Geosynthetics International Gives Free Access to Best Papers

Annual, editor-selected "Best Of" papers from Geosynthetics International are available for free access online. Thomas Telford Ltd's division ICE Publishing—part of the UK-based Institution of Civil Engineers—has published up to three from each calendar volume going back to 2010.

Visit the "Editor's Choice" page on the journal's website.

Members of the International Geosynthetics Society (IGS) have free digital access to Geosynthetics International, but the open sharing of these honors-earning papers is a tremendous service to the larger geosynthetics and geotechnical engineering field.

Geosynthetics International is a Top 5-rated geotechnical journal in the world (as tracked by SCImago). ICE Publishing arranges institutional subscriptions. If you have academic or professional libraries in your daily research or work which are not already subscribed, recommend to the librarians that they contact sales@icepublishing.com.

GEOSYNTHETICS INTERNATIONAL BEST PAPERS

2015

- Fox, P. J. & Stark, T. D.
  State-of-the-art report: GCL shear strength and its measurement – ten-year update (Best paper)

- Take, W. A., Brachman, R. W. I. and Rowe, R. K.
  Observations of bentonite erosion from solar-driven moisture migration in GCLs covered only by a black geomembrane (second best paper)

2014

- Kuwano, J., Miyata, Y. & Koseki, J.
  Performance of reinforced soil walls during the 2011 Tohoku earthquake

- Blanc, M., Thorel, L., Girout R. and Almeida, M.
  Geosynthetic reinforcement of a granular load transfer platform above rigid inclusions: comparison between centrifuge testing and analytical modelling

- Abdelaal, F. B., Rowe, R. K. and Brachman, R. W. I.
  Brittle rupture of an aged HPDE geomembrane at local gravel indentations under simulated field conditions

For access to 2010 – 2013, please use the links provided on the journal's Editor's Choice page via ICE Publishing. Those papers are as follows:

2013

- Rowe, R. K., Abdelaal, F. B. & Brachman, R. W. I.
  Antioxidant depletion of HDPE geomembrane with sand protection layer

- Tanyu, B. F., Aydilek, A. H., Lau, A. W. Edil, T. B. & Benson, C. H.
  Laboratory evaluation of geocell-reinforced gravel subbase over poor subgrades

- Lim, S. Y. & McCartney, J. S.
  Evaluation of effect of backfill particle size on installation damage reduction factors for geogrids

2012

- Chappel, M. J., Rowe, R. K., Brachman, R. W. I. & Take, W. A.
  A comparison of geomembrane wrinkles for nine field cases

- Munoz, H., Tatsuoka, F., Hirakawa, D., Nishikiori, H., Soma, R., Tateyama, M. & Watanabe, K.
  Dynamic stability of geosynthetic-reinforced soil integral bridge

- Yee, T. W. & Lawson, C. R.
  Modelling the geotextile tube dewatering process

2011

- Brandl, H.
  Geosynthetics applications for the mitigation of natural disasters and for environmental protection

- Fox, P.J., Ross, J.D., Sura, J.M. and Thiel, R.S.
  Geomembrane damage due to static and cyclic shearing over compacted gravelly sand

- Rowe, R.K., Rayhani, M.T., Take, W.A., Siemens, G. and Brachman, R.W.I.
  GCL hydration under simulated daily thermal cycles

2010

- Zornberg, J. G., Bouazza, A. & McCartney, J. S.
  Geosynthetic capillary barriers: current state of knowledge

- Kongkitkul, W., Tatsuoka, F., Hirakawa, D., Sugimoto, T., Kawahata, S. & Ito, M.
  Time histories of tensile force in geogrid arranged in two full-scale high walls

- Mendes, M. J. A., Touze-Foltz, N., Palmeira, E. M. & Pierson, P.
  Influence of structural and material properties of GCLs on interface flow in composite liners due to geomembrane defects

Learn more about Geosynthetics International: http://www.icevirtuallibrary.com/journal/jgein

Learn more about the International Geosynthetics Society (IGS) and its chapters at www.geosyntheticssociety.org.

(Chris Kelsey, October 27, 2016, http://www.geosynthetica.net/geosynthetics-international-best-papers-access)

ΠΡΟΣΕΧΕΙΣ ΓΕΩΤΕΧΝΙΚΕΣ ΕΚΔΗΛΩΣΕΙΣ

Για τις παλαιότερες καταχωρήσεις περισσότερες πληροφορίες μπορούν να αναζητηθούν στα προηγούμενα τεύχη του «περιοδικού» και στις παρατιθέμενες ιστοσελίδες.

NEMO International Conference Probing the Santorini volcano for 150 years / Διεθνές συνέδριο NEMO 150 χρόνια μελέτης ηφαιστείου της Σαντορίνης, 3-5 November 2016, Santorini, Greece, http://nemo.conferences.gr

GeoAsia 6 - 6th Asian Regional Conference on Geosynthetics 8-11 November 2016, New Delhi, India, http://seags.ait.asia/news-announcements/11704

3rd Annual Underground Infrastructure & Deep Foundations UAE, 13 - 15 November 2016, Dubai, United Arab Emirates, www.undergrounduae.com

Risk Management in Underground Construction, November 14-16, 2016, Florida University, USA, http://undergroundriskmanagement.com/agenda

5th International Conference on Geotechnical Engineering and Soil Mechanics, 14-16 November 2016, Tehran, Iran, www.icgesm2016.ir

RARE 2016 Recent Advances in Rock Engineering 16-18 November 2016, Bangalore, India, www.rare2016.in

TBM DiGs Istanbul 2016 2nd International conference on "TBM DiGs in difficult grounds", 16-18 November 2016, Istanbul, Turkey, www.tbmdigsturkey.org

International Seminar on Roads, Bridges and Tunnels, 18-24 November 2016, Thessaloniki, Greece, http://isrbt2016.civil.auth.gr

GEOTEC HANOI 2016, The 3rd International Conference on Geotechnics for Sustainable Infrastructure Development, 24-25 November, Hanoi, Vietnam, www.geotechn.vn

TUNNELLING SUMMIT - Pinpointing project opportunities and exploring innovation in tunnelling, 7-8 December 2016, London, U.K., https://tunnelling.newcivilengineer.com

5th International Conference on Forensic Geotechnical Engineering, 8-10 December 2016, Bangalore, Karnataka, India, http://5icfge.com

International Symposium on Submerged Floating Tunnels and Underwater Tunnel Structures (SUFTUS-2016), 16-18 December 2016, Chongqing, China, www.cmct.cn/suftus

MPM 2017 - First international conference on the material point method for Modelling Large Deformation and Soil–Water–Structure Interaction, 10 – 13 January 2017, Delft, The Netherlands, http://mpm2017.eu

International Workshop on "Advances in Multiphysical Testing of Soils and Shales", 18-20 January 2017, Villars, Switzerland, http://atmss.epfl.ch

ICNCGE-2017 International Conference on New Challenges in Geotechncial Engineering, 23 January 2017, Lahore, Pakistan, www.pges-pak.org/home/icncge-2017

Tunnelling Asia' 2017 - Design, Construction and Risk Management in Underground Construction : Issues & Challenges, 9 - 10 February, 2017, Mumbai, India, sunil@cbip.org; cbip@cbip.org; www.cbip.or

International Congress and Exhibition HYDROPOWER CASPIAN AND CENTRAL ASIA, 15-16 February 2017, Tbilisi, Georgia, www.hydropowercongress.com

4th Arabian Tunnelling Conference & 20th Gulf Engineering Forum - Advancing Underground Space, 21-22 February 2017, Dubai, UAE, www.atcita.com

AFRICA 2017 - Water Storage and Hydropower Development for Africa, 14-16 March 2017, Marrakech, Morocco, www.hydropower-dams.com/AFRICA-2017.php?c_id=89

3rd Annual Urban Underground Space & Tunnelling, 27th-29th March 2017, Singapore, http://isocarp.org/events/3rd-annual-urban-underground-space-tunneling

Instrumentation and Monitoring Conference 2017 - Innovation, best practice and projects, 29- 30 March 2017 | Inmarsat, London, U.K., https://monitoring.geplus.co.uk

2nd International Conference on Geotechnical Research and Engineering (ICGRE'17), April 3 - 4, 2017, Barcelona, Spain, http://icgre.org

IS - São Paulo 2017, 9th International Symposium on Geotechnical Aspects of Underground Construction in Soft Ground, April 4 and 5 2017, São Paulo, Brazil, www.is-saopaulo.com

Southeast Asian Conference and Exhibition in Tunnelling and Underground Space 2017 (SEACETUS 2017) - Innovation and Sustainable Underground Space Development, 18 – 19 April 2017, Subang Jaya, Selangor, Malaysia, nora@iem.org.my

EURO:TUN 2017 IV International Conference on Computational Methods in Tunneling and Subsurface Engineering, 18 – 20 April 2017, Innsbruck, Austria, www.eurotun2017.com

SEE TUNNEL 2017 Zagreb 7th International Symposium on Tunnels and Underground Structures in South-East Europe, May 4-5, 2017, Zagreb, Croatia, www.promovere.hr

YSRM2017 & NDRMGE 2017 Challenges and Innovations in Rock Mechanics and Engineering, 10-13 May 2017, Jeju Island, South Korea, www.ysrm2017.com

TechnoHeritage 2017 3rd International Congress Science and Technology for the Conservation of Cultural Heritage, May 20-23, 2017, Cádiz, Spain, http://technoheritage2017.uca.es

EPS'17 5th International Conference on the Use of EPS Geofoam Blocks in Construction Applications, 22-24 May 2017, Istanbul, Turkey, www.geofoam2017.org

Rapid Excavation and Tunneling Conferrence, June 4-7, 2017, San Diego, USA, www.retc.org

IV International Course on Geotechnical and Structural Monitoring, June 2017, Rome, Italy, www.geotechnicalmonitoring.com/en

PRF 2017 Progressive Rock Failure, 5-9 June 2017, Ascona, Switzerland, www.prf2017.ethz.ch

EAgs - EurAsian Geotextiles Symposium 2017, 07 - 08 June 2017, Beijing, China, www.edana.org/education-events/conferences-and-symposia/event-detail/eurasia-geotextiles-symposium-2017

World Tunnel Congress 2017 Surface challenges – Underground solutions, 9 to 16 June 2017, Bergen, Norway, www.wtc2017.no

EUROCK 2017 Human Activity in Rock Masses, 20-22 June 2017, Ostrava, Czech Republic, www.eurock2017.com

BCRRA 2017 Tenth International Conference on the Bearing Capacity of Roads, Railways and Airfields, 28th to 30th June 2017, Athens, Greece, www.bcrra2017.com

85th Annual Meeting of International Commission on Large Dams, July 3-7, 2017, Prague, Czech Republic, www.icold2017.cz

6th International Conference on Coupled THMC Processes in Geostystems, 5-7 July 2017, Paris, France, https://geoproc2017.sciencesconf.org

10th World Congress on Water Resources and Environment "Panta Rhei", 5-9 July 2017, Athens, Greece, http://ewra2017.ewra.net

GeoMEast2017, 15 - 19 July 2017, Sharm El-Sheik, Egypt, www.geomeast2017.org

3rd International Conference on Performance-based Design in Earthquake Geotechnical Engineering (PBD-III), July 16 - 19, 2017, Vancouver, Canada, http://pbdiiivancouver.com

ICTUS17 The 2017 International Conference on Tunnels and Underground Spaces, 28 August 2017 - 1 September 2017, Seoul, Korea, www.i-asem.org/new_conf/asem17.htm

19th International Conference on Soil Mechanics and Geotechnical Engineering, 17 - 22 September 2017, Seoul, Korea, www.icsmge2017.org

SIFRMEG 2017 Shaoxing International Forum on Rock Mechanics and Engineering Geology, September 20, 2017, http://forum.hmkj.com.cn/index.php/Index/show/tid/20

AfriRock 2017, 1st African Regional Rock Mechanics Symposium, 2 – 7 October 2017, Cape Town, South Africa, www.saimm.co.za/saimm-events/upcoming-events/afrirock-2017

Geotechnique Symposium in Print 2017 Tunnelling in the Urban Environment, http://www.icevirtuallibrary.com/pb-assets/Call%20for%20Papers/Geo-Symposium-CFA-AW.pdf

HYDRO 2017 Shaping the Future of Hydropower, 9-11 October 2017, Seville, Spain, hydro2017@hydropower-dams.com

GeoAfrica 2017 3rd African Regional Conference on Geosynthetics, 9 – 13 October 2017, Morocco, http://geoafrica2017.com

3ο Πανελλήνιο Συνέδριο Φραγμάτων και Ταμιευτήρων - Διαχείριση Έργων και Προοπτικές Ανάπτυξης, 12 - 14 Οκτωβρίου 2017, Αθήνα, www.fragmata2017.gr

XIII International Conference
"Underground Infrastructure of Urban Areas 2017"
24-26 October 2017, Wroclaw, Poland
http://uiua.pwr.edu.pl/?lang=en

The aim of conference is to create a forum in order to develop an exchange of experiences and provoke a discussion on the topics related to building of tunnels and underground infrastructure in the cities. The issues such as geotechnical tests and town planning could also be brought up in this forum. The discussion on various problems related to underground infrastructure such as tunnels (traffic and railway tunnels, and underground), water and sewage ducts, garages, and subways is anticipated. It is hoped that the possibilities of using an underground space associated with town planning and modernization of cities will be analysed as well. The important inspirations for the conference are starting the construction of the road tunnel on the way to Zakopane and studies on the design of tunnel in Świnoujście. The organizers wish to involve a wide body of people from different sectors. Scientists, investors, designers, contractors, and students have different point of view and thus possibly varying opinions. It is hoped that the analysis and the comparison of these different views will allow drawing a fruitful conclusions. The subject matter of conference is very crucial and up-to-date due to a current need for adjusting underground infrastructures to nowadays standards and requirements. The impact of these structures on the environment and the principles of sustainable development have to be considered nowadays.

CORRESPONDENCE ADDRESS

Wrocław University of Technology
Institute of Civil Engineering
50-370 Wrocław, Wybrzeże Wyspiańskiego 27,
with a postscript:
"Underground Infrastructure of Urban Areas 2014"

CONFERENCE INFORMATION

Marta DUDEK (webmaster) marta.dudek@pwr.edu.pl

Andrzej KOLONKO
Tel.: 0048 71 320 29 14, Mobil Tel.: +48 507043537
e-mail: andrzej.kolonko@pwr.edu.pl

Arkadiusz SZOT
Tel. 0048 71 320 3466, Mobil Tel.: +48 606639424
e-mail: arkadiusz.szot@pwr.edu.pl

PARIS 2017 AFTES International Congress "The value is Underground", 13-16 November 2017, Paris, France, www.aftes2017.com

World Tunnel Congress 2018
20-26 April 2018, Dubai, United Arab Emirates

EUROCK 2018
22-26 May 2018, Saint Petersburg, Russia

Contact Person: Prof. Vladimir Trushko
Address: 21-st line V.O., 2
199106 St. Petersburg
Russia
Telephone: +7 (812) 328 86 71
Fax: +7 (812) 328 86 76
E-mail: trushko@spmi.ru

16th European Conference on Earthquake Engineering (16thECEE), 18-21 June 2018, Thessaloniki, Greece, www.16ecee.org

CPT'18 4th International Symposium on Cone Penetration Testing, 21-22 June 2018, Delft, Netherlands, www.cpt18.org

RockDyn-3 - 3rd International Conference on Rock Dynamics and Applications
26-27 June 2018, Trondheim, Norway

Sem Sealands veg 1
749 Trondheim
Norway
Telephone: +47 98630706
E-mail: charlie.c.li@ntnu.no

UNSAT2018 The 7th International Conference on Unsaturated Soils, 3 - 5 August 2018, Hong Kong, China, www.unsat2018.org

11th International Conference on Geosynthetics (11ICG), 16 - 20 Sep 2018, Seoul, South Korea, www.11icg-seoul.org

ARMS10
10th Asian Rock Mechanics Symposium
ISRM Regional Symposium
29 October - 3 November 2018, Singapore
www.arms10.org

Contact Person: Prof. Yingxin Zhou
Address: 1 Liang Seah Street
#02-11 Liang Seah Place
SINGAPORE 189022
Telephone: (+65) 637 65363
Fax: (+65) 627 35754
E-mail: zyingxin@dsta.gov.sg

14th ISRM International Congress
20-27 September 2019, Foz de Iguaçu, Brazil

Contact Person: Prof. Sergio A. B. da Fontoura
E-mail: fontoura@puc-rio.b

ISDCG 2019
7th International Symposium on Deformation Characteristics of Geomaterials
26-28 June 2019, Strathclyde, Scotland, UK,

Organizer: TC101

The 17th European Conference on
Soil Mechanics and Geotechnical Engineering
1st - 6th September 2019, Reykjavik Iceland
www.ecsmge-2019.com

The theme of the conference embraces all aspects of geotechnical engineering. Geotechnical engineering is the foundation of current as well as future societies, which both rely on complex civil engineering infrastructures, and call for mitigation of potential geodangers posing threat to these. Geotechnical means and solutions are required to ensure infrastructure safety and sustainable development. Those means are rooted in past experiences enhanced by research and technology of today.

At great events such as the European Geotechnical Conference we should: Spread our knowledge and experience to our colleagues; Introduce innovations, research and development of techniques and equipment; Report on successful geotechnical constructions and application of geotechnical design methods, as well as, on mitigation and assessment of geohazards and more.

Such events also provide an opportunity to draw the attention of others outside the field of geotechnical engineering to the importance of what we are doing, particularly to those who, directly or indirectly, rely on our services, knowledge and experience. Investment in quality geotechnical work is required for successful and safe design, construction and operation of any infrastructure. Geotechnical engineering is the key to a safe and sustainable infrastructure and of importance for the society, economy and the environment. This must be emphasized and reported upon.

ΕΝΔΙΑΦΕΡΟΝΤΑ ΓΕΩΤΕΧΝΙΚΑ ΝΕΑ

Opening Earth
Sinkholes: The Groundbreaking Truth

Εντυπωσιακές εικόνες και video από sinkholes και άλλες εδαφικές θραύσεις και αποσπάσματα από το βιβλίο "Earth Changes and the Humen-Cosmic Connection - The Sectret History of the World - Book 3", σύμφωνα με το οποίο οι sinkholes αλλά και η σεισμική και ηφαιστειακή δραστηριότητα οφείλονται στον ηλεκτρισμό ...

Something is happening to the ground beneath our feet.

The earth is literally opening up.

Before 2010, sinkholes were a relatively uncommon phenomenon. Now they are appearing almost daily.

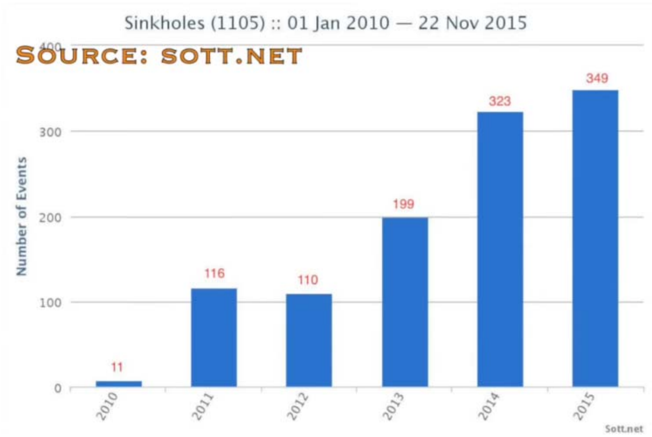

But why so many sinkholes and why now? In a word... ELECTRICITY. Strange it may sound. The Electric Universe Theory, or Plasma Cosmology, can account for this unprecedented phenomenon.

Plasma cosmology sees the universe as a giant electric motor being driven by the exchange of charged particles.

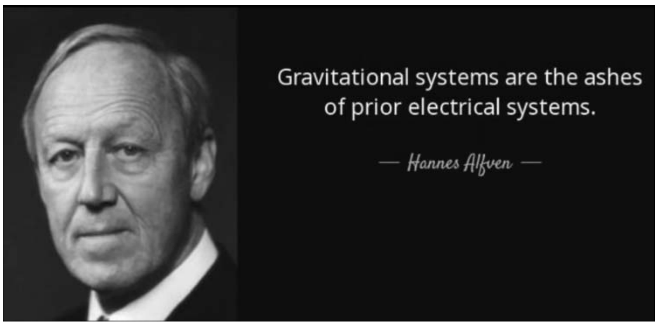

Which explains the mechanical and electromagnetic forces responsible for sinkhole formation.

Sinkholes are usually explained away by ruptured underground water pipes or gradual soil erosion. Even in places where no such piping exists. While standard scientific theories may account for a few, they do not explain ones like these:

Nor can it account for the vast number of new sinkholes forming around the globe.

Here is a simple illustration of the electromagnetic and mechanical forces behind sinkhole formation.

The activity of the sun is directly related to the rotational speed of the earth. The more energy that is produced by the sun, the faster the earth spins.

Like an electric motor, there is a charged potential difference that drives our planet rotation.

The sun is currently in a period similar to the Maunder Minimum with very low solar activity.

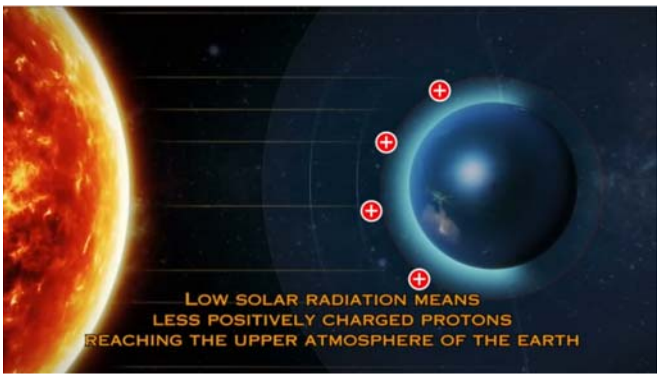

Low solar radiation means less positively charged protons reaching the upper atmosphere of the earth.

The potential difference between the positively charged upper atmosphere and the negatively charged earth decreases, resulting in a slowdown of the earth's rotation.

A slower spin causes the earth to become les oblong like an oval and more circular like a sphere.

The induced mechanical stress causes deformations resulting in cracks, cavities and fissures.

There is also a potential difference between the earth's crust and the core and because the upper atmosphere is now less positive, it also attracts less electrons from inside the earth to its surface, thus decreasing the potential difference between the surface and the core.

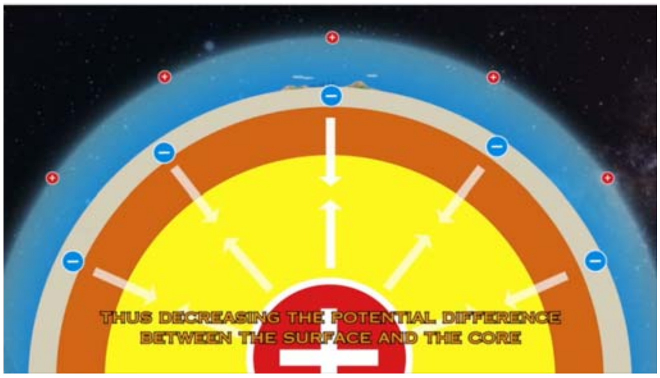

This potential difference acts as a binder of the planet pulling the surface and the core together.

When the potential difference drops, the earth's crust becomes loose. creating pockets of space beneath the surface. The stress on the crust produced by these two combined mechanical and electrical forces results in an increase in earthquake activity.

The loosening of the earth's crust produces cracks and openings resulting in an increase of volcanic activity and,

lastly, the subterranean space created by the loosening, results in the increased formation of sinkholes.

Sinkholes are not an isolated phenomenon. They are also related to earthquakes, volcanoes, tsunamis, strange sounds and extreme weather. This is only the beginning. For more information ...

https://www.youtube.com/embed/TLUgEXI9RYI?rel=0

‘Thinking soil’ made of bacteria could keep buildings from collapsing

It can be quite costly, even catastrophic, when the land under a building subsides. But genetically engineered microbes may one day keep that from happening if researchers in the United Kingdom are successful. Inspired by undergraduates who made a concrete-repairing bacterium—dubbed Bacilla Filla—for a synthetic biology competition (https://2010.igem.org/Team:Newcastle), a biodesigner and his colleagues have been pushing hard to develop biocement, a material that custom-built soil microbes would produce in response to the changing pressures in soil to help shore up the ground under foundations. Toward that end, the team grew a common gut bacterium in surrogate soil—a “hydrogel” shaped into a cylinder. They subjected the bacteria-laden hydrogel to pressures up to 10 times that experienced at sea level. They identified 122 bacterial genes that increased their activity by at least threefold by the pressure change. The team then modified the bacterial genome so that the regulatory DNA responsible for activating one of these genes was attached to a gene for a protein that glows when produced. The more pressure exerted on the microbe, the more intensely it glows (http://www.synbio.construction/2016/07/11/computational-colloids-project-at-acadia-2016), the scientists will report 29 October at the Association for Computer Aided Design in Architecture conference in Ann Arbor, Michigan. In addition, at the meeting, they will describe a computer program that predicts how the microbe will react to forces, such as water pressure, transferred through soil under a building foundation (as depicted in the illustration). Eventually the researchers plan to replace the glowing protein gene with genes that make biocement, creating a “thinking soil” that will keep buildings safe and be a self-constructing foundation. The effort is part of a growing movement to incorporate biology into architecture, they note.

(Elizabeth Pennisi / Science, 27 October 2016, http://www.sciencemag.org/news/2016/10/thinking-soil-made-bacteria-could-keep-buildings-collapsing)

Τα θεμέλια του Πύργου του Eiffel

ΕΝΔΙΑΦΕΡΟΝΤΑ - ΛΟΙΠΑ

Ενδιαφέροντες γεωλογικοί σχηματισμοί ανά τον κόσμο

Τελικά η φύση μπορεί να ξεπεράσει μερικές φορές και την πιο ακραία φαντασία...

Το Σπήλαιο Των Κρυστάλλων, Μεξικό

Οι σταλακτίτες και οι σταλαγμίτες που περιέχει μπορούν να φτάσουν σε μέγεθος πολυκατοικίας και είναι μακράν οι μεγαλύτεροι κρύσταλλοι που είδε ποτέ άνθρωπος.

Οι Περιπλανώμενες Πέτρες, Racetrack Playa, Κοιλάδα του Θανάτου

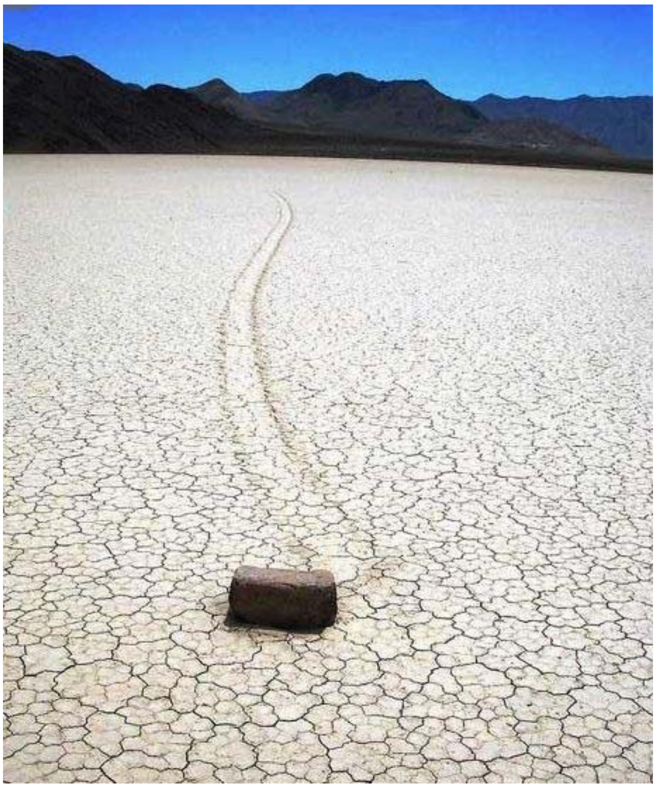

Οι πέτρες αυτές φαίνονται να περιπλανώνται μόνες τους στην άγονη αυτή κοιλάδα, αφήνοντας πίσω γραμμές στο έδαφος. Οι επιστήμονες αναφέρουν ότι ο πάγος που σχηματίζεται γύρω από τις πέτρες τους χειμερινούς μήνες τις κάνει να γλυστρούν.

Το Μάτι της Σαχάρα, Μαυριτανία

Γνωστό και ως Ριχάτ, μοιάζει με ένα μάτι με διάμετρο 50 χιλιομέτρων. Λόγω του μεγέθους του είναι ορατό από το διάστημα, τόσο που οι αστροναύτες το χρησιμοποιούν σαν σημείο αναφοράς. Εκτιμάται ότι ο αέρας και το νερό έχει διαβρώσει σε διαφορετικό βάθος το έδαφος δημιουργώντας αυτό το εκπληκτικό θέαμα.

Οι Παγωμένοι Πύργοι του Βουνού Έρεβος, Ανταρκτική

Το όρος Έρεβος είναι το πιο θερμό μέρος στην παγωμένη ήπειρο καθώς εκεί βρίσκεται το μόνο ενεργό ηφαίστειο. Η κορυφή του, σε υψόμετρο 3.794 μέτρα, καλύπτεται από εκατοντάδες εκπληκτικούς παγωμένους πύργους που συνεχώς εκπέμπουν ατμούς στον ουρανό. Ο ατμός παγώνει μέσα στους πύργους και οδηγεί στην επέκταση και επιμήκυνση των πύργων, που φτάνουν σε ύψος περίπου 20 μέτρων.

Το Μονοπάτι Του Γίγαντα, Βόρεια Ιρλανδία

Αποτελείται από περισσότερες από 40.000 ηφαιστειογενείς και βραχώδεις σχηματισμούς σαν κίονες. Ο θρύλος λέει ότι ο γίγαντας Finn McCool έφτιαξε αυτό το μονοπάτι για να βγει μέχρι τη θάλασσα της Σκωτίας για να συναντήσει τον αντίπαλο του Benandonner. Οι επιστήμονες λένε ότι σχηματίστηκε από εκροές λάβας περίπου 60 εκατομμύρια χρόνια πριν.

Τα Απομεινάρια Ενός Φυσικού Πυρηνικού Αντιδραστήρα, Γκαμπόν

Πριν από 2 δισεκατομμύρια χρόνια, σε αυτό το φυσικό ορυχείο στη Δυτική Αφρική, "λειτουργούσε" ένας φυσικός πυρηνικός αντιδραστήρας που είχε ουράνιο. Φαίνεται πως λειτουργούσε για περισσότερα από 150.000 χρόνια και στη διάρκεια της ζωής του παρήγαγε τόση ενέργεια όση θα ισοδυναμούσε σε 100 μεγατόνους πυρηνικών βομβών.

Το Μονοπάτι Tessellated στο Λαιμό του Σταυραετού, Τασμανία

Παρ' ότι θα έλεγε κανείς ότι κάτι τέτοιο δεν θα μπορούσε να δημιουργηθεί χωρίς ανθρώπινη παρέμβαση, είναι 100% φυσικός σχηματισμός. Σχηματίστηκε πριν από 60 έως 160 εκατομμύρια χρόνια λόγω διάβρωσης του εδάφους.

Η Παγωμένη Σπηλιά του Eisriesenwelt, Γερμανία

... ή αλλιώς "ο κόσμος των γιγάντων του πάγου" είναι η πιο γνωστή σπηλιά με πάγους στον κόσμο.

Pamukkale - Ο Πύργος του Βαμβακιού, Τουρκία

Το όνομα του το περιγράφει γλαφυρά "Ο Πύργος Του Βαμβακιού". Μοιάζει ίσως με πάγο αλλά στην πραγματικότητα είναι άλατα τα οποία καταλήγουν σε εξαιρετικά καυτές λίμνες πλούσιες σε μεταλλικά στοιχεία και άλατα.

Σοκολατένιοι λόφοι, Φιλιππίνες

Παρόλο που οι λόφοι είναι κατά βάση πράσινοι, σε περιόδους ανομβρίας το χόρτο μετατρέπεται σε καφέ και έτσι στ' αλήθεια οι λόφοι μοιάζουν με σοκολάτα. Οι λόφοι αυτοί βρίσκονται στις Φιλιππίνες και απαριθμούνται γύρω στους 1300. Ο τρόπος με τον οποίον σχηματίστηκαν συνεχίζει να αποτελεί μυστήριο ακόμη και σήμερα. Υπάρχουν πολλές θεωρίες σχετικά με το πως δημιουργήθηκαν.

Κυματιστός βράχος, Αυστραλία

Ο κυματιστός βράχος πήρε το όνομα του από το σχήμα του, που μοιάζει με τεράστιο ωκεανό έτοιμο να σαρώσει τα πάντα στο πέρασμα του. Βρίσκεται κοντά στην πόλη Hyden στη Δυτική Αυστραλία.

Το Κύμα, Ηνωμένες Πολιτείες

Βρίσκεται στην Αριζόνα, κοντά στα σύνορα με τη Γιούτα. Το ηλικίας 190 εκατομμυρίων ετών θαύμα της φύσης σχηματίστηκε από αμμόλοφους που μετατράπηκαν έπειτα σε βράχο.

Το φαράγγι της Αντιλόπης, Ηνωμένες Πολιτείες

Το φαράγγι της Αντιλόπης αποτελεί αναμφισβήτητα ένα από τα πιο πολυφωτογραφημένα μέρη στις ΗΠΑ. Βρίσκεται τοποθετημένο στη γη των ινδιάνων Ναβάχο στην Αριζόνα. Στην πραγματικότητα, υπάρχουν δυο ξεχωριστά φαράγγια της Αντιλόπης. Το ανώτερο φαράγγι ονομάζεται Tse' bighanilini, που σημαίνει "το μέρος που το νερό διαπερνά τους βράχους," ενώ το χαμηλότερο φαράγγι ονομάζεται Hasdestwazi, δηλαδή "σπειροειδείς αψίδες βράχου." Το φαράγγι σχηματίστηκε από μια διάβρωση των βράχων που έλαβε χώρα λόγω ξαφνικής πλημμύρας αλλά με την πάροδο του χρόνου οι άκρες λειάνθηκαν με αποτέλεσμα να δημιουργηθεί ένα από τα πιο όμορφα αξιοθέατα στον κόσμο.

Η πύλη της κόλασης, Ισλανδία

Το μικρό νησί στο τέλος του κόσμου συγκεντρώνει έναν μεγάλο αριθμό από θαύματα της φύσης, κυρίως λόγω των ηφαιστείων του. Η πύλη της κόλασης, ή Namaskar όπως το αποκαλούν οι Ισλανδοί, είναι μια ομάδα ηφαιστείων που από πάνω τους αιωρείται συνεχώς ατμός περικλείοντας τα, ακριβώς όπως η κόλαση περιγράφεται στους μύθους. Παρόλα αυτά, αν αποφασίσετε να επισκεφθείτε το μέρος δεν θα συναντήσετε την κόλαση, αλλά τον επίγειο παράδεισο.

Salar de Uyuni, Βολιβία

Το Salar de Uyuni βρίσκεται στις Άνδεις της Βολιβίας και αποτελούσε τη μεγαλύτερη λίμνη από αλάτι στον κόσμο. Η λίμνη έχει ξεραθεί εδώ και πολλά χρόνια με αποτέλεσμα να έχει δημιουργηθεί ένα συμπαγές ίζημα από αλάτι που περιλαμβάνει το 50- 70% των παγκόσμιων αποθεμάτων λιθίου. Ωστόσο, δεν είναι αυτός ο λόγος που το μέρος αυτό είναι τόσο διάσημο. Κατά τη διάρκεια της περιόδου των βροχών, το νερό της λίμνης δημιουργεί τον μεγαλύτερο καθρέφτη πάνω στη γη. Μπορεί δηλαδή κάποιος να δει τον ουρανό και τα σύννεφα κάτω από τα πόδια του και να νοιώσει σαν να περπατά πάνω σε αυτά. Παρά το γεγονός ότι είναι ένα απομονωμένο μέρος, προσελκύει πολλούς τουρίστες από όλο τον κόσμο.

Πέτρινο δάσος, Μαγαδασκάρη

Το πέτρινο δάσος, ή "εκεί που δεν μπορείς να περπατήσεις ξυπόλυτος" όπως οι ντόπιοι χαρακτηριστικά λένε, βρίσκεται στο εθνικό πάρκο της Μαγαδασκάρης Tsingy de Bemaraha. Το δάσος αποτελεί μέρος της Παγκόσμιας Κληρονομιάς χάρη στο γεγονός ότι εκεί φιλοξενείται ένας μεγάλος αριθμός ειδών υπό εξαφάνιση. Τα "δέντρα" του δάσους αποτελούν πόλο έλξης για πολλούς τουρίστες από όλο τον κόσμο που επισκέπτονται το παραδεισένιο νησί κάθε χρόνο.

Η Σπηλιά Φίνγκαλ, Σκωτία

Μοιάζει με καθεδρικό ναό. Έχει βάθος περίπου 75 μέτρα μέσα στο βράχο και βρίσκεται στις δυτικές ακτές της Σκωτίας. Στη Βικτωριανή εποχή ήταν εξαιρετικά διάσημος τουριστικός προορισμός τον οποίο είχε επισκεφθεί και η Βασίλισσα της Αγγλίας, Βικτωρία.

Η Μεγάλη Μπλε Τρύπα, Κεντρική Αμερική

Η μεγάλη μπλε τρύπα στο Μπελίζ είναι παγκοσμίως γνωστή ως ένα ιδανικό μέρος για καταδύσεις. Η σχεδόν τέλεια κυκλική τρύπα στον στη θάλασσα είναι κομμάτι της ατόλης Lighthouse Reef και έχει 450 μέτρα βάθος.

http://www.news.gr/perivallon/planhths-gh/article/79375/oi-10-pio-periergoi-geologikoi-shhmatismoi-ston.html

http://lefteria.blogspot.qa/2015/09/10_8.html

ΝΕΕΣ ΕΚΔΟΣΕΙΣ ΣΤΙΣ ΓΕΩΤΕΧΝΙΚΕΣ ΕΠΙΣΤΗΜΕΣ

TBM Excavation in Difficult Ground Conditions: Case Studies from Turkey

N. Bilgin, H. Copur, C. Balci

The book relates experience of TBM drives in difficult geology, making use of case studies from Turkey to demonstrate the influence of the local geotechnical conditions on the selection of a tunnel boring machine and the selection of tools. There is an extensive description how various geological phenomena, such as for example transition zones, dikes, rock discontinuities, blocky ground, squeezing ground, swelling clays and high strength and abrasive rocks, can reduce the advance rate and what countermeasures can be introduced. There is also a discussion of necessary advance probing and safety measures. Since the presented practical experience from Turkey can also be applicable for other tunnel projects in difficult geology, the book represents a valuable source of knowledge for every tunneler.

(WILEY / Ernst & Sohn, November 2016)

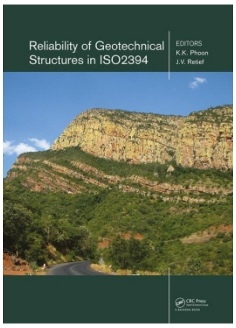

Reliability of Geotechnical Structures in ISO2394

K.K. Phoon, J.V. Retief

The latest 4th edition of the international standard on the principles of reliability for load bearing structures (ISO2394:2015) includes a new Annex D dedicated to the reliability of geotechnical structures. The emphasis in Annex D is to identify and characterize critical elements of the geotechnical reliability-based design process. This book contains a wealth of data and information to assist geotechnical engineers with the implementation of semi-probabilistic or full probabilistic design approaches within the context of established geotechnical knowledge, principles, and experience.

The introduction to the book presents an overview on how reliability can play a complementary role within prevailing norms in geotechnical practice to address situations where some measured data and/or past experience exist for limited site-specific data to be supplemented by both objective regional data and subjective judgment derived from comparable sites elsewhere. The principles of reliability as presented in ISO2394:2015 provides the common basis for harmonization of structural and geotechnical design. The balance of the chapters describes the uncertainty representation of geotechnical design parameters, the statistical characterization of multivariate geotechnical data and model factors, semi-probabilistic and direct probability-based design methods in accordance to the outline of Annex D.

This book elaborates and reinforces the goal of Annex D to advance geotechnical reliability-based design with geotechnical needs at the forefront while complying with the general principles of reliability given by ISO2394:2015. It serves as a supplementary reference to Annex D and it is a must-read for designing geotechnical structures in compliance with ISO2394:2015.

Features

- provides interpretation and application of general principles of ISO 2394 to geotechnical design
- serves as an informative supplement to ISO2394 Annex D *Reliability of geotechnical structures*
- provides valuable authoritative statistical data and reliability models needed for any code calibration
- provides efficient methods for reliability analysis and design
- provides a systematic process for deriving reliability based design procedures whilst fully taking account of the unique character of geotechnical design
- resulting overall in a significant advancement in reliability based geotechnical design practice

(CRC Press, September 12, 2016)

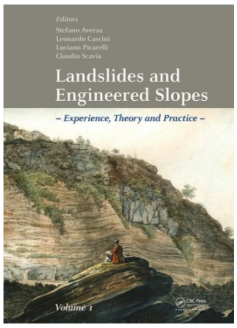

Landslides and Engineered Slopes. Experience, Theory and Practice

Proceedings of the 12th International Symposium on Landslides (Napoli, Italy, 12-19 June 2016)

Stefano Aversa, Leonardo Cascini, Luciano Picarelli, Claudio Scavia (ed.)

Landslides and Engineered Slopes. Experience, Theory and Practice contains the invited lectures and all papers presented at the 12th International Symposium on Landslides, (Naples, Italy, 12-19 June 2016). The book aims to emphasize the relationship between landslides and other natural hazards. Hence, three of the main sessions focus on Volcanic-induced landslides, Earthquake-induced landslides and Weather-induced landslides respectively, while the fourth main session deals with Human-induced landslides. Some papers presented in a special session devoted to "Subareal and submarine landslide processes and hazard" and in a "Young Session" complete the books.

Landslides and Engineered Slopes. Experience, Theory and Practice underlines the importance of the classic approach of modern science, which moves from experience to theory, as the basic instrument to study landslides. Experience is the key to understand the natural phenomena focusing on all the factors that play a major role. Theory is the instrument to manage the data provided by experience following a mathematical approach; this allows not only to clarify the nature and the deep causes of phenomena but mostly, to predict future and, if required, manage similar events. Practical benefits from the results of theory to protect people and man-made works.

Landslides and Engineered Slopes. Experience, Theory and Practice is useful to scientists and practitioners working in the areas of rock and soil mechanics, geotechnical engineering, engineering geology and geology.

(CRC Press, June 6, 2016)

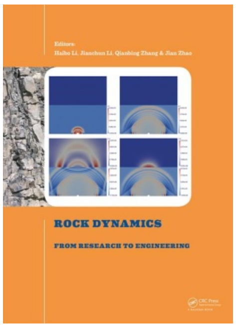

Rock Dynamics: From Research to Engineering

Proceedings of the 2nd International Conference on Rock Dynamics and Applications

Haibo Li, Jianchun Li, Qianbing Zhang, Jian Zhao

Rock Dynamics: From Research to Engineering is a collection of the scientific and technical papers presented at the Second International Conference on Rock Dynamics and Applications (RocDyn-2, Suzhou, China, 18-19 May 2016). The book has four sections. The first section contains 8 keynote papers, covering a wide range of dynamic issues related to rock mechanics and rock engineering, from rock failure mechanism and stress wave propagation to seismic behaviour and impact. Section 2 includes papers on rock dynamic theory and numerical modelling, focussing on theoretical aspects of rock fracture dynamics, wave propagation, numerical methods and numerical modelling works. Papers on laboratory testing and experimental techniques are collected in Section 3, including new testing facilities, data monitoring and data analysis. Section 4 deals with case studies and engineering applications, and presents state-of-the-art papers on rock engineering related to dynamic conditions such as earthquake and blasting.

Rock Dynamics: From Research to Engineering will serve as a must-have reference, presenting the results of recent developments in rock dynamics scientific research and rock dynamics engineering applications.

(CRC Press, April 19, 2016)

ΗΛΕΚΤΡΟΝΙΚΑ ΠΕΡΙΟΔΙΚΑ

http://www.geoengineer.org/geonews139.html

Κυκλοφόρησε το Τεύχος #139 του **Newsletter του Geoengineer.org** (Οκτωβρίου 2016) με πολλές χρήσιμες πληροφορίες για όλα τα θέματα της γεωμηχανικής. Υπενθυμίζεται ότι το Newsletter εκδίδεται από τον συνάδελφο και μέλος της ΕΕΕΕΓΜ Δημήτρη Ζέκκο (secretariat@geoengineer.org).

Ενδεικτικά αναφέρονται:

- Earthquake Measuring 6.9 Strikes Papua New Guinea
- Project Summary in the city of Memphis about Riverside Drive Slope Stabilization
- Colima Volcano in Mexico Erupts Causing Evacuations
- DFI Releases Report from Workshop on Quality Assurance for Post-Grouted Drilled Shafts
- Combining geological modelling and BIM for infrastructure
- Energy Plant Dam Collapses Due to Flooding in North Carolina (video)
- Shallow 5.3 Magnitude Earthquake Strikes Greece
- Simple post-processing to estimate hydraulic conductivity and water table elevation
- Bridge Collapse in Indonesia Leaves 8 Dead

cs Ꟊ

The International Journal of Geoengineering Case Histories, an official Journal of the International Society for Soil Mechanics and Geotechnical Engineering (ISSMGE), is pleased to launch its third issue of its third volume. This is a special issue with Case Histories on geotechnical challenges from Singapore, organized by the Geotechnical Society of Singapore and edited by Prof. Siau Chen Chian and Prof. Kok Kwang Phoon.

Papers published in this refereed journal are freely available in color and are accompanied by databases that include the electronic data presented in the paper as well as additional figures (as necessary). The locations of the case histories are also positioned in a downloadable Google Earth database, also available in GeoMap.

The Special Issue includes the following papers:

- Cham, W. M. (2016). Singapore Case Histories on Performance of Piles Subjected to Tunnelling-Induced Soil Movement. International Journal of Geoengineering Case Histories, Volume 3, Issue 3, pp. 128-148, doi: 10.4417/IJGCH-03-03-01
- Goh, K. H., Ng, S.S.G., and Wong, K. C. (2016). Case Histories of Bored Tunnelling Below Buildings in Singapore Downtown Line. International Journal of Geoengineering Case Histories, Volume 3, Issue 3, pp. 149-161, doi: 10.4417/IJGCH-03-03-02
- Senthilnath, G.T., and Velu, D. (2016). Stacked Tunnelling Induced Surface Settlements in Soft Soil. International Journal of Geoengineering Case Histories, Volume 3, Issue 3, pp. 162-175, doi: 10.4417/IJGCH-03-03-03
- Soh, K. K., Wai, T.T., Yeo, L., and Lim, P. K. (2016). Reclamation and Safety of High Cantilever Strong Box Pipe Pile Seawall in Marine Clay. International Journal of Geoengineering Case Histories, Volume 3, Issue 3, pp. 176-189. doi: 10.4417/IJGCH-03-03-04
- Zhang, W., and Goh, A. T. C. (2016). General Behaviour of Braced Excavation in Bukit Timah Granite Residual Soils. International Journal of Geoengineering Case Histories, Volume 3, Issue 3, pp. 190-202, doi: 10.4417/IJGCH-03-03-05

Follow this link (http://casehistories.geoengineer.org/volume/volume3/issue3/issue3.html) in order to download and read the papers of the latest issue of the journal and access the digital data.

The truly open-source mission of the journal is funded annually by not more than four companies and organizations who have an action-based commitment to the advancement of the geoengineering profession. These organizations are acknowledged on our website and in every single paper of the journal. IJGCH is proudly funded by Shamsher Prakash Foundation and Dar Group. Our sponsors make possible the circulation of the journal to thousands of readers at no cost.

Geotechnical engineers are encouraged to submit a paper for review and potential publication by the ISSMGE International Journal of Geoengineering Case Histories.

cs Ꟊ

THE ITA@NEWS #61 - October 2016

https://www.ita-aites.org/en/?option=com_acymailing&ctrl=archive&task=view&mailid=139&key=889CxjDS&subid=1894-74d7627ed3e51b67271afdd9255b5891&tmpl=component&Itemid=843

Κυκλοφόρησε το τεύχος αρ. 61, Οκτωβρίου 2016 των ITA@NEWS με τα ακόλουθα περιεχόμενα:

- Message from Tarcisio CELESTINO, ITA President
- ITA Tunnelling Awards 2016
- Workshop on "Best Practices for Safe Cross Passage"

- DFTU International Tunnelling Symposium
- SIG Conference
- BEFIPS meeting
- 4th Arabian Tunnelling Conference & 20th Gulf Engineering Union
- 4th Brazilian Tunnelling Congress, 3- 6 th April 2017 in São Paulo
- Southeast Asian Conference & Exhibition in Tunnelling and Underground Space 2017 (SEACETU 2017)
- 7th International Symposium on Tunnels and Underground Structures in South-East Europe, 4 - 5th May 2017, Croatia

ΕΕΕΕΓΜ
Τομέας Γεωτεχνικής
ΣΧΟΛΗ ΠΟΛΙΤΙΚΩΝ ΜΗΧΑΝΙΚΩΝ
ΕΘΝΙΚΟΥ ΜΕΤΣΟΒΙΟΥ ΠΟΛΥΤΕΧΝΕΙΟΥ
Πολυτεχνειούπολη Ζωγράφου
15780 ΖΩΓΡΑΦΟΥ

Τηλ. 210.7723434
Τοτ. 210.7723428
Ηλ-Δι. secretariat@hssmge.gr ,
geotech@central.ntua.gr
Ιστοσελίδα www.hssmge.org (υπό κατασκευή)

«ΤΑ ΝΕΑ ΤΗΣ ΕΕΕΕΓΜ» Εκδότης: Χρήστος Τσατσανίφος, τηλ. 210.6929484, τοτ. 210.6928137, ηλ-δι. ctsatsanifos@pangaea.gr, editor@hssmge.gr, info@pangaea.gr

«ΤΑ ΝΕΑ ΤΗΣ ΕΕΕΕΓΜ» «αναρτώνται» και στην ιστοσελίδα www.hssmge.gr